Characterization of Photodegradable Polymers for UV-triggered Release from Microcapsules

Master's thesis in Materials Chemistry

SZILVIA VAVRA

Department of Chemistry and Chemical Engineering
CHALMERS UNIVERSITY OF TECHNOLOGY
Gothenburg, Sweden 2019

Master's thesis 2019

Characterization of Photodegradable Polymers for UV-triggered Release from Microcapsules

SZILVIA VAVRA

Department of Chemistry and Chemical Engineering
Division of Applied Chemistry
Chalmers University of Technology
Gothenburg, Sweden 2019

Characterization of Photodegradable Polymers for UV-triggered Release from Microcapsules

Characterization of Photodegradable Polymers for UV-triggered Release from Microcapsules
Szilvia Vavra
Department of Chemistry and Chemical Engineering
Chalmers University of Technology

Abstract

Characterization of photodegradation mechanisms of polymers has key importance in materials engineering both when the degradation process is unwanted so as in cases when it is intentionally desired and tailored. In microcapsules with solid polymer wall that are designed to be capable of instantaneous release of core phase content upon UV-light irradiation the photodegradation of the polymer wall has to be rapid and controlled. Therefore, use of characterization method that is fast, easy and provides physical and chemical information on photodegradation is crucial in evaluating high number of polymers as possible wall material candidates. The aim of this work is to support choice of material for microcapsule wall by characterization of photodegradation mechanisms of various potentially suitable photodegradable polymers. To achieve this, weightlosses of the studied polymers nanofilms were measured in function of UV-light irradiation time by QCM-D coupled with IRRAS to gain also chemical information on their degradation process. Additionally, some of the polymer microfilms photodegradation was characterized with NMR, ATR-IR, DSC, and TGA.

From the obtained dataset UV-light degradation mechanisms and time dependencies of the different polymers could be described. Six different kinds of polymers (PMMA, PS, PPhA, PPC, PSu, PVCi) were studied, in case of PMMA with two different molecular weights and in case of depolymerizable polymers (PPhA, PPC, PSu) with photo catalyst added to the neat polymer. Among depolymerizable polymers even with added catalyst in PSu and PPC the depolymerization remained restricted proposedly due to their high ceiling temperature. PMMA, independently from molecular weigth, degraded with main chain scission followed by incomplete unzipping of the mainchain that resulted moderate weightloss. Low molecular weigth PS showed photooxidation that resulted more rapid weightloss, however, only after one hour-long offset proposedly due to diffusion control of oxygen. In case of PVCi photocrosslinking could not be observed but instead photooxidative degradation happened upon UV light that was still moderate compared to PS. Among the studied polymers the most suitable candidate as microcapsule wall is PPhA, preferably with added photo acid generator as it showed extremely rapid depolymerization that could be further enhanced with photo acid catalysis.

Chemical changes and mass loss of different polymer nanofilms upon UV-light could be measured relatively fast and easy with coupling QCM-D and IRRAS methods. Due to the robustness of the measurement procedure, several types of polymers could be compared and evaluated on their suitability as possible microcapsule walls under the same UV-light irradiation conditions. Huge advantage is that photodegradation could be studied on nanofilms that have the same thickness range as microcapsule wall thickness. Also, it is important to note that more rapid photodegradation could be observed on nanofilms than on microfilms making it possible to study degradation mechanisms in a less time-consuming way.

Keywords: microcapsule, UV, photodegradation, photodegradable polymer, photo catalyst

Table of Content

1. Background

1.1. Microencapsulation and triggered release

Microencapsulation is the process of packaging solids, liquids or gases with another material into sealed capsules with diameter varying from few microns to few millimeters [7] [8] [9]. Regarding morphology and internal structure, several types of microparticles can be obtained by microencapsulation; among them the product is called microcapsule when it has core-shell structure [9] [10]. The core-shell structure typically consists of an internal phase (also referred as core) that is covered with one or more outer layer (also referred as shell, coating or wall) [7] [9]. The microcapsules that are capable of releasing core content are often further classified based on their release properties and mechanism of possible triggering and targeting [8] [11] [12] [13] [14].

Several methods have been developed to achieve triggered release of the encapsulated content; beside conventional methods like shell wall melting or mechanical degradation of the wall, response phenomena of stimuli-responsive systems are also widely utilized [11]. Stimuli-responsive systems show non-linear change in properties as response to an external signal and their common classification is based on the type of the trigger for release; such triggers can be biological, chemical, photo, thermal, electrical and magnetic stimuli, Figure 1.1 [11] [15] [16]. Among these triggers, using light (photo stimulus) is advantageous for its potential to be remotely applied with extremely high spatial and temporal precision and tailored using a broad range of parameters (e.g. irradiation time, intensity, etc.) [17]. In general, there are two basic ways to prepare stimuli-responsive microcapsules: i) grafting or incorporating stimuli-responsive material into the microcapsule wall and ii) forming the wall directly from stimuli-responsive material [18].
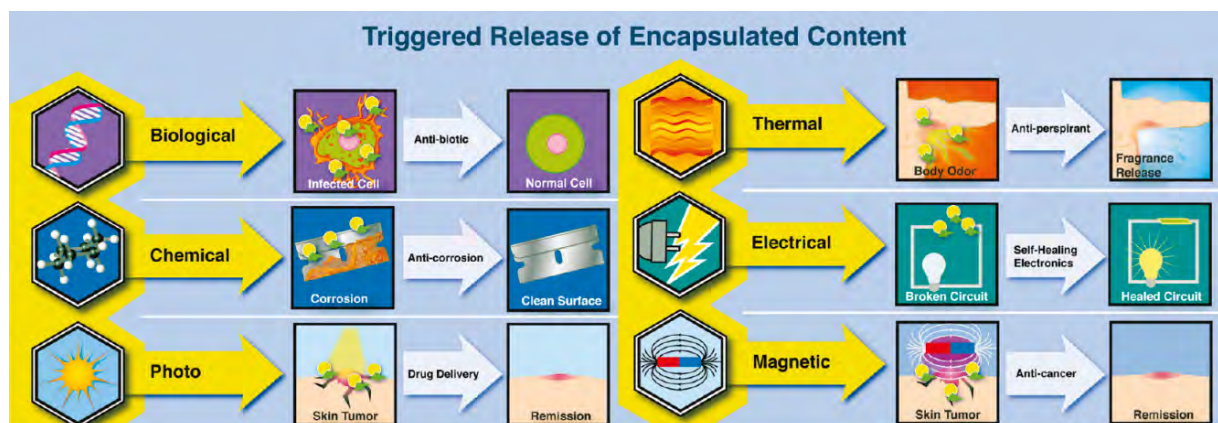

Figure 1.1. Triggers and potential applications of microcapsules [9]

1.2. UV-triggered release from microcapsules

Numerous light-responsive microcapsule-based systems have been developed for controlled release based on a variety of UV-triggered chemical and physical mechanisms. Here, only response mechanisms that can be used in microcapsules with solid, polymeric wall under UV-light are discussed. Even though it is extremely difficult to make quantitative comparison of these systems due to deviations in experimental conditions some of their important attributes still can be noted.

UV-light can induce stereoisomerisation and rearrangement in certain chemical groups that can be utilized also in light-responsive microcapsules, usually by altering the hydrophilic lipophilic balance. When photo-sensitive groups are introduced into the polymer backbone or side chain, the entire material of the polymeric wall undergo on physical and chemical change upon irradiation [14]. One of the most studied photoinduced stereoisomeric phenomenon is the *cis-trans* isomerization of molecules with double bonds. Double bonds are restricted in rotation thus molecules like azobenzes, stilbenes, etc. can switch from a thermally stable, linear *trans* orientation to an energetically less favorable *cis* orientation upon irradiation of UV-light [17]. Permeability of a microcapsule wall that contains polyelectrolyte multilayers with azo groups can be controlled by UV-light; the photoinduced stereochemical change of azo groups leads to increased permeability of the capsules that provides long term release of their content [19]. Huge advantage of these systems is the reversibility of *cis-trans* transformation thus rendering the microcapsules reusable [11].

Photochemical degradation of polymer microcapsule wall upon UV-light irradiation is also suitable to trigger release from the core [9]. A wide variety of photochemical reactions might be utilized for such purpose, some of them discussed more detailed in Chapter 3.3. Even though there are several suitable degradation mechanisms, most articles focus on polymers that can show complete or incomplete unzipping of the polymer chain to its monomers or other small molecules upon UV-light irradiation. Complete unzipping can be initiated by UV-light irradiation in depolymerizable polymers that are also called self-immolative polymers [11] [20]. Depolymerizable polymers, are thermodynamically unstable in room temperature and are therefore able to spontaneously depolymerize [20] [21]. To avoid undesired depolymerization, protecting head groups are attached to the ends of the polymer chain [11]. Triggered destruction of microcapsule wall made of such polymers can be achieved by removal of these protecting headgroups by UV-light, initiating degradation of the wall via depolymerization [11]. Self-immolative reactions are irreversible and in some cases extremely rapid compared to other degradation mechanisms [11] [20]. Thus, self-immolative polymer-based microcapsules are potentially suitable for short, rapid release of their content. This idea is relatively novel, however, much progress has been made since their first publication in 2010 [11]. Such systems are highly studied not only because of their fast reaction kinetics, but also because the mechanism of self-immolative polymers allows the activation of capsules by lower amount of stimulant [11].

Another suitable method is the incorporation of a photocatalyst into the microcapsule shell, by which UV-light induced degradation of the polymeric wall can be significantly enhanced [22] [1]. Nanoparticles with photocatalytic activity are highly suitable candidates

for this purpose, however nanoparticle/polymer composite systems used as microcapsule walls are seldom reported [22]. As a prominent proof of concept titanium dioxide (titania) nanoparticles were proven to show photocatalytic activity in photodegradation of polystyrene microcapsule wall, achieving UV-light triggered release of fluoroalkyl silane [22].

Also, cross-link removal reaction upon UV-light irradiation can be utilized in UV-light triggered content release of microcapsules. The crosslinks are usually evenly distributed in the wall material and the speed of the release can be controlled by the concentration of the crosslinks. By increasing the concentration of crosslinks faster disintegration of the wall and faster release can be achieved upon the same UV-light irradiation conditions. Providing tunability on release profile is a huge advantage of these systems, however, implementation of large number of crosslinks requires more complex microcapsule synthesis [11].

Macroscopic physical changes in the microcapsule wall can be generated by UV-light, thus such phenomena can be used for UV-light triggered content release of microcapsules. There are several physical changes that can be suitable; the most important mechanisms are pressure-induced rupture, shell wall melting, change in porosity, and thermomechanical degradation [11]. In addition, from this point of view, as shrinkage and pore formation in the polymeric material can be achieved by photocrosslinking, also crosslinking as degradation process can potentially be utilized [17].

2. Objective

This study is part of a research project that aims to obtain microcapsules that are capable of instantaneous release of content from the core phase upon UV-light irradiation preferably with high core/shell ratio. Beside release profile and trigger mechanism, further considerations are related to a possible scaled-up production are beneficial to be taken even at basic research stage, for example simplicity of synthesis, availability of raw materials and stability in air. To achieve this, UV-light sensitive, polymeric material is designed to be used as solid microcapsule wall. They highly meet the requirements of this use: microcapsules could be synthetized from them by simple internal phase separation, they are mechanically stable due to their solid state and show rapid photodegradation that can provide instantaneous release.

Thus, the main goal of this work is to support the choice of material by studying potentially suitable photodegradable polymers. For the sake of simplicity, commercially available photosensitive polymers were chosen to be characterized as potential wall materials. Due to the key importance of the possible release rate of capsule content, the thesis focuses primarily on studying degradation rates and mechanisms, moreover the related change in physical and chemical properties of photodegradable polymers. By comparison of the potential polymers, the objective is to give assessment on which polymers might be the most suitable wall materials of UV-triggered microcapsules.

3. Theoretical Background

3. 1. Fundamentals in Photochemistry of Polymers

3. 1. 1. UV light and its interaction with matter

The behaviour of electromagnetic radiation can he attributed either to its wave-like (quantum) character or to its corpuscular (photon) character, together called as wave-particle duality [23] [24]. In the wave model, electromagnetic radiation is characterized by its wavelength, λ , and frequency, v, that are inversely proportional to one other with velocity, c, eq. 3. 1.. The value of the velocity depends on the medium [24]. The energy of a photon, E, depends on its frequency (or wavelength); according to eq. 3. 2. where h is Planck's constant [24].

$$\lambda = \frac{c}{v}$$
<div align="right">eq. 3. 1.</div>

$$E = hv = \frac{hc}{\lambda}$$
<div align="right">eq. 3. 2.</div>

The electromagnetic spectrum is divided into regions based on the wavelength of the electromagnetic radiation so-called „optical radiation" refers to ultraviolet (UV), visible (VIS) and infrared (IR) radiations, Figure 3. 1. [23] [24]. UV radiation is further divided into near UV (NUV) and far UV (FUV), or according to another classification UVA (315-400 nm), UVB (315-280 nm) and UVC (280-100 nm) regions [23] [25].

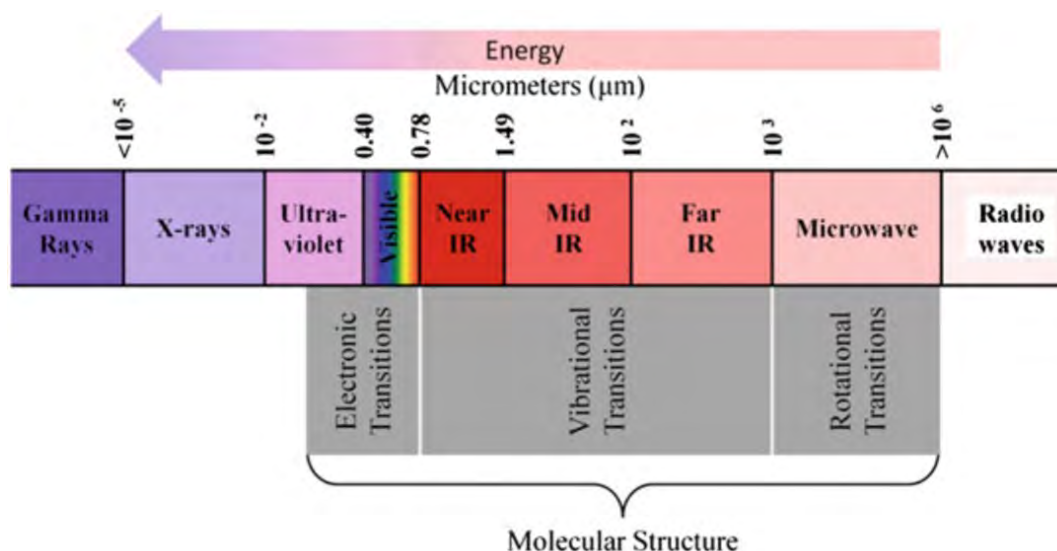**Figure 3. 1.** The electromagnetic spectrum [24]

Energies that are needed to change the electron distributions of molecules are of the order of several electronvolts (>1 eV), that is equivalent to about 100 kJ/mol. Thus, photons in the visible and ultraviolet regions of the spectrum with similar energies emitted or absorbed cause change in the electronic state of molecules [26]. Moreover, photons at wavelength

around 250 nm possess enough energy to be able of breaking certain bonds in polymers, energies of abundant bonds can be seen in Table 3.1. [23]. However, it is important to note that under irradiation of polymer molecules, bonds are seldom broken at random. Instead, the excited molecules undergo fairly selective reactions of bond breaking, rearrangements, or bimolecular reactions [23].

Table 3. 1. Energies for dissociation of typical chemical bonds [23].

Bond	Energy (kcal/mol)	λ (nm)
C=C	160	179
C–C	85	336
C–H	95–100	286–301
C–O	80–100	286–357
C–Cl	60–86	332–477
C–Br	45–70	408–636
O–O	35	817
O–H	85–115	249–336

3. 1. 2. Photochemical Laws

To describe photochemical processes, the following fundamental laws have been established [25] [27] [23].

(i) light absorption by at least one of the reactants participating in a photophysical process or a photochemical reaction is necessary and only the radiation absorbed is effective in producing a photochemical change [25] [23]

(ii) each photon absorbed activates one molecule in the primary excitation step of a photochemical sequence [23]

(iii) each photon absorbed by a molecule has a certain probability of populating either the lowest excited singlet state (S_1) or lowest triplet state (T_1) [23]

(iv) reciprocity law: all mechanisms of the photochemical processes are exclusively dependent on total absorbed energy and independent of exposure time and radiant intensity –however the legitimacy of this law is still under debate [25]

3. 1. 3. Electronically Excited States and Photodissociation

The electrons of most unexcited molecular systems, such as polymers, are in singlet ground state (with the exception of radicals and para- or ferromagnetic transition metals) in which the electron spins are paired. Since direct excitation from the singlet ground state to the triplet state is spin forbidden, the absorption of a photon with appropriate frequency will result in an excited electronic state which is also singlet. This process can be represented in a Jablonsky diagram, Figure 3.2. The higher the energy of the absorbed photon with appropriate frequency, the higher the energy of the excited singlet state (S_1, S_2...S_i) will be [2] [23]. In comparison, triplet states cannot be achieved via direct excitation from the ground state.

Instead, the lowest excited triplet state (T_1) can be formed mainly by non-radiative transition called intersystem crossing (ISC) from the lowest excited singlet state (S_1) via vibrational overlapping states. Higher triplet states (T_2, T_3, ... T_j;) may be formed when the lowest triplet state (T_1) absorbs a new photon (triplet-triplet absorption) [27].

In polymers containing single and double covalent bonds and lone pair electrons, the excitation of a single electron may occur from the σ, π or n orbital in the ground state to the antibonding π^* or n* orbital, depending on the energy of the incident UV-light, see Figure 3. 3. [27] [25].
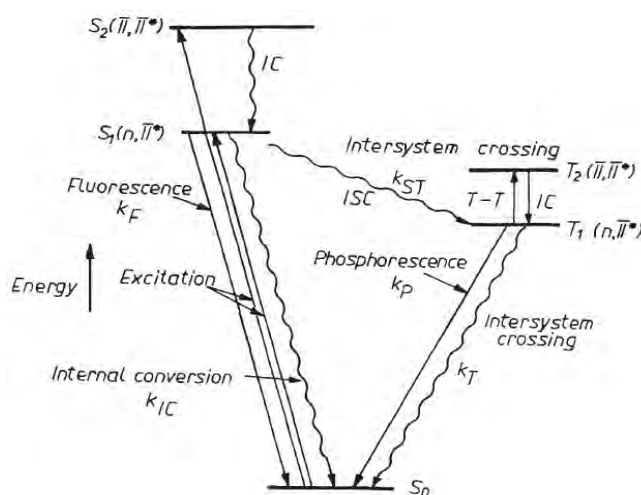

Figure 3. 2. Jablonsky diagram of electronical states and processes [23]
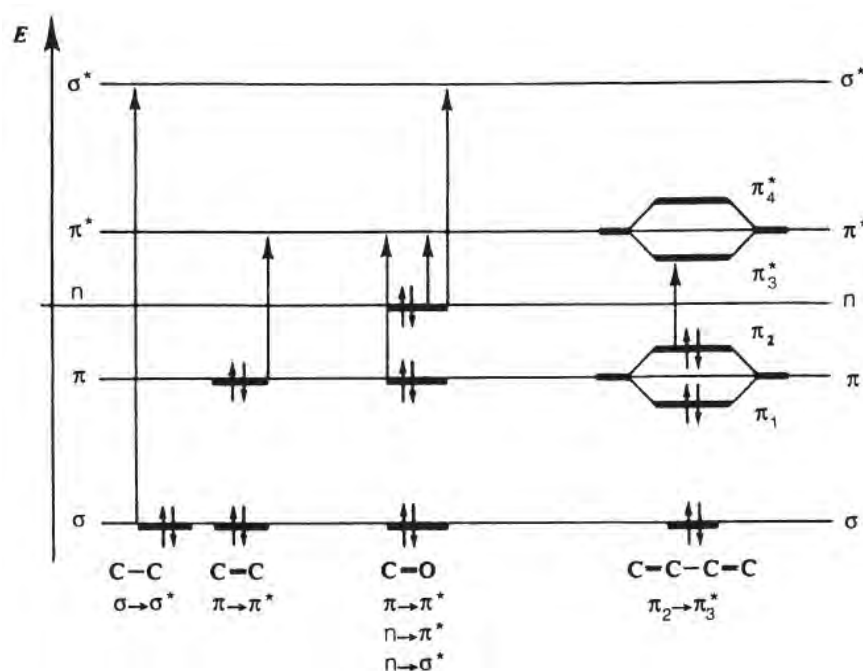
Figure 3. 3. Relative energies of molecular orbitals and different electronic transitions [27]

Photodissociation processes have key role not only in radical formation in general, but also in direct chain scission of polymers and formation of substances with catalytic effect on polymer degradation. Photodissociation of a molecule may occur *via* both singlet and triplet excited states. Figure 3. 4. shows schematized potential energy curves of molecules and their states during photodissociation. Figure 3. 4. A represents dissociation from a stable excited singlet or triplet state to a point beyond the dissociation limit of the upper states. Figure 3. 4. B displays electronic excitations bringing the molecule to dissociative excited states where the atoms repel each other at any separation distance (r). Since excited triplet states have much longer lifetimes due to longer relaxational pathways, more photodissociation processes are likely to occur from levels of that excited state [23].

Figure 3. 4. Photodissociation of a molecule from the ground state S_0 via an excited singlet S_1 (left) or triplet state T_1 (right) by excitation above the dissociative limit of the upper state (A) or through a dissociative excited state (B) [23]

3. 2. Photodegradation of Polymers in General

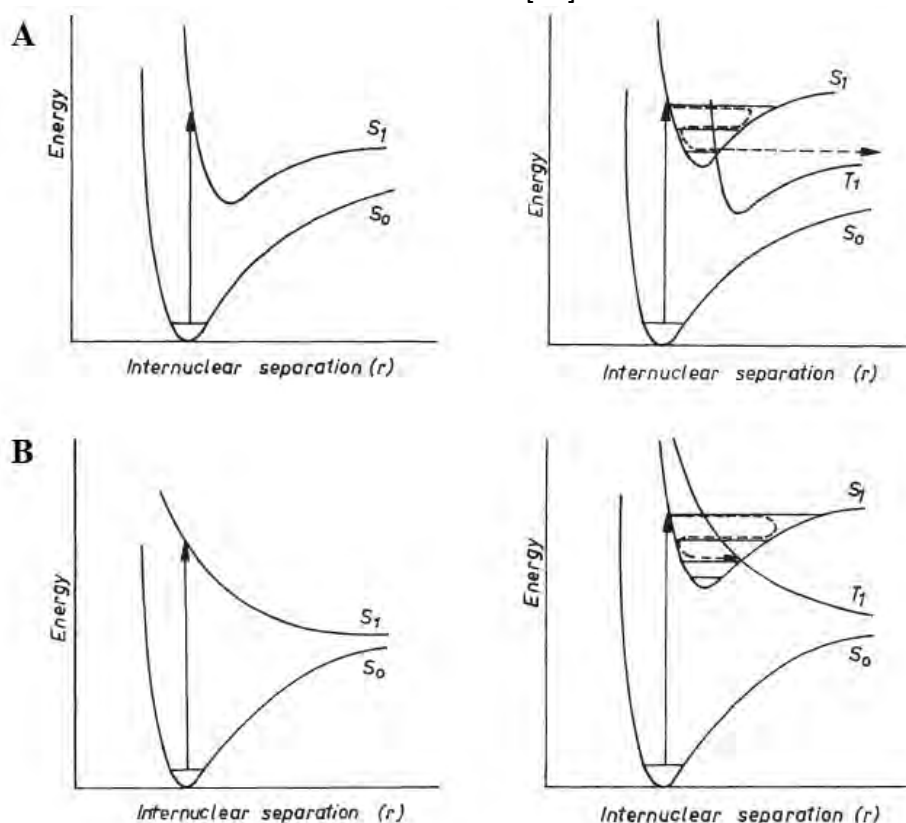### 3. 2. 1. Basic Steps of Photodegradation

Photochemical reactions can be described by three major stages [23] :
- (i)   photon absorption that leads to electronical excitation of a molecule
- (ii)   primary photochemical process which involve electronically excited states
- (iii)   secondary or "dark" (thermal) reactions of the radicals, radical ions, ions and electrons produced by the primary photochemical process

Photodegradation is generally described as a result of primary (photo-) and secondary (dark) reactions which change the primary structure of a polymer by chain scission, crosslinking and oxidative processes [23] .

3. 2. 2. Degree of Polymerization during Photodegradation

The change in degree of polymerization (DP) and in the related physical and chemical properties highly depends on the mechanism of photodegradation of the main chain. Basically, the first step of it can be: (i) random breaks of internal bonds in the main chain (ii) reaction at the ends of the main chain. Depolymerization may further occur by a partial unzipping or by a complete unzipping. Accordingly, in Figure 3. 5. relative degree of polymerization is shown for different degradation mechanisms as a function of fraction of depolymerization which latter is related to the progress of the main chain photodegradation. The relative degree of polymerization is defined as the average degree of polymerization relative to the initial average degree of polymerization [23]. The following basic mechanisms are shown by:

(i) Line A: initial end-group depolymerization followed by complete unzipping
In this case the photo-induced elimination of the end-group of the main chain cause small change in DP of the polymer that is followed by complete unzipping of the chain to small molecules. Thus, the DP of the remaining polymeric material is still high even at high fraction of depolymerization.

(ii) Line B: random initial depolymerization followed by complete unzipping
When the photodissociation of main chain happens in the middle of the chain it effects the DP significantly, thus line B will run below line A.

(iii) Line C: chain-end initiation followed by partial (incomplete) unzipping
Linear decrease of average DP appears when chain-end photodissociation is followed by incomplete unzipping. Linearity can be explained by that DP of the remaining polymeric material is decreased only by the one-by-one elimination of repeating units from the chain end. Thus, for example when 50% of the repeating units depolymerized the average DP of the remaining polymeric material with various molecular weights is half of the initial DP.

(iv) Line D: random initial depolymerization followed by partial (incomplete) unzipping
Compared to line C, line D runs below it because in this case the depolymerization can appear

not only at the chain ends but also in the middle of the chain that cause the DP of the remaining polymeric material decrease non-linear.
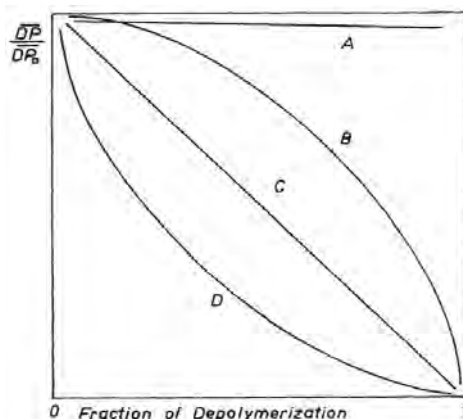
Figure 3. 5. Changing of the relative average degree of polymerization as a function of fraction of depolymerization for different depolymerization (A-D) mechanisms [23]

3. 2. 3. Photooxidative Degradation

In air, photooxidation is often the main photodegrading process due to the presence of oxygen [23]. Photooxidative degradation of polymers includes many simultaneous or consecutive reactions. For the sake of simplicity these reactions can be summarized in a simplified degradation cycle, Figure 3. 6. [6]. The photodegradation process itself can be divided into three basic steps: (i) initiation, (ii) propagation and (iii) termination, Figure 3.7. [23] [6]. As a result of photooxidative processes, several types of groups with different oxidation states might be added onto the polymer chain providing additional functionalities [23] [27]. In the following sub-sections, the most important types of main chain scissions *via* photo-oxidation are described. Random breakage of C-C bonds are described previously in Subchapter 3. 1. 3.

Figure 3. 6. Simplified cycle of photooxidative degradation of polymers [6]

Initiation

$$PH, O_2 \xrightarrow{h\nu} HO_2^{\cdot}, P^{\cdot}, H_2O_2$$

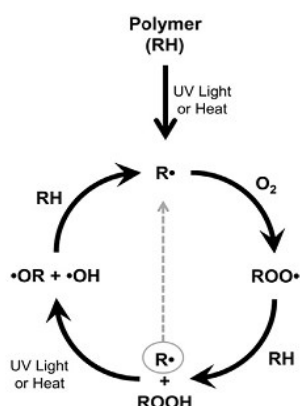$$H_2O_2 \xrightarrow{h\nu} 2\,^{\cdot}OH$$

$$^{\cdot}OH + PH \longrightarrow H_2O + P^{\cdot}$$

Propagation

$$P^{\cdot} + O_2 \longrightarrow PO_2^{\cdot}$$

$$PO_2^{\cdot} + PH \longrightarrow POOH + P^{\cdot}$$

$$HO_2^{\cdot} + PH \longrightarrow HOOH + P^{\cdot}$$

$$PO_2^{\cdot} + PH \xrightarrow{h\nu} P^{\cdot} + HO_2^{\cdot} + P^{\cdot}$$

$$HO_2^{\cdot} + PH \xrightarrow{h\nu} H^{\cdot} + HO_2^{\cdot} + P^{\cdot}$$

$$PO_2^{\cdot} \xrightarrow{h\nu} P^{\cdot} + HO_2^{\cdot}$$

$$PO_2^{\cdot} \xrightarrow{h\nu} -C{\overset{H}{\underset{O}{<}}} + CH_2{=}CH{-} + \,^{\cdot}OH$$

$$(POOH)_s + PH \xrightarrow{h\nu} P{=}O + H_2O + PH$$

$$(POOH)_t \xrightarrow{h\nu} P_1{-}\underset{\underset{O}{\|}}{C}{-}R + CH_2{=}CH{-}P_2 + H_2O$$

$$(POOH)_t + P_1CH_2CH_2P_2 \xrightarrow{h\nu} POH + H_2O + P_1{-}CH{=}CH{-}P_2$$

$$P{=}O \xrightarrow{h\nu} P_1{-}\underset{\underset{O}{\|}}{C}^{\cdot} + \,^{\cdot}CH_2{-}P_2 \quad (\text{Norrish Type I})$$

(...)

Termination

$$PO_2^{\cdot} + PO_2^{\cdot} \longrightarrow P{=}O + P{-}OH + O_2$$

$$PO_2^{\cdot} + HO_2^{\cdot} \longrightarrow \begin{cases} POOH + O_2 \\ P{=}O + H_2O + O_2 \end{cases}$$

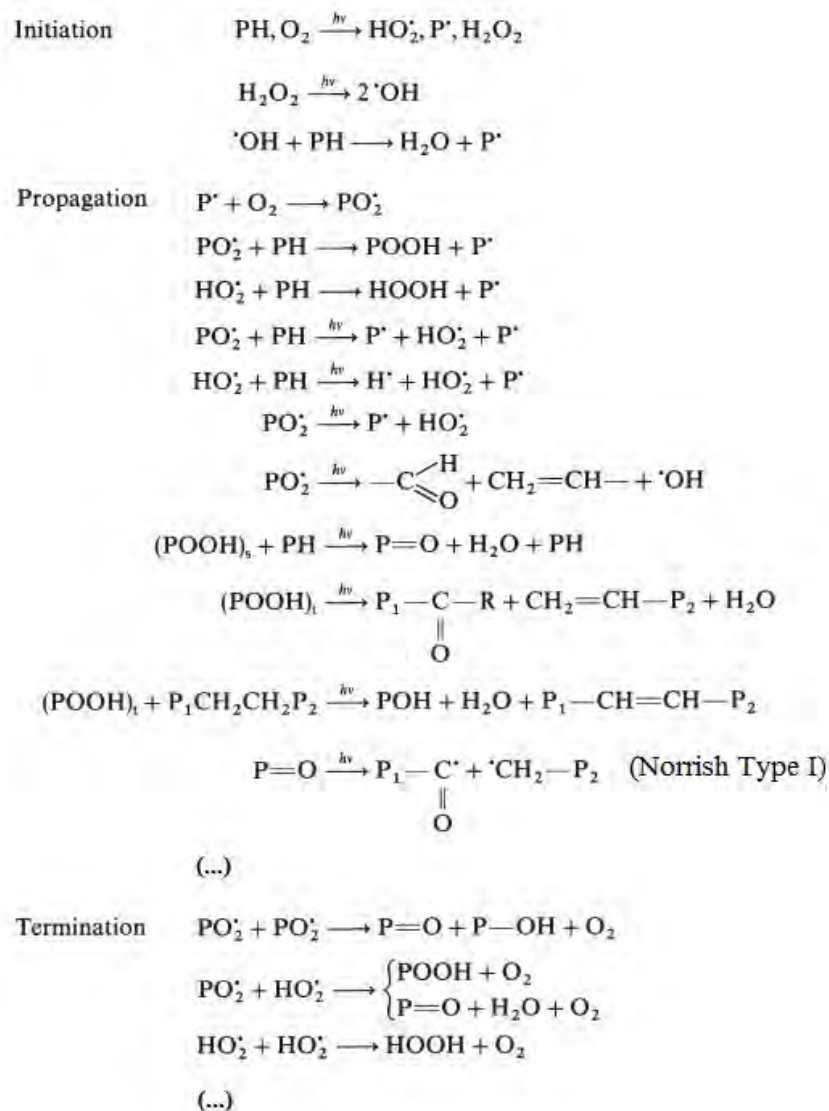$$HO_2^{\cdot} + HO_2^{\cdot} \longrightarrow HOOH + O_2$$

(...)

Figure 3. 7. Photooxidative degradation of polymers [23] [27]

β–Scission

Decomposition of the alkoxy radicals - that formed during photooxidation- by β-scission is the principal mode of chain scission in the photooxidative degradation of almost all polymers, Figure 3.8 [23]. As can be seen in Figure 3. 6., the key propagation reaction is the formation of polymer peroxide radicals (ROO·). These radicals are highly reactive and may abstract an adjacent hydrogen atom thus generating a new chain alkyl radical (R·) and chain hydroperoxide (ROOH) [27]. Due to its instability, hydroperoxide decomposes by photolysis and/or thermolysis into hydoxyl radical (HO·) and chain alkoxy radical (RO·) [27] [6]. This alkoxy radical will then further decompose via β–scission into an alkyl radical and a ketone according to Figure 3.8..
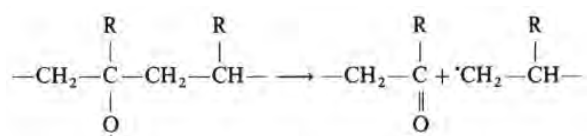
Figure 3.8: β-scission of polymers [23]

The decomposition of hydroperoxide as described above may also result direct chain scission *via* the reaction route in Figure 3. 9. into a ketone, an olefin and water [23].
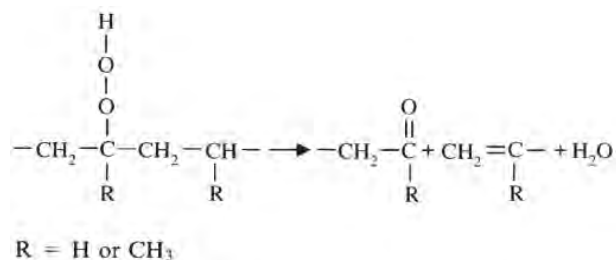

Figure 3. 9. Decomposition of polymer hydroperoxides [23]

Photoreactions of Carbonyl Group

Carbonyl groups which may be present in the pristine polymer or formed from polymer alkoxy radicals can give Norrish Type I and Norrish Type II reactions, eventually leading to chain scissions [23] [27]. Norrish Type I. reaction of the carbonyl group, also called α-cleavage, yields two polymeric radicals and carbon monoxide, Figure 3. 10., [23] [27].
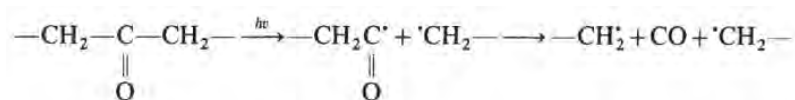

Figure 3. 10. Norrish Type I reaction [23]

Norrish type II reaction is a non-radical, intermolecular process which results in a ketone and an olefin *via* formation of a six-membered cyclic intermediate, Figure 3.11. [23] [27]. Note that for this type of reaction, the oxygen of the carbonyl group must not necessarily be attached to a main chain carbon in order to result in chain scission in contrast to the Norrish Type I reaction.
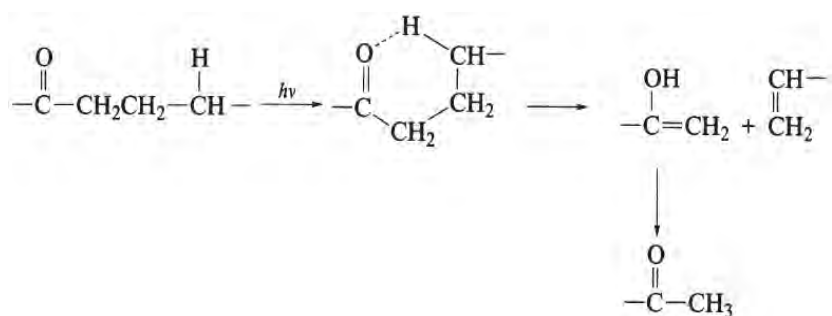

Figure 3. 11. Norrish Type II reaction [23]

3. 3. Specific Photodegradation Mechanisms

3. 3. 1. Commodity Polymers

3. 3. 1. 1. Poly(methyl methacrylate)

Even though photodegradation of poly(methyl methacrylate) (PMMA) has been the subject of extensive studies, several articles are published without specifying precisely the applied wavelength and irradiation dose. This makes it difficult to summarize reaction pathways [3]. The following processes have been proven by different kind of analytical methods such as MS (mass spectrometry), IR (infrared spectroscopy), XPS (X-ray photoelectron spectroscopy), NMR (nuclear magnetic resonance spectroscopy) [3].

Direct photodissociation of main chain and unzipping

Photodissociation of the polymer backbone can be directly induced by UV-photons with $\lambda <$ 320 nm, the number of main chain scission shows maximum at 280 nm (at $3.83 \cdot 10^{19}$ photons/cm^2) [3] [4] [27]. After photolytic scission of the main chain, degradation of the chain can continue by incomplete unzipping, forming free methylmethacrylate monomers, Figure 3. 12.. Maximum zip length in room temperature is about five monomer units per scission [3].
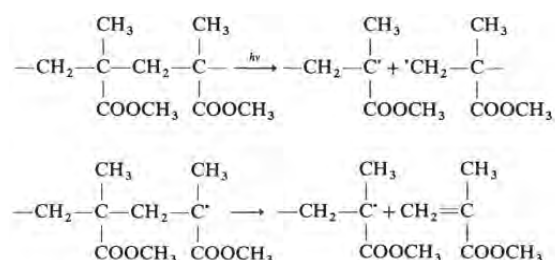

Figure 3. 12. Random main chain scission and depolymerization of PMMA [27]

Photolysis of methyl side chain

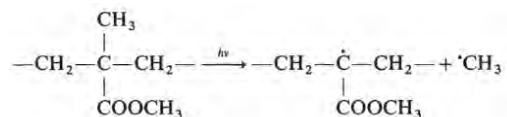Also scission of the methyl side group can be induced by UV-light, Figure 3. 13. [27].

Figure 3.13. Photolysis of methyl side chain of PMMA [27]

Photolysis of ester side chain

Both complete and incomplete ester side chain cleavage of PMMA can occur depending on the irradiation wavelength and dose, see Figure 3. 14. [27] [3]. At a lower UV-irradiation dose (375-5000 pulses of 45 mJ/cm^2= $5.6 \cdot 10^{16}$ photon/cm^2/pulse), at 248 nm, complete side chain separation from the main chain *via* Norrish Type I reaction resulting in a methyl formate radical and formation of a radical electron on the α-C-atom. The generation of the radical electron on the α-C-atom can provoke hydrogen abstraction or main chain scission, both

reactions result in C=C double bond formation [3]. At high irradiation intensity, C=C double bonds can absorb so much UV-light that in the following relaxation processes enough heat is released for photothermal degradation of the polymer that generates small molecules [3]. At low UV-irradiation dose (maximum 400 pulses of 15 mJ/cm^2= 1.6·10^{16} photon/cm^2/pulse) and 193 nm incomplete separation of the side chain occur on the ester bond via Norrish Type I reaction. The main chain is less destabilized due to the absence of the radical electron on the α-C-atom [3]. In addition, side chain photolysis can also occur *via* so-called ester elimination which results in the formation of methyl radicals [27] [5].

Figure 3. 14. Photolysis of ester side chain of PMMA [3] [27]
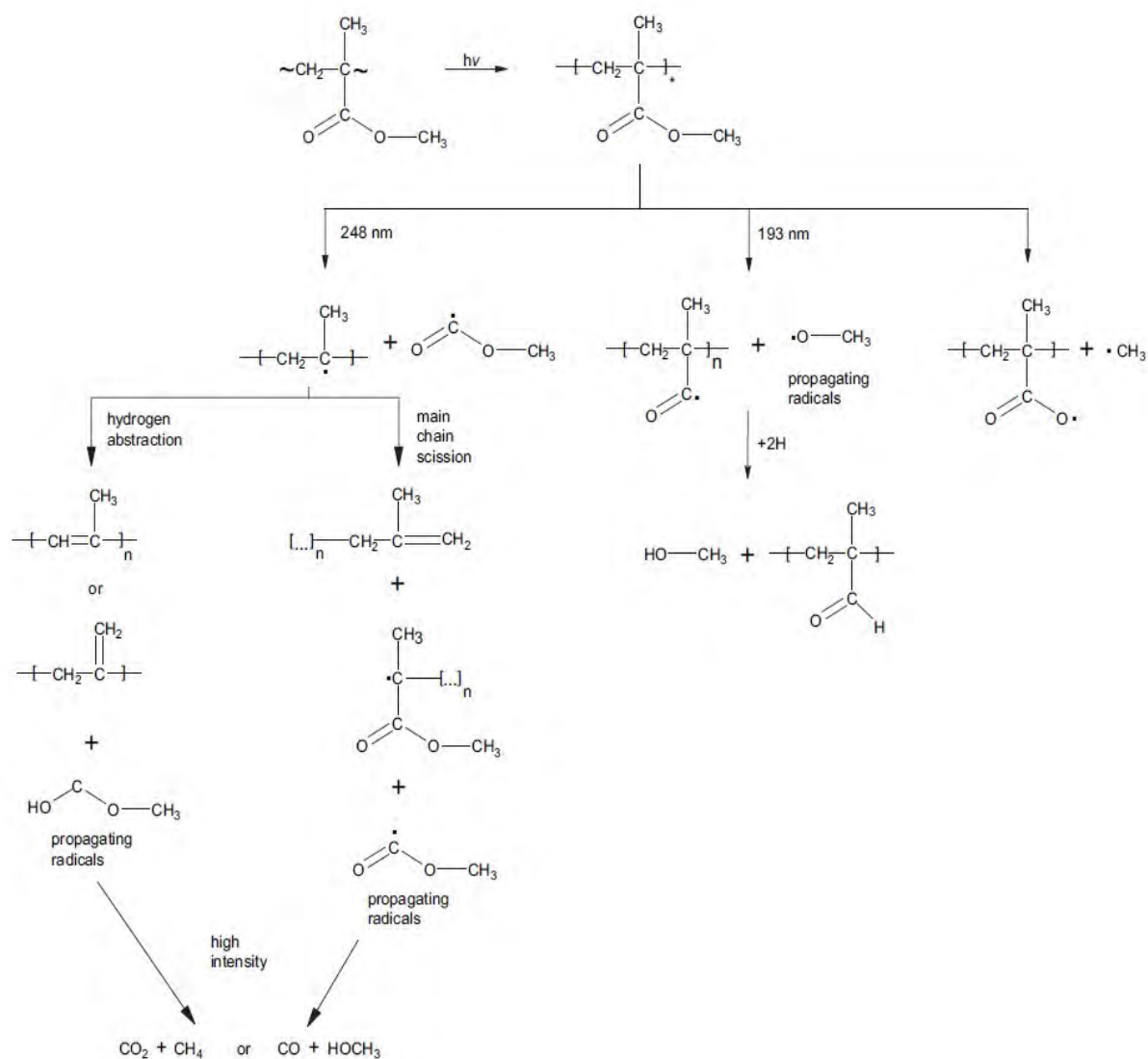
Crosslinking

Even though crosslinking of PMMA under UV-radiation has been discarded as a potential degradation mechanism, recent studies have verified their existence [3]. Yet, the general absence of crosslinking can be explained by the photochemical defragmentation processes prevailing over crosslinking processes and also, main chain can break even after crosslinking

through Norrish Type II reaction [3]. At low irradiation dose (375 pulses of 45 mJ/cm^2= 5.6·10^{16} photon/cm^2/pulse), at 248 nm wavelength, crosslinking between the ester side chains of two adjacent PMMA polymer molecules may occur *via* acid anhydride bond, leading to formation of methyl and methoxy radicals, see Figure 3.15 [3].
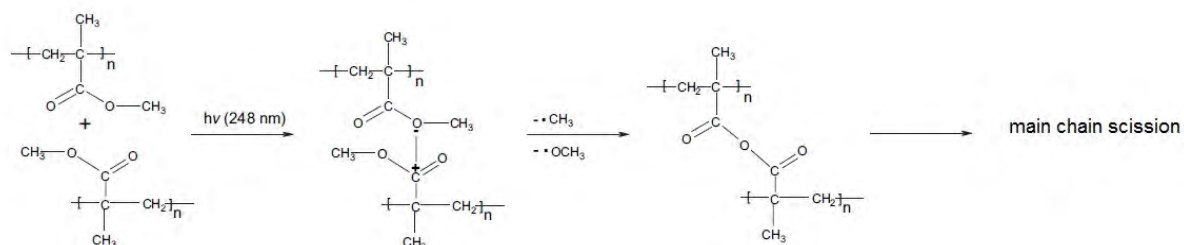
Figure 3. 15. Crosslinking of PMMA chains via acid anhydride group [3]

When PMMA is irradiated with 193 nm UV-light (maximum 5000 pulses of 15 mJ/cm^2= 1.6·10^{16} photon/cm^2/pulse) crosslink is formed by the two methyl groups, see Figure 3. 16. [3].

Figure 3. 16. Crosslinking of PMMA chains via ethyl group [3]

Also, the crosslinking reaction in Figure 3. 17 resulting cyclic ether has been proposed, however, as of yet, not irrefutably confirmed [3].

Figure 3. 17. Proposed cross-linking of PMMA chains via cyclic ether group [3]

As a commodity polymer, photooxidative degradation of polystyrene is intensively studied. Photooxidation of polystyrene in air results in loss of mechanical properties, cracking, yellowing and decrease of the molecular 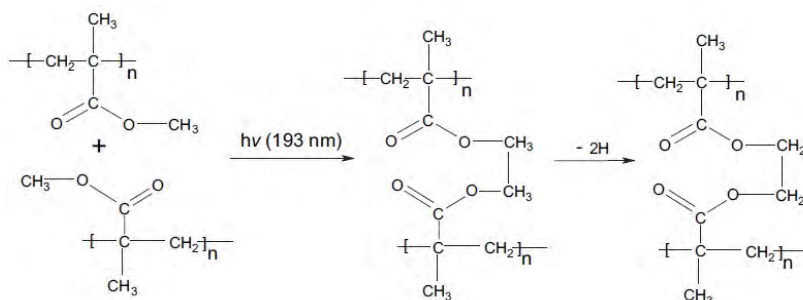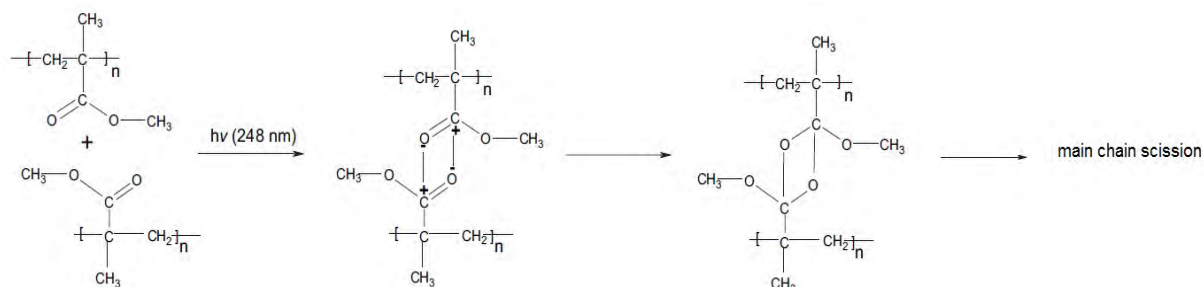weight [6]. Due to the complexity of the process, not all reactions pathways have been entirely explored [27], here only the most important, previously reported ones will be discussed.

As a first step of photodegradation, UV light absorption by the benzene ring occurs, resulting in the excitation of the ring to singlet states that can be transformed by intersystem crossing (ISC) to triplet states, Figure 3. 18. [28]. From triplet state $C_6H_5 - C$ bond or via energy transfer processes $C - H$ or $C - C$ bonds can dissociate.
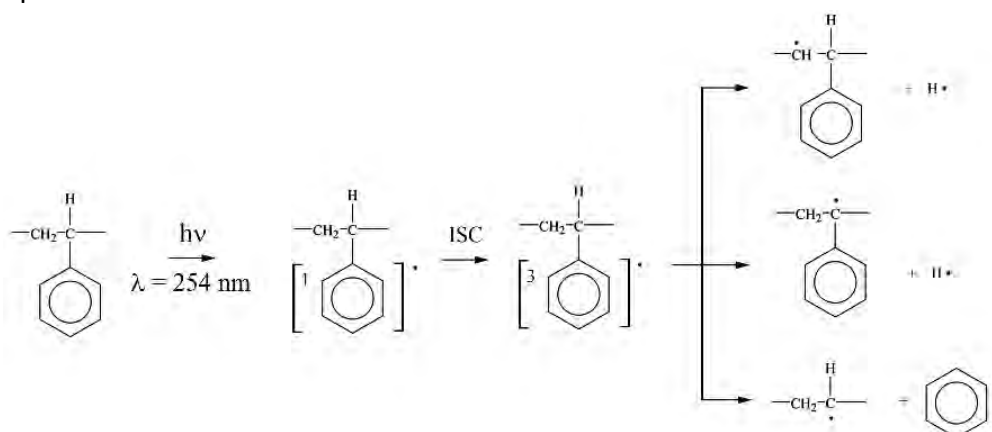
Figure 3. 18. Radical decomposition of PS from triplet state [28]

The polystyrene alkyl radicals can further react. One possible reaction is crosslinking when two macro radicals are near to each other. Furthermore, when oxygen is present, singlet oxygen $^1O_2$ may be formed by energy transfer from excited singlet or triplet state benzene ring to the ground state molecular oxygen $^3O_2$ leading to formation of peroxy radicals [28] [27] [6] [29] Figure 3. 19.. Polymer peroxy radical can abstract hydrogen from surrounding polystyrene chains, resulting in alkoxy polymer radicals that besides giving other reactions, can decompose by beta-scission, Figure 3. 20. [28].

Figure 3. 19. Reactions of PS alkyl radical [28]

Figure 3. 20. Reactions of PS alkoxy radical [28]

When an end group radical is formed unzipping may occur as well, Figure 3. 21. [28]

Figure 3. 21. Unzipping of PS from its end group alkyl radical [28]

3. 3. 2. Depolymerizable Polymers

3. 3. 2. 1. Thermodynamics and Kinetics of Depolymerization

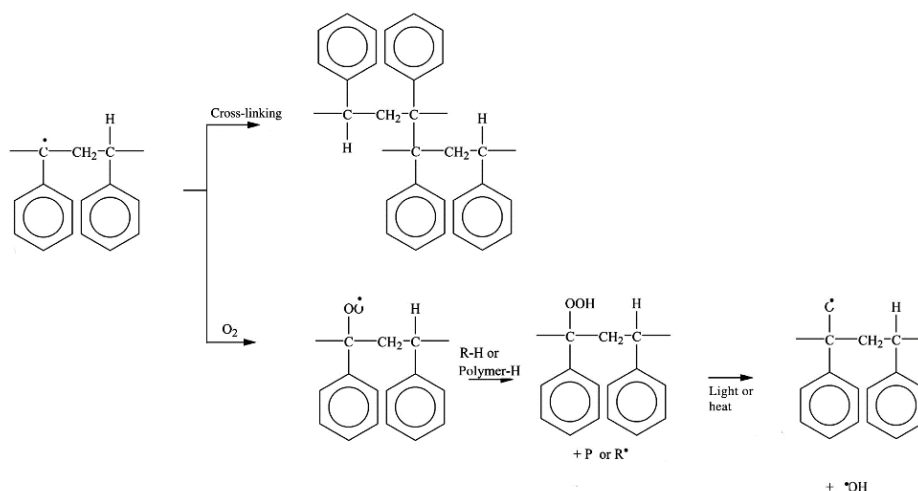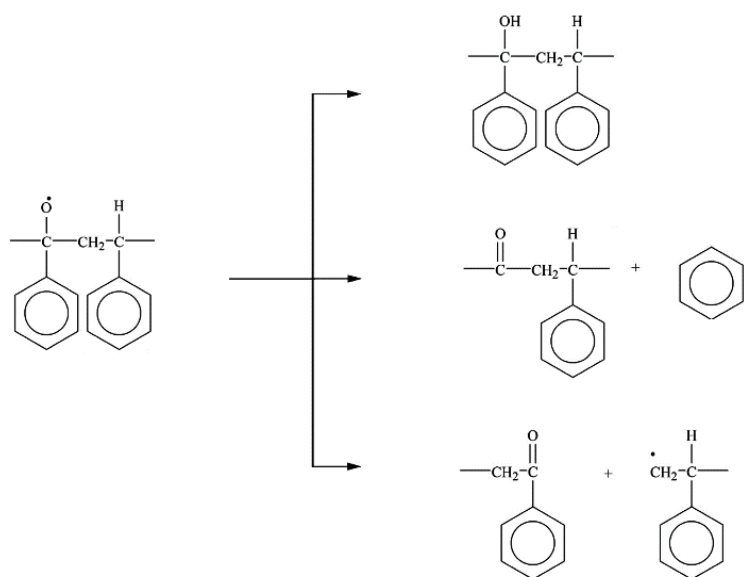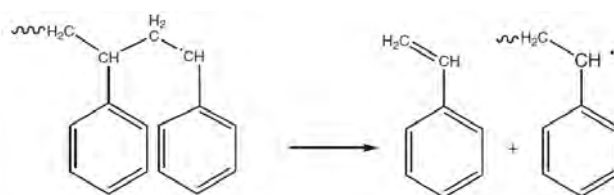Whether or not the reversible polymer propagation or depropagation step can proceed depends on its thermodynamics, in particular on the free enthalpy change of this step [21]. The free enthalpy of the polymerization is determined by the free enthalpy of the monomer and the polymer, eq. 3. 3. [21] [21]. With a few exceptions, polymerization reaction is exothermic and exoentropic ($\Delta H < 0$ and $\Delta S < 0$) [20].

$$M + P_n^* \underset{k_{dp}}{\overset{k_p}{\rightleftharpoons}} P_{n+1}^* \qquad \text{eq. 3. 3.}$$
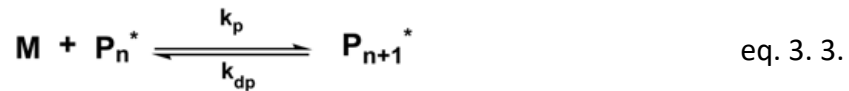
$$G_{polymer} - G_{monomer} = \Delta G = \Delta H - T\Delta S$$
$$= H_{polymer} - H_{monomer} - T(S_{polymer} - S_{monomer}) < 0$$

As the entropy of a polymer is smaller than that of its monomer the slope of the free enthalpy of the polymer vs. temperature is less negative than that of the monomer, Figure 3. 22. [21]. At some temperature, when the free enthalpies of polymer and monomer are equal (the lines cross each other, ($\Delta G=0$)) the rate of propagation is equal to the rate of depropagation. This temperature is called ceiling temperature, T_c [20] [21]. Accordingly, below this temperature polymerization process is thermodynamically favored, whereas above this temperature the polymer is unstable and thus will depolymerize [21].

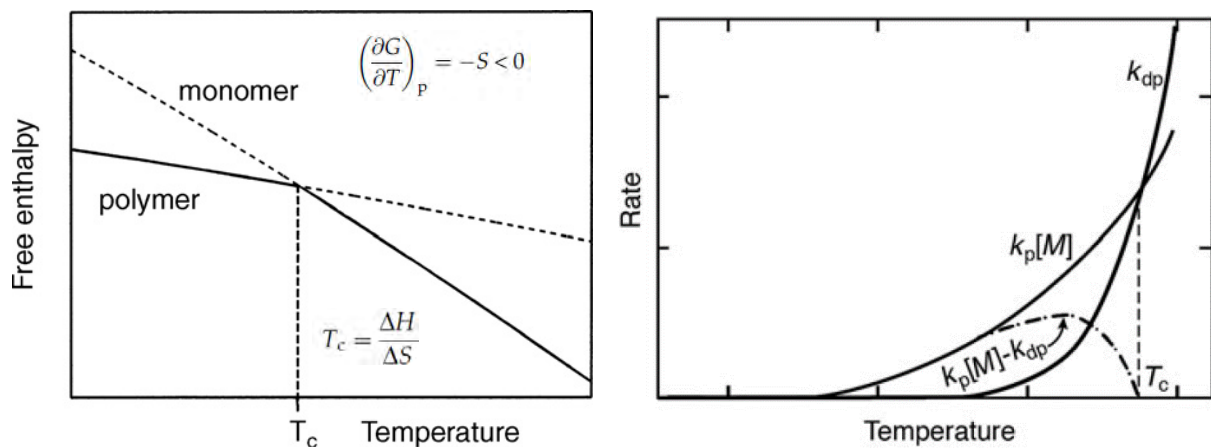**Figure 3. 22.** Free enthalphy in function of temperature for a polymer and its monomer (left) Polymer propagation and depropagation rates as a function of temperature (right)

The actual conversion can be estimated from the equilibrium constant which temperature dependence is described by the van`t Hoff equation, eq. 3. 4.

$$lnK_{eq} = -\frac{\Delta G^0}{RT} - \frac{\Delta H^0}{RT} + \frac{\Delta S^0}{R} \qquad \text{eq. 3. 4.}$$

Besides, considering the Arrhenius equation, it can be seen that the reaction rate grows exponentially with the decrease of activation energy and increase of temperature, eq. 3. 5.. Activation energy can be drastically lowered by use of catalytic compounds reaching increased reaction rate [30]

$$lnk = -\frac{E_{act}}{RT} + lnA$$

eq. 3. 5.

3. 3. 2. 2. Poly(phthalaldehyde)

Poly(phthalaldehyde) (PPhA) is a thermodynamically unstable polymer that decompose rapidly to its monomer via so-called head-to-tail depolymerization reaction on room temperature due to its extremely low, -10 °C ceiling temperature, Figure 3. 23. [30] [31]. Thus, to keep it thermally stable, an end cap group is necessary to prevent unzipping [30]. In special applications, removal of the end cap is designed to be triggered by an external stimulus that subsequently results in the controlled degradation of the polymer [31]. When the polymer is aimed to be photo-responsive, the end cap contains chromophore groups eg. carbonyl and aromatic groups in carboxybenzyl end cap.
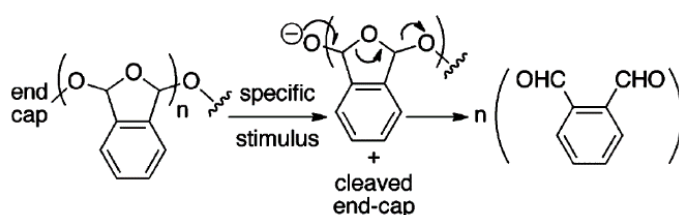
Figure 3. 23. Depolymerization of PPhA [28]

So-called chemical amplification resists containing depolymerizable polymers that were introduced in the 80`s and offered higher sensitivity than PMMA analogs and allowed the use of deep UV light with lower intensity [32]. In case of poly(phthalaldehyde) depolymerization reaction can be catalyzed by protons formed upon UV-light irradiation from compounds called photo acid generators [30]. Poly(phthalaldehyde) can be protonated on both ether groups generating cationic hydroxyl compounds that decompose to the identical cation intermediate, which can unzip itself to phthalaldehyde monomers, Fig. 3. 24. [30] [32]. The overall activation energy for the degradation reaction was calculated to less than 12.8 kcal/mol with and 50 kcal/mol without acid catalysis [30] [33].
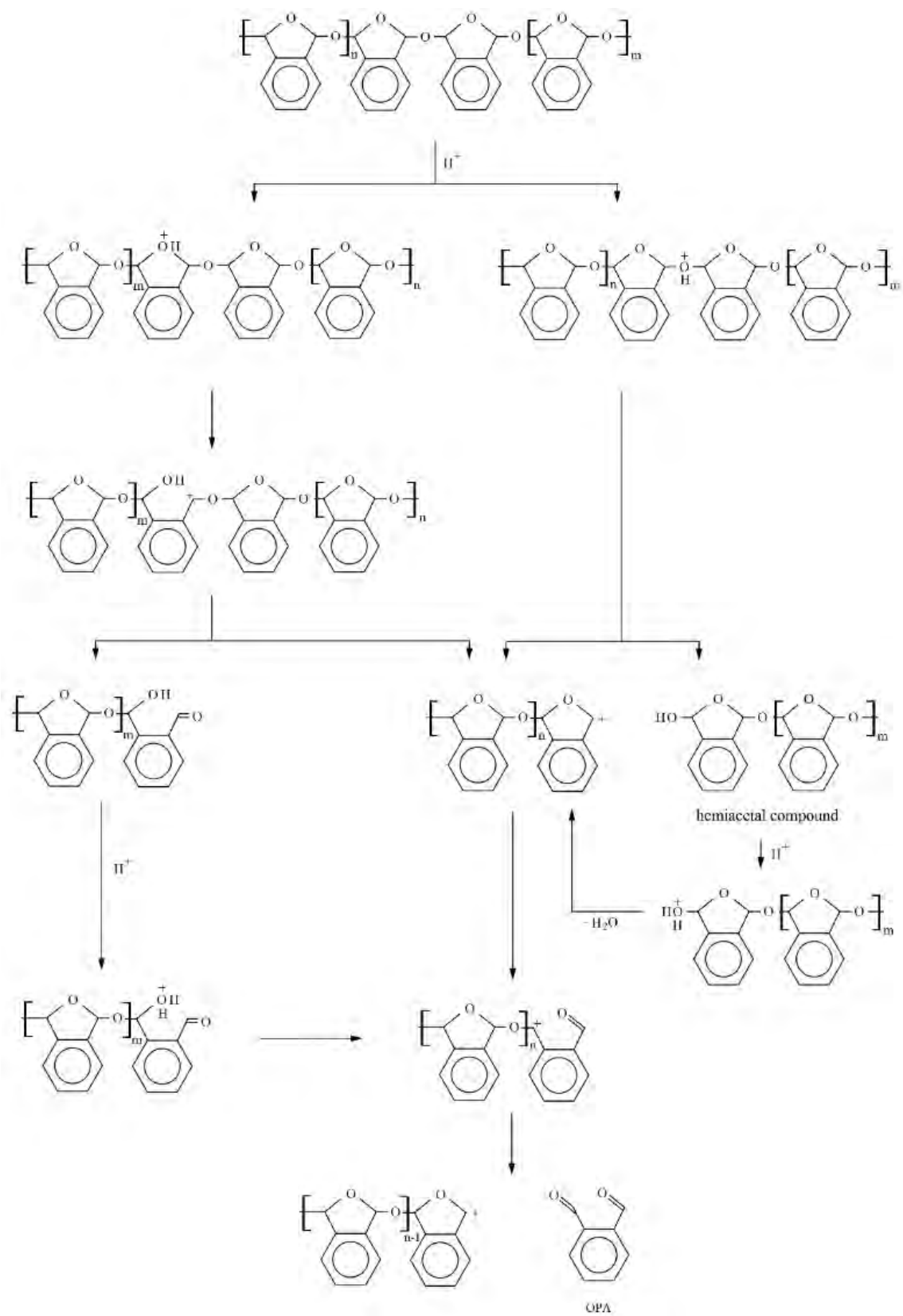
Figure 3. 24. Acid catalyzed depolymerization of PPhA [30]

3. 3. 2. 3. Poly(propylenecarbonate)

Poly(propylene carbonate) (PPC) is intensively studied as sacrificial material that can degrade via thermal decomposition. In air, the decomposition takes place at around 200 °C in two-steps, first scission of the backbone that is followed by unzipping, Figure 3. 25 [34]. Polycarbonates with uncapped end groups and with lower molecular weight have higher tendency for chain unzipping, Figure 3. 26. [34]. By adding photo acid generator to the system, the decomposition temperature can be decreased close to room temperature upon UV-light irradiation because the activation energy of the process is decreased via acid catalyzation [35].
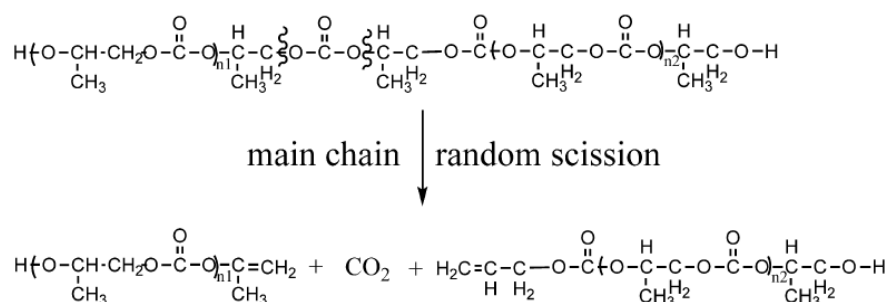
Figure 3. 25. Main chain scission of PPC [34]
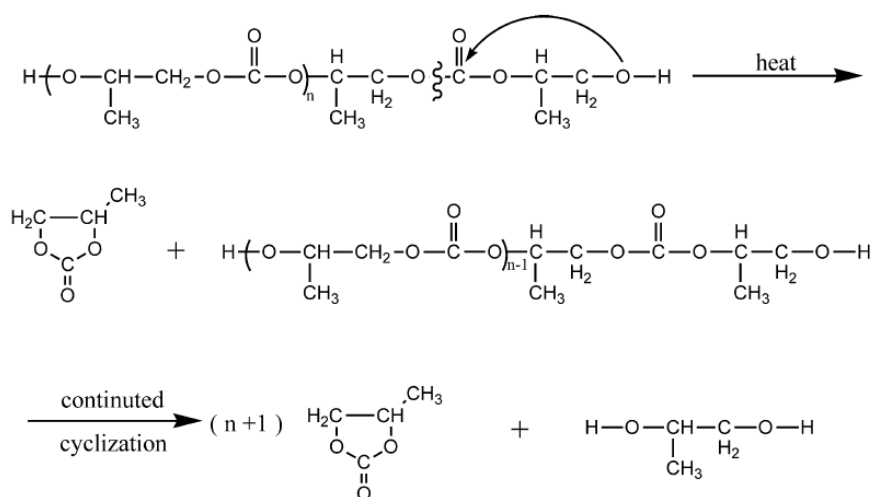
Figure 3. 26. Chain unzipping of PPC [34]

The ceiling temperature of poly(olefin sulfone)s (PSus) lies at or below room temperature, depending on the olefin structure [36] [37]. Since the sulfonyl group is a strong electron-withdrawing moiety, adjacent carbon atoms became electron-poor that results higher acidity of the neighbouring hydrogen, thus protons on that carbon can easily be abstracted by bases. After proton abstraction, chain reaction occurs in which the main-chain of the poly(olefin sulfone) is depolymerized to the olefin monomer and sulfur dioxide, Figure 3. 27. [38]. Thus, the reaction can be catalyzed by bases [38].

Depolymerization chain reaction
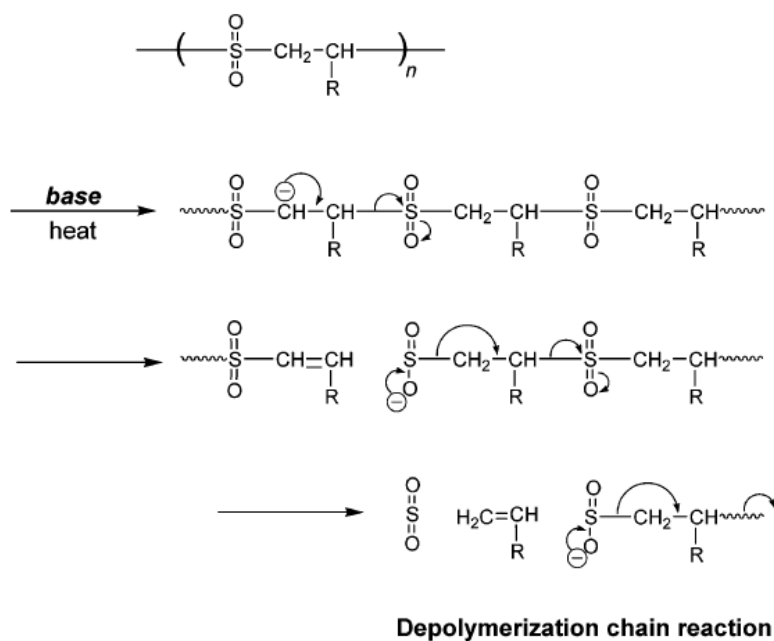
Figure 3. 27. Acid catalized **d**epolymerization of PSu [38]

29

3. 3. 2. 5. Photo acid and base generators

Addition of photo acid and base generators can enhance photodegradation processes of depolymerizable polymers by catalysis [39] [32]. The mechanism of the generation of acidic or alkaline species is generator compound specific . In Figure 3. 28. and 3. 29., acid generation from 2-(4-methoxystyryl)-4,6-bis(trichloromethyl)-1,3,5-triazine (AG1) and bis(4-tert-butylphenyl)iodonium perfluoro-1-butanesulfonate (AG2) are shown, respectively. In AG1 highly reactive Cl· radical is generated that abstracts a hydrogen from the environment to form hydrochloric acid (HCl) upon exposure to UV light (λ_{max} = 379 nm) [40]. In case of AG2 the mechanism is a slightly different multi-step reaction, but similarly involving subtraction of hydrogen [39].
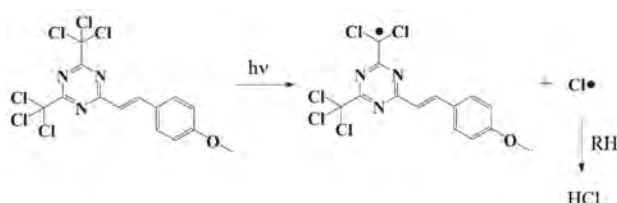
Figure 3. 28. Acid generation from 2-(4-Methoxystyryl)-4,6-bis(trichloromethyl)-1,3,5-triazine (AG1) [40]
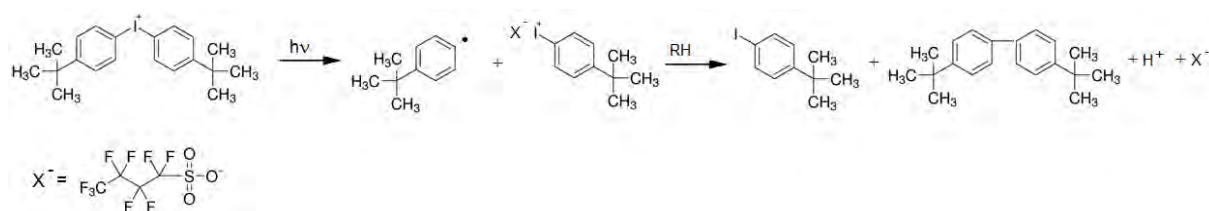
Figure 3. 29. Acid generation from bis(4-tert-butylphenyl)iodonium perfluoro-1-butanesulfonate (AG2) [39]

As an example of photo base generators (PBGs), α-keto carbamates are photo-sensitive in range of 300 nm or longer wavelength light [41]. In general, upon such UV-light irradiation carbamates cleave, release carbon dioxide, and liberate an amine, shown on N-hexylcarbamate compound on Figure 3. 30. [42]. One photon yields one base molecule [42]. Accordingly, diethylamine release from 9-anthrylmethyl N,N-diethylcarbamate (BG) upon UV-light is expected, the chemical structrure of BG is shown on Figure 3. 31. [41].

Figure 3. 30. Base generation from N-hexylcarbamate compound [42]
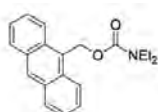
Figure 3. 31. 9-anthrylmethyl N,N-diethylcarbamate

3. 3. 3. Photocrosslinkable Polymer

3. 3. 3. 2. Poly(vinylcinnamate)

Poly(vinylcinnamate) (PVCi) can undergo both *trans-cis* isomerization and cycloaddition under UV-light irradiation. However, isomerization is suppressed in the solid state [43]. Cycloaddition reaction involves formation of truxinic or truxillic dimers that both consist cyclobutane ring, Figure 3. 32. [44]. Thus, crosslinks form between the double bonds on the same or different chains [45]. Inoue et al. showed that photocrosslinking reaction of PVCi results significant size decrease of capsules in which it was used as wall material [45].
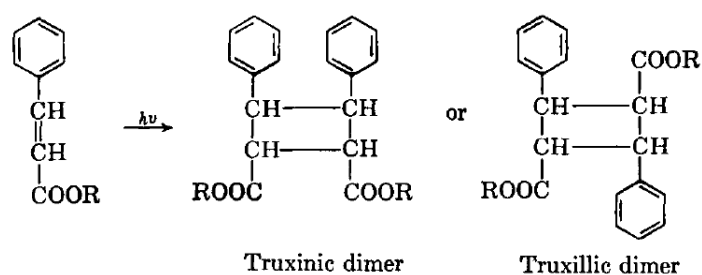
Figure 3. 32. Photocrosslinking of PVCi [44]

3. 4. Characterization Techniques

3. 4. 1. Quartz Crystal Microbalance with Dissipation Monitoring (QCM-D)

Quartz-crystal microbalance with dissipation monitoring (QCM-D) is a surface sensitive technique that is suitable to measure mass of a layer with thickness in nanometer range on quartz crystal (resolution < 10 ng/cm^2). Also, in certain cases, information on homogeneity and rheological properties of this film can be gained [46] [47]. The instrumentation principle of QCM-D relies on the inverse piezoelectric effect. First, when the frequency of the applied voltage on the quartz crystal matches the crystal's resonance frequency (or its multiples of positive integers (n) called overtones (f_n)) a standing wave is generated inside the crystal. AT-cut crystals, widely used in QCM-D devices, vibrate in thickness-shear mode that allows to treat the propagation of the shear wave one-dimensionally, schematically shown on Figure 3. 33. [46]. Then, during ring-down method, the driving voltage is switched off and the decay in time of the oscillation is measured. The obtained decay curve gives two important parameters: the dissipation factor (D) and the resonance frequency (f), Figure 3. 33.. [46] [48].
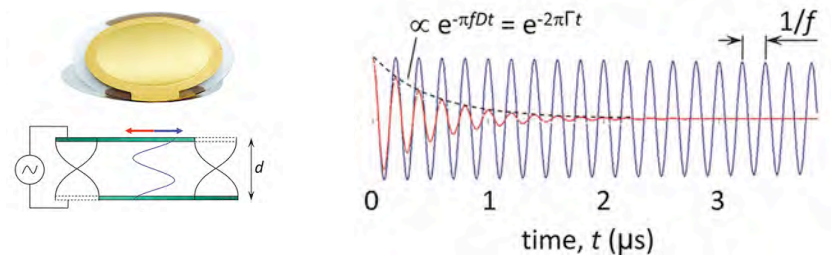
Figure 3. 33. AT-cut quartz crystal (Q-Sense) and its shear vibration (right) and decay curve – amplitude of oscillation in function of time (left) [46] [48].

The dissipation factor measured on the crystal with the film attached onto it is related to the ratio of the energy dissipated by the system during one oscillation (E_d) and the energy stored (E_s), eq. 3. 6. [48] [47]:

$$D = \frac{1}{2\pi} \frac{E_d}{E_s}$$

eq. 3. 6.

Using viscoelastic models describing ideal fluids and solids, it can be noted that larger value of D reflects higher ratio of dissipated and stored energy and the presence of softer layer on the crystal, whereas a smaller D indicates relatively high storage energy and a rigid layer [48] [47]. In practice, this layer is considered rigid solid measured on a 5 MHz crystal when the following critera is fulfilled, where Δ indicates difference between bare crystal and crystal with a studied material layer on it, eq. 3. 7. [46]:

$$\frac{\Delta D_n}{\Delta f_n / n} < 4 \cdot 10^{-7} Hz$$

eq. 3. 7.

In this case Sauerbrey equation, which is valid only on rigid films, can be applied to calculate the mass of the layer, from the resonance frequency which is decreased by added mass on the crystal, eq. 3. 8.:

$$\Delta\Gamma = C\frac{\Delta f_n}{n} \qquad \text{eq. 3. 8.}$$

where $\Delta\Gamma$ is the adsorbed mass per unit area and C=17.7 ng/cm^2/Hz.

3. 4. 2. Infrared Vibrational Spectroscopy

The energy of a molecule is quantized, thus allowed to have certain discrete values called energy levels, Figure 3. 34. [26]. This energy is the sum of contributions from its different modes of motion and electronic contribution, eq. 3. 9.:

$$\epsilon_i = \epsilon_i^T + \epsilon_i^R + \epsilon_i^V + \epsilon_i^E \qquad \text{eq. 3. 9.}$$

where T denotes translation, R rotation, V vibration, and E the electronic contribution. The difference in rotational energy levels is smaller than that of the vibrational energy levels which itself is smaller than that of the electronic energy levels, Figure 3. 34. [26]. The energy that is needed for vibrational excitation can be supplied by absorption of infrared light and the energy of the absorbed light is characteristic to the given molecules vibrational motion [47] [49]. In practice, the infrared absorption spectrum (IR spectrum) is mostly acquired in the 400-4000 cm^{-1} wavenumber range.

At temperatures higher than 0 K, molecules are excited into higher energy states; more energy levels are significantly populated if they are energetically close together and thus comparable with the thermal energy (such as rotational and translational states), than if they are far apart (such as vibrational and electronic states). This leads to two important features of the IR spectrum of a molecule obtained at room temperature: (i) bands will be broadened due to the different rotational states of the vibrationally excited molecules (however it is not the only reason for band broadening) (ii) only vibrational transitions v=0→1 are relevant due to the high population of the ground state [26] [47] [50].
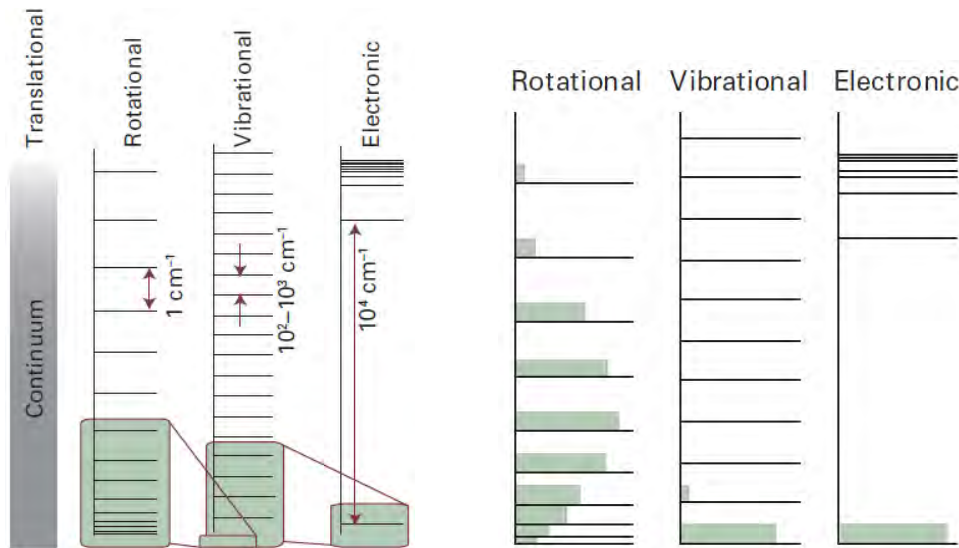
Figure 3. 34. Energy level separations expressed as wavenumbers (left) and Boltzmann distribution of populations for rotation, vibration, and electronic energy levels at room temperature [26]

When vibrational excitation is generated by absorption of electromagnetic wave the resonance condition requires that the frequency of the radiation equals that of the vibration and that the dipole moment of the atoms involved in the vibration changes, eq. 3. 10.. Also, generally polar bonds display high intensity of absorption [47]

$$\frac{\delta\mu}{\delta r} \neq 0 \qquad\qquad \left(\frac{\delta\mu}{\delta r}\right)^2 \propto I \qquad\qquad \text{eq. 3. 10.}$$

The vibrational motion can be modelled with a harmonic oscillator in which atoms are connected by „springs" obeying Hook's law representing bonds, Figure 3 35.. This approach is useful to quantify energy difference of vibrational states close to the ground state and describe modes of vibration [47] [51]. Relevant limitation of the model is the deviation of the potential energy well of a simple harmonic oscillator from the actual potential energy well, that can be described with a harmonic oscillator allowing to show dissociation energy. Moreover, in real systems energy difference between vibrational states are not equivalent unlike in the harmonic oscillator model [51]   [50].
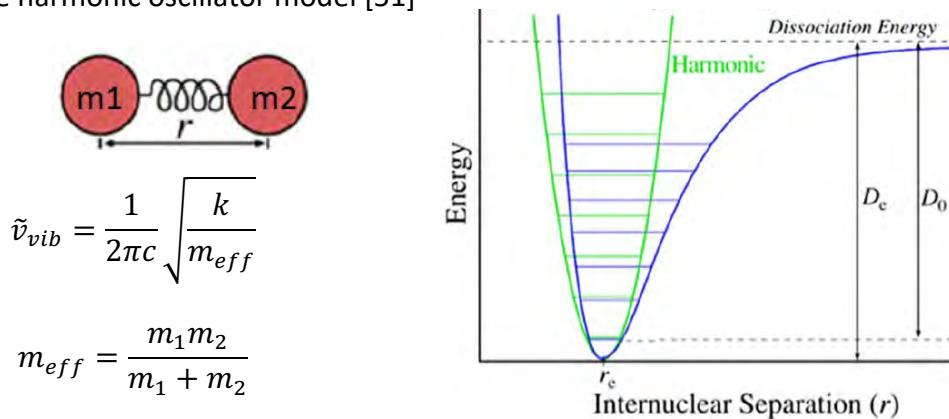
Figure 3. 35. Harmonic oscillator model (left) and the parabolic potential energy as a simple harmonic oscillator and the actual potential energy (right) [50] [47]

Four vibrational modes are distinguised, listed in Table 3. 2. [47]. The number of vibrational modes of a molecule can be determined from the number of atoms that it contains (N). A non linear molecule possesses 2N-6, linear possesses 3N-5, and polymers posess 3N or less vibration modes, in this case N is the number of atoms in the repeating unit. The vibrational energies usually follow the order: $\upsilon > \delta > \gamma > \tau$.

Table 3. 2. Vibrational Modes

Vibrational modes

| Symbol	Name	Mode of deformation
υ	Stretch	Stretching of valence bond
δ	In plane bend	1 or more bond angle changes, constant bond length
γ	Out of plane bend	1 atom oscillates through a plane of at least 3 atos
τ	Torsion	Dihedral angle is changed

3. 4. 3. Nuclear Magnetic Resonance Spectroscopy (NMR)

NMR spectroscopy is a robust, non-invasive spectroscopic technique that utilizes information on magnetic resonance of a nucleus with either odd mass, odd atomic number, or both under an external magnetic field. As magnetic resonance frequency is affected by the electronic environment of the nucleus and the presence of magnetic nuclei in its vicinity, NMR spectroscopic methods are suitable to study molecular structure, dynamics, reaction state, and chemical environment [21] [49].

Atomic nuclei that possess either odd mass, odd atomic number, or both have quantized spin angular momentum and magnetic moment [49]. Correspondingly, the nuclear spin quantum number, I, is a fixed characteristic property of these nuclei and either an integer or a half-integer [26]. From the spin quantum number, the number of allowed spin states can be expressed as 2I+1 with integer differences ranging from +I to −I [49]. In absence of external magnetic field spin states are degenerate and should be almost equally populated. As the nucleus is a moving charged particle, it has a magnetic field and magnetic moment of its own. Thus, under external magnetic field spin states have different energies depending on the alignment of the magnetic moment with the external field; more aligned configuration of magnetic fields results lower energy spin state(s) and vice versa. The energy difference between the states is proportional with the strength of the external magnetic field (B) and magnetogyric ratio (g) characteristic for a given nucleus, schematically represented in Figure 3. 36. [49].

Nuclear spin transition from lower to higher energy can be generated via absorption of irradiated electromagnetic wave with suitable energy. For energy transfer via absorption, the frequency of the oscillating electric field component of the incoming radiation must match the frequency of the electric field generated by the precessing nucleus under the external magnetic field so that the two fields can couple. This condition is called resonance [49]. The

magnitude of energy separation between upper and lower energy level is relatively small; the frequency of the exciting electromagnetic radiation is on the radiofrequency range [49] [26].
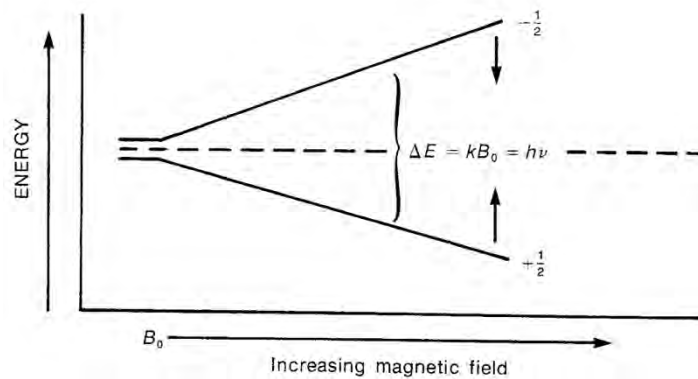
Figure 3. 36. Splitted nuclear spin states proportional with the external magnetic field strength

3. 4. 4. Differential Scanning Calorimetry (DSC)

Differential scanning calorimetry (DSC) is a widely used technique for thermal analysis of materials *via* studying physical or chemical changes in them that are connected with the generation or consumption of heat [26] [47] [52].

Power compensating DSC instrument, that was used also in this study, contains two cells; one for the sample and one for the reference material that does not undergo a physical or chemical change during the measurement, Figure 3. 37. [26]. The instrument measures the required amount of heat that is given or withdrawn to keep the sample and the reference in thermal equilibrium [47]. The recorded DSC thermogram (also called DSC curve) shows the input or output heat flow difference between the sample and the reference in function of the temperature that is scanned in a given range and heating rate, Figure 3. 37. [52].
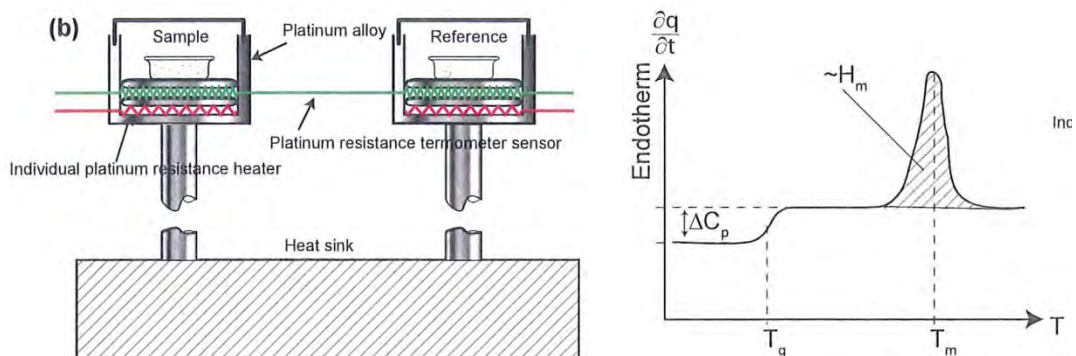
Figure 3. 37. DSC measurement cell (left) and schematic DSC thermogram (left) [47]

DSC is commonly used to investigate first and second order phase transitions as several important parameters can be determined from the DSC curve [52] . On the thermogram,

under isobaric condition, constant-pressure heat capacity (C_p) is related to the slope of the curve based on the following relation, eq. 3. 11. [52] [47]:

$$dq_p = C_p(T)dT$$
<div align="right">eq. 3. 11.</div>

Thus, step on the thermogram shows change in constant-pressure heat capacity (C_p) and indicates second order phase transition, such as glass transitions. In the case of glass transitions, the heat capacity increases because of the increased rotational and translational freedom and the glass temperature T_g can be determined from this step. Also, first-order transitions can be indicated by appearance of peak on the DSC curve [52] [47]. Absolute amount of the heat input or output related to first-order transition can be determined by its peak area and equals to the enthalpy change of the transition under constant pressure and next to negligible surface area change, eq. 3. 12. [52].

<div align="right">eq. 3. 12.</div>

$$\Delta H_p = H(T) - H(T_0)$$

$$\Delta H_p = Q_p = \int_{T_0}^{T} C_p(T)\, dT$$

In practice, signal can be enhanced by increasing heating rate, but it is limited by occurring thermal lag at too high heating rates. To obtain true transition temperatures the thermogram may be extrapolated to zero heating rate, however, for example for T_g determination it is often sufficient to measure at low heating rates (0-10 K/min).

3. 4. 5. Thermogravimetric Analyisis (TGA)

Thermogravimetric analysis (TGA) is an experimental technique in which mass of a sample is measured as a function of sample temperature and time. Depending on the instrument setup, not only heating or cooling rate, but atmosphere can be controlled as well. In this way chemical and physical changes can be studied that are connected with mass change of the sample. The result of the measurement is usually presented on a TGA curve that shows mass or per cent mass plotted against temperature or time. An alternative presentation is to derivate the TGA curve with respect to the temperature or time. This shows the rate of mass change and is known as the differential thermogravimetric or DTG curve [53].

4. Materials and Methods

4. 1. Materials

Materials that were used for experiments are listed in Table 4. 1.. They were used as received and aqueous solutions were prepared with Milli Q water.

4. 2 Preparation of Nano- and Micofilms

Nanofilms were prepared on QCM-D crystals with spin-coating of 0.5 w/w% polymer solution in DCM. First, 50 μl solution was spread quickly then dried during continued spinning. The overall spinning process took 180 s at 2000 rpm.

Microfilms of polymers were prepared by casting their 5 w/w% solution on a 2.2 x 2.2 cm square-shaped glass plate. The complete drying of the microfilm could be reached overnight and in case of PPhA the film was kept under aluminium foil. The estimated thickness of the film was 65 μm.

4. 3. UV light irradiation

The samples were irradiated with an OSRAM HBO 100 W/2 mercury short-arc discharge UV lamp operating at 90 V. According to calibration with Ocean Optic Spectra Suit USB 2000+, the spectrometer accumulated light intensity between 250 and 400 nm was 437 W/m^2, the photon flux was $7.56 \cdot 10^{16}$ #photon/cm^2/s at the hitting spot. The distance between the lamp and the sample was kept constant at 55 cm . The spectrum of the lamp can be seen on Figure 4. 1..
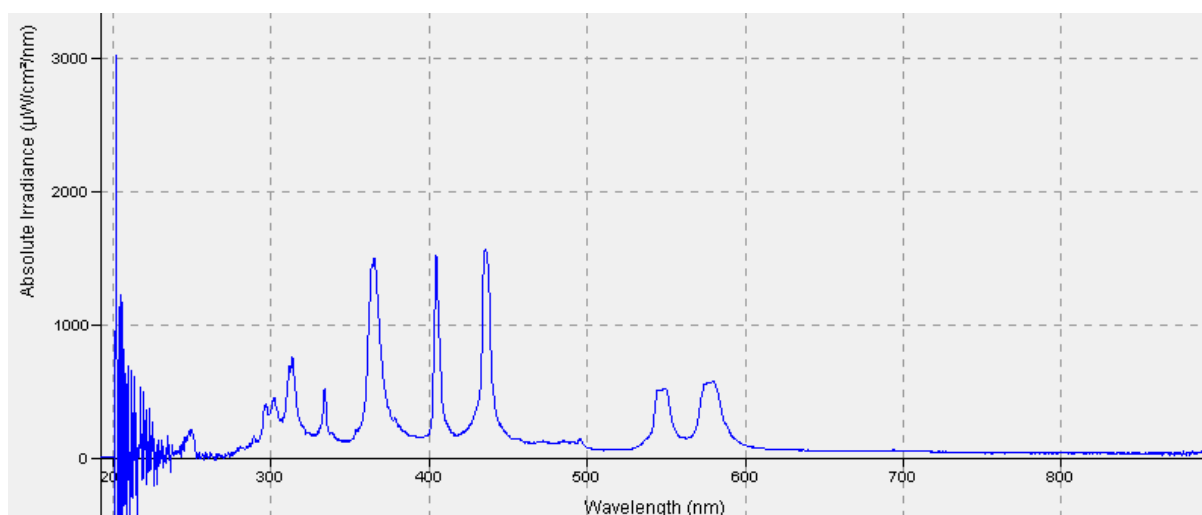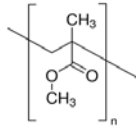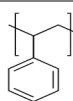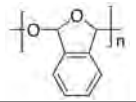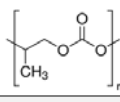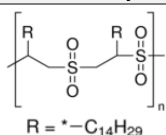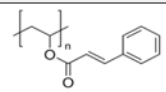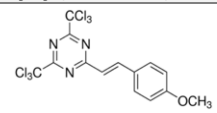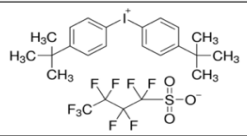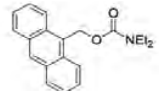
Figure 4. 1. Spectrum of OSRAM HBO 100 W/2 lamp

Table 4. 1. Materials used during experiments

MATERIALS			
Abbrevation	Structural formula	Supplier	Infromation from supplier
Solvent			
Dichloromethane			
DCM	CH_2Cl_2	Sigma Aldrich	ρ:1.325 g/mL at 25 °C, Molecular Weight: 84.93 g/mol, BP.: 39.8-40 °C, MP.:−97 °C, ≤50 ppm water
Polymers			
Poly(methyl methacrylate)			
PMMA (highM)		Sigma Aldrich	MW: 350,000, Tg: 122.0 °C, ρ= 1.17 g/mL (25 °C)
PMMA (lowM)		Polysciences Inc.	MW: ca. 25,000, atactic beads; 200μm polydispersity ~3.0, Tg: 105°C, ρ: 1.20 g/mL
Polystyrene			
PS		Polymer Sources	MW: 5000, Mn: 4000, Tg ~60 °C
Poly(phthalaldehyde)			
PPhA		Sigma Aldrich	Average M_n 5000-8000, DPI<2, linear
Poly(propylenecarbonate)			
PPC		Sigma Aldrich	Mn ~ 50,000, storage temperature: 2 - 8 °C
Poly(1-hexadecene-sulfone)			
PSu		Sigma Aldrich	Mw ~10,000,000, Tm: 50.4 °C , ρ= 0.985 g/mL at 25 °C
Poly(vinylcinnamate)			
PVCi		Sigma Aldrich	average M_n 40,000, powder
Photo acid and base generators			
2-(4-Methoxystyryl)-4,6-bis(trichloromethyl)-1,3,5-triazine			
AG1		Sigma Aldrich	MP: 192-195 °C, λmax 379 nm
Bis(4-tert-butylphenyl)iodonium perfluoro-1-butanesulfonate			
AG2		Sigma Aldrich	MP: 175-177 °C, Molecular Weight: 692.42 g/mol
9-anthrylmethyl N,N-diethylcarbamate			
BG		Wako Pure Chemical Corporation	Molecular weight ＝ 307.39 g/mol, MP: 72～74°C, generates diethylamine by photoirradiation

4. 4. Characterization Procedure

4. 4. 1. Quartz Crystal Microbalance with Dissipation Monitoring (QCM-D)

QCM-D measurements were conducted on a Q-sense QE401-F1257 instrument using 4.95 MHz AT-cut quartz crystal (QuartzPRO), Figure 4. 2.. Each nanofilm was measured three times before spin-coating, after spin-coating, and after UV-light irradiation. The 3rd resonant frequencies and the associating dissipations were averaged. In addition, values of $\Delta D_3/(\Delta f_3/3)$ were calculated for every steps concluding that all films can be considered rigid ($<4 \cdot 10^{-7}$ Hz). Consequently, the Sauerbrey equation could be applied to calculate the weight and from that the thickness of the films.
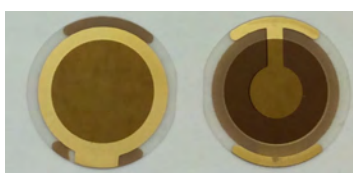
Fig. 4. 2. AT-cut quartz crystal (QuartzPRO)

4. 4. 2. Infrared Vibrational Spectroscopy (IR)

The IR spectra were measured with a PerkinElmer Fourier Transform Infrared (FT-IR) spectrophotometer instrument in both Attenuated Total Reflectance (ATR) and Reflection Absorption Spectroscopy (RAS) mode; in case of ATR mode diamond crystal (GladiATR, Pike Technologies) was used thus the spectrum had to be cut between 2600 and 1900 cm^{-1}. The optical range was 4000 cm^{-1} to 400 cm^{-1} and for all experiments 64 scans were collected and averaged. The recorded data was subjected to baseline correction. The resolution was set to 1 cm^{-1}.

4. 4. 3. Nuclear Magnetic Resonance Spectroscopy (NMR)

^{1}H NMR spectra were recorded on an Agilent 400 MHz spectrometer at 25 °C. Shimming and tuning of the magnet were done automatically. The measurement was carried out in liquid state by preparing a 0.5 w/w% solution of the polymers before and after irradiation of UV-light. Deuterated chloroform was used as solvent. The reference of chemical shifts was tetramethylsilane (TMS).

4. 4. 4. Differencial Scanning calorimetry (DSC)

The glass temperature (Tg) of the polymer microfilms before and after UV light irradiation was determined with differential scanning calorimetry carried out on a DSC 2 Stare power compensating instrument (Mettler Toledo) in sealed 40 microliter aluminium sample holder. The heating and cooling rate was 10 K/min from 25 °C to 150 °C run in two cycles, the Tg was determined from the second heating run.

4. 4. 5. Thermogravimetric Analyisis (TGA)

Thermogravimetric measurement was performed on a TGA/DSC 3+ Stare instrument (Mettler Toledo). During the temperature program the samples were heated up from 25 °C to 550 °C with 10 °/min rate in 100 microliter aluminium sample holder under 60 ml/l nitrogen gas flow.

5. Results

5. 1. Commodity Polymers

5. 1. 1. Poly(methyl methacrylate) (PMMA)

5. 1. 1. 1. PMMA nanofilms

The weight of PMMA nanofilms relative to their initial weight as a function of irradiation time can be seen on Figure 5. 1.. The mass decreases upon UV-light irradiation with a similar degradation rate in case of both high and low molecular weight PMMA. After 5-hour long UV-light irradiation the prior's relative weight reduced to 57.7% while that of the the latter kept 63.2% of its initial weight.
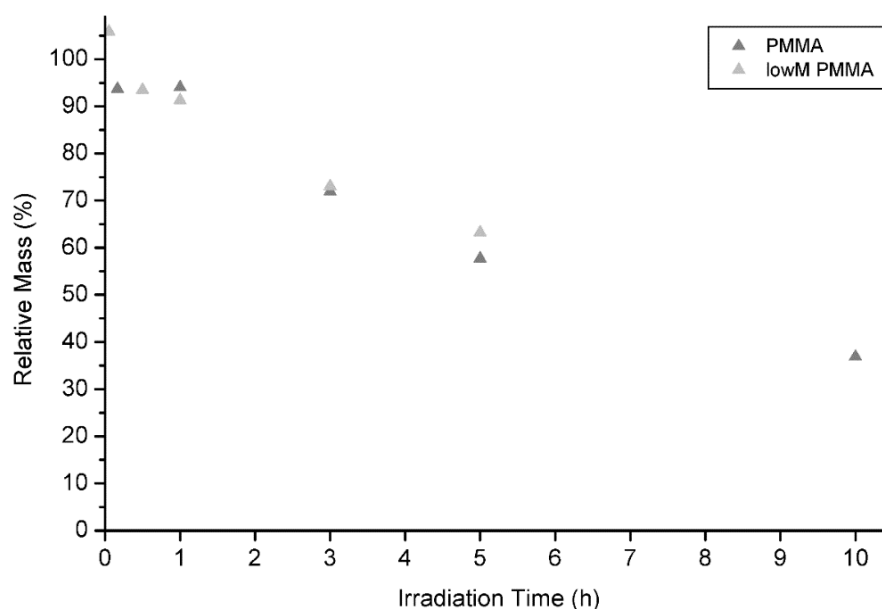
Figure 5. 1. Relative mass of PMMA nanofilms after UV-light irradiation

IR spectra that were taken after given irradiation time periods on both high and low molecular weight PMMA are shown in Figure 5. 2. and Figure 5. 3., respectively. Same characteristic bands appear independent from molecular weight. Methylene group in the main chain of PMMA can be identified by its bending motion that results in a broad band around 1465 cm^{-1} on its IR spectra and the C-H stretch that gives bands around 2950 cm^{-1}. As C-H stretch appears also in methyl groups, the latter band can represent absorption of both methylene and methyl groups. Considering the ester group of PMMA, the strong band of the carbonyl C=O stretch appears at 1740 cm^{-1} and the C-O stretch can be indicated by the bands occurring in the range of 1300-1000 cm^{-1} [49]. Upon UV-light irradiation there is no change in the position of the peaks but they become slightly broader.
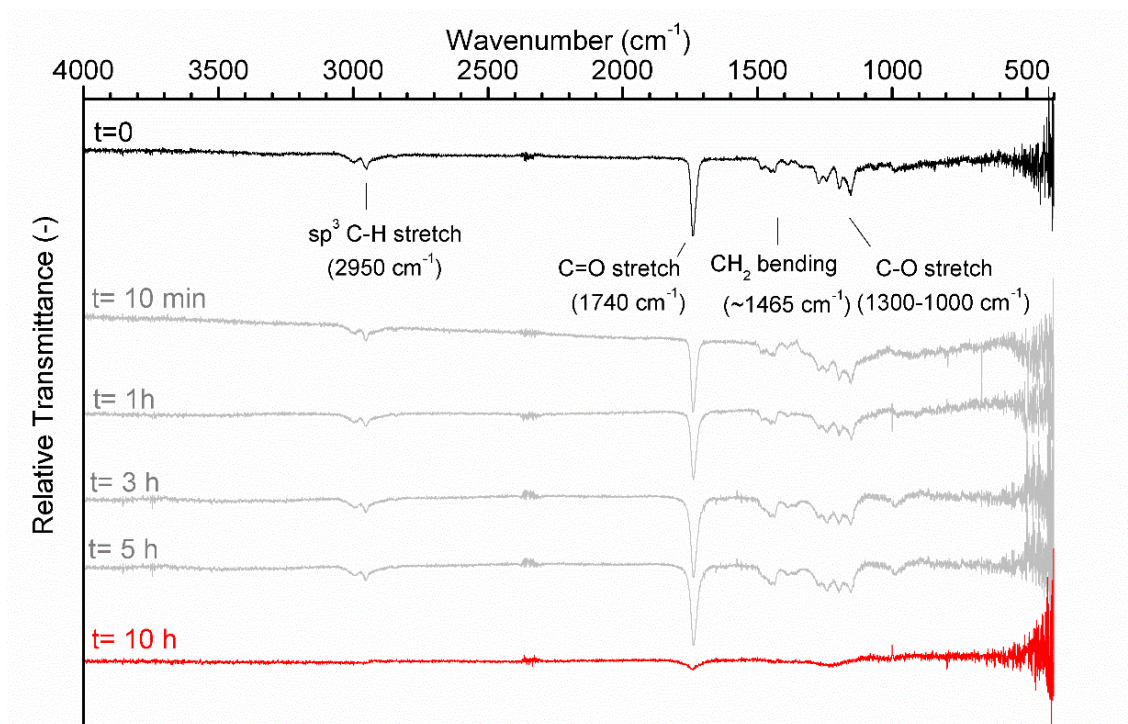
Figure 5. 2. IR-RAS spectra of PMMA (high M) nanofilms after different UV-light irradiation times
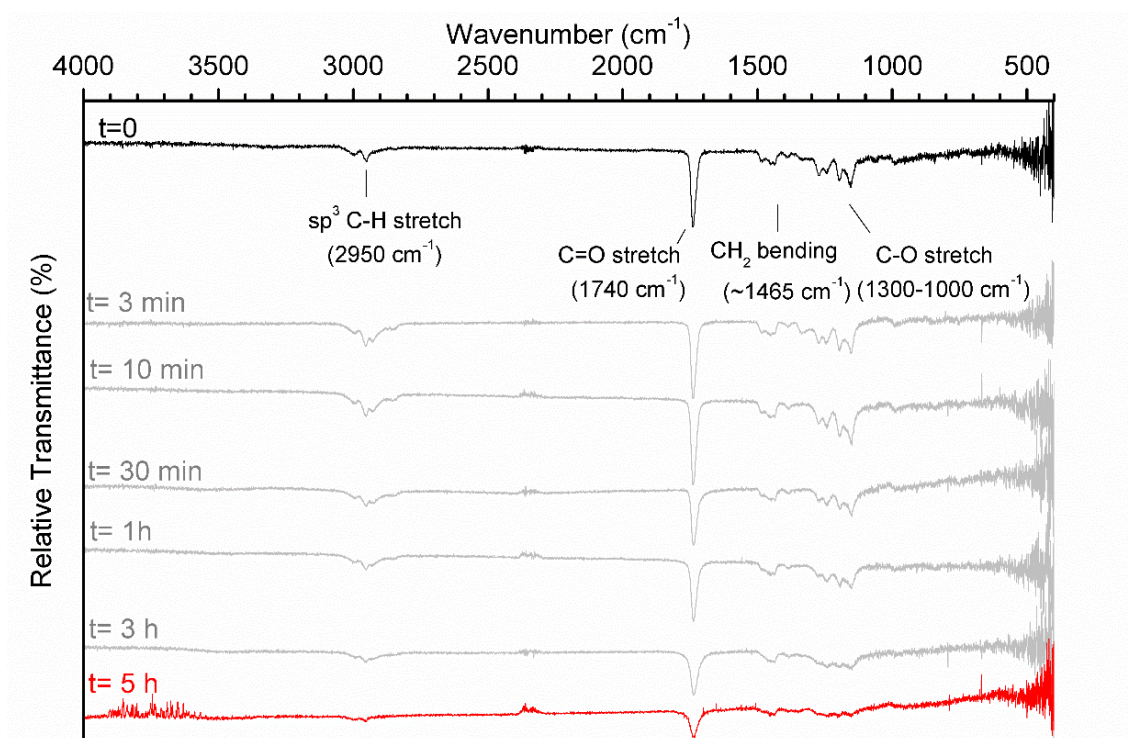
Figure 5. 3. IR-RAS spectra of PMMA (low M) nanofilms after different UV-light irradiation times

Significant differences could be observed visually between the PMMA samples before and after irradiation , Figure 5. 4.. High molecular weight PMMA film contracts more at its surface than in the bulk upon UV light irradiation and remain non-transparent. Contraction can be observed also in case of low molecular weight PMMA that leads to cracking of the material. Moreover, transparent areas of the film become non-transparent.

Weightlosses of microfilms with different molecular weights are similar and much lower than the nanofilms after 5 hours of UV-light irradiation. The relative mass of high molecular weight PMMA microfilm remains relatively high, 95.5%, in comparison to its nanofilm that decreases to 57.7%. In the case of low molecular weight PMMA the weightloss depends on the thickness in similar way, while the relative mass of the microfilm is 95.6%, the nanofilm is 63.2% of its initial weight after the UV-light irradiation.
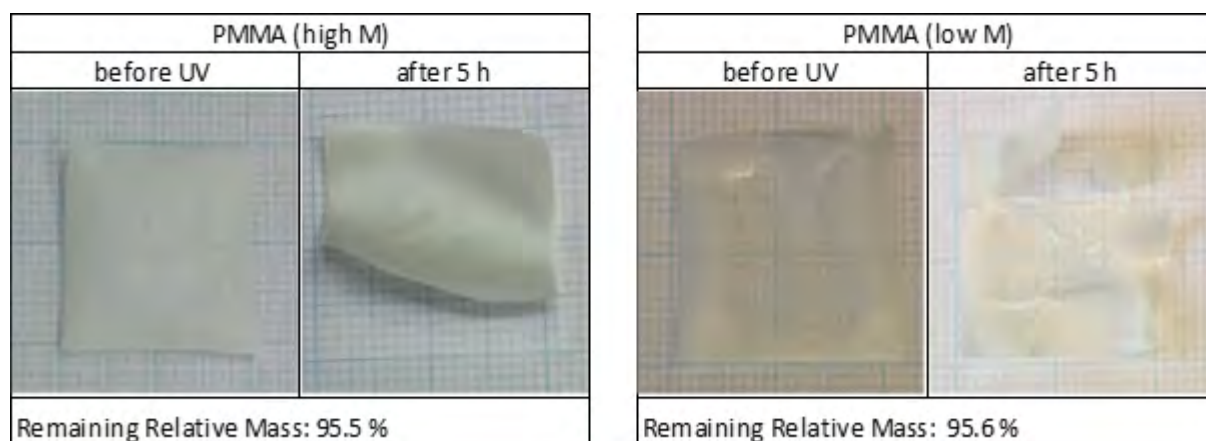
Figure 5. 4. Microfilm of PMMA (high M) (left) and PMMA (low M) (right) before and after 5 h UV-light irradiation and their remaining relative mass

ATR-IR spectra of the PMMA (high M) and PMMA (low M) microfilms are shown on Figure 5. 5. and Figure 5. 6.. Similar to the nanofilms, the IR spectra of the microfilms display the same characteristic bands before and after UV-light irradiation independent of molecular weight. However, beside the characteristic bands of PMMA discussed previously (see page 42) a band corresponding to a C-Cl stretch at 730 cm^{-1} appears that indicates the presence of residual DCM [49]. After 5-hour long UV-light irradiation the position of the peaks do not change, but broaden like in the spectra of corresponding nanofilms.

NMR spectra of high and low molecular weight PMMA microfilms are very similar; the same type of protons can be identified by their peaks appearing at the same chemical shifts, Table 5. 1., Table 5. 2., Figure 5. 7.. The most highly deshielded type of proton is in the chlorinated solvent used for solvent casting; absorption peak of the hydrogen in DCM is present at 5.3 ppm on every spectrum. Besides, all hydrogens in PMMA gave NMR absorption signal. Among them the highest chemical shift at 3.6 ppm belongs to the hydrogen of methyl group which is attached to the carboxyl oxygen, then between 2.2 and 1.6 ppm the methylene group of the main chain gives several peaks. The methyl side-group of PMMA can be identified
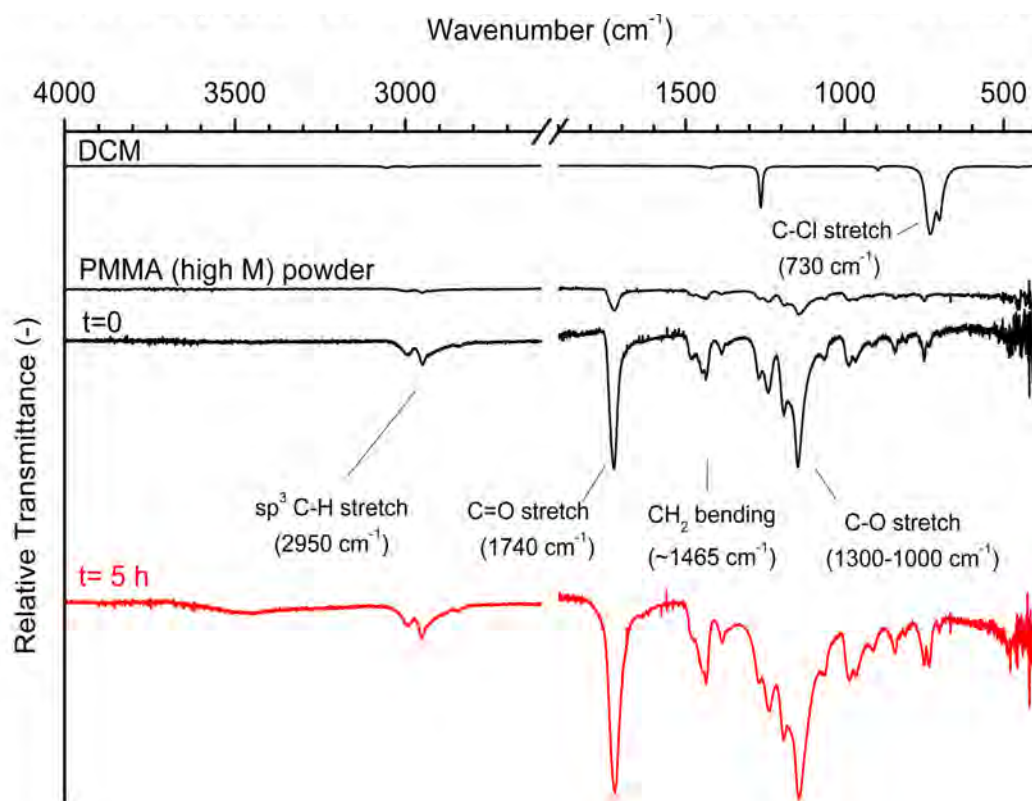
Figure 5. 5. ATR-IR spectra of DCM, PMMA (high M) powder and microfilms before and after 5-hour long UV-light irradiation
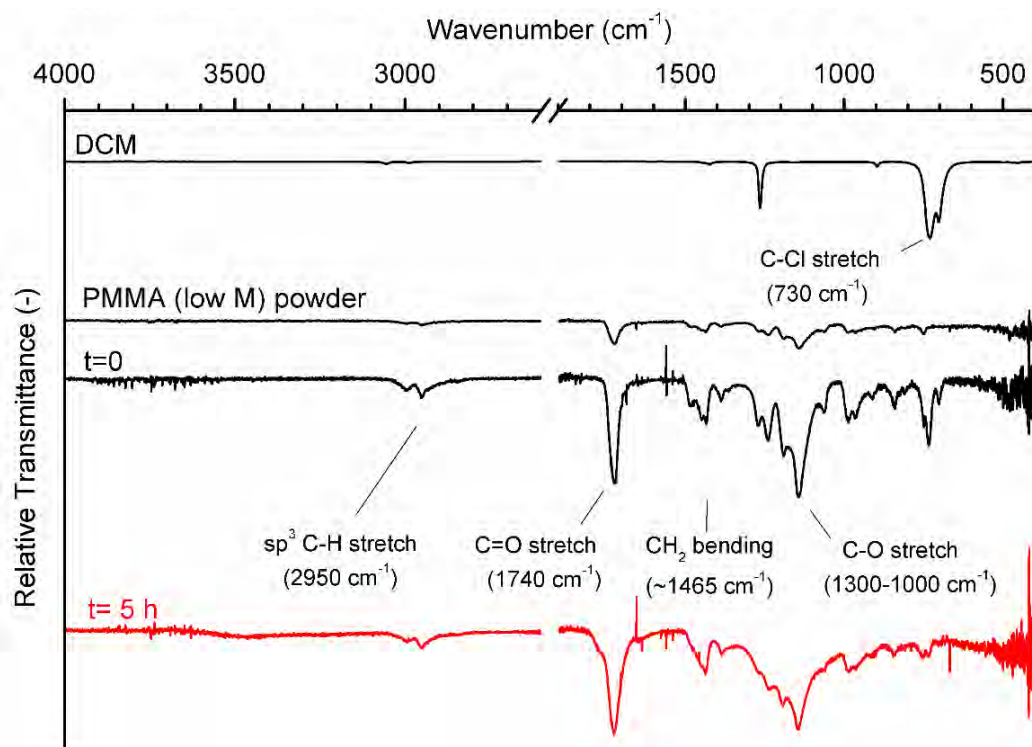
Figure 5. 6. ATR-IR spectra of DCM, PMMA (low M) powder and microfilms before and after 5-hour long UV-light irradiation

by its double peak at 1.0 and 0.8 ppm. Additionally, water was present its peak is at 1.6 ppm. In addition, the monomer of PMMA (methyl methacrylate) could not be detected based on the absence of peak at around 5.0 ppm that would belong to the hydrogens at the carbon-carbon double bond [54]. Furthermore, any new, relevant photoproduct could not be detected either. Correspondingly, the distribution of hydrogen atoms among the components of the microfilms are very similar showing that the microfilms contained the relatively same amount of PMMA before and after UV-light irradiation in case of both high and low molecular weight PMMA.

Table 5. 1. Fractions of different types of H atoms in PMMA (high M) microfilms before and after 5 h UV-light irradiation based on their NMR spectra

PMMA (high M) microlayer before UV			
Type of proton	Range of Integral		Fractions of hyrogen atoms
	ppm		
CH_2Cl_2	5,3	5,3	0,029
OCH_3	3,5	3,7	0,358
CH_2	1,6	2,2	0,275
H_2O	1,5	1,6	0,006
CH_3	1,0	1,1	0,139
	0,7	0,9	0,193

PMMA (high M) microlayer after 5 h UV			
Type of proton	Range of Integral		Fractions of hyrogen atoms
	ppm		
CH_2Cl_2	5,3	5,3	0,019
OCH_3	3,5	3,7	0,377
CH_2	1,6	2,2	0,284
H_2O	1,5	1,6	0,007
CH_3	1,0	1,1	0,137
	0,7	0,9	0,176

Table 5. 2. Fractions of different types of H atoms in PMMA (low M) microfilms before and after 5 h UV-light irradiation based on their NMR spectra

PMMA (low M) microlayer before UV			
Type of proton	Range of Integral		Fractions of hyrogen atoms
	ppm		
CH_2Cl_2	5,3	5,3	0,028
OCH_3	3,5	3,7	0,357
CH_2	1,6	2,2	0,217
H_2O	1,5	1,6	0,058
CH_3	1,0	1,1	0,129
	0,7	0,9	0,211

PMMA (low M) microlayer after 5 h UV			
Type of proton	Range of Integral		Fractions of hyrogen atoms
	ppm		
CH_2Cl_2	5,3	5,3	0,028
OCH_3	3,5	3,7	0,365
CH_2	1,6	2,2	0,278
H_2O	1,5	1,6	0,006
CH_3	1,0	1,1	0,127
	0,7	0,9	0,195
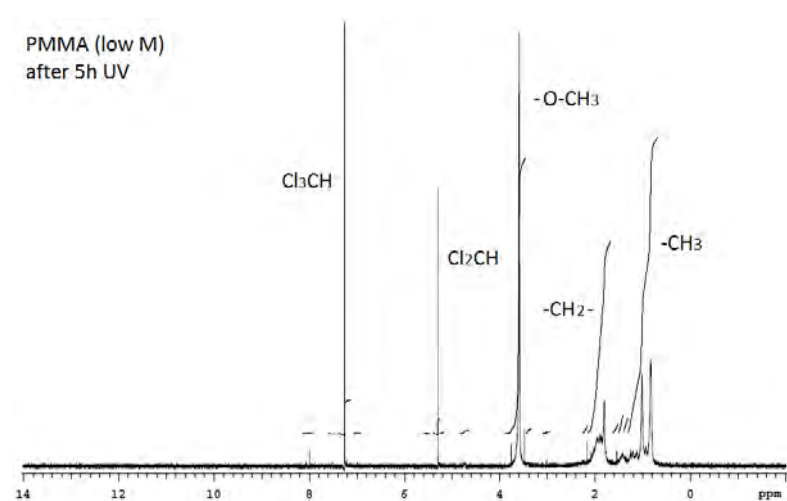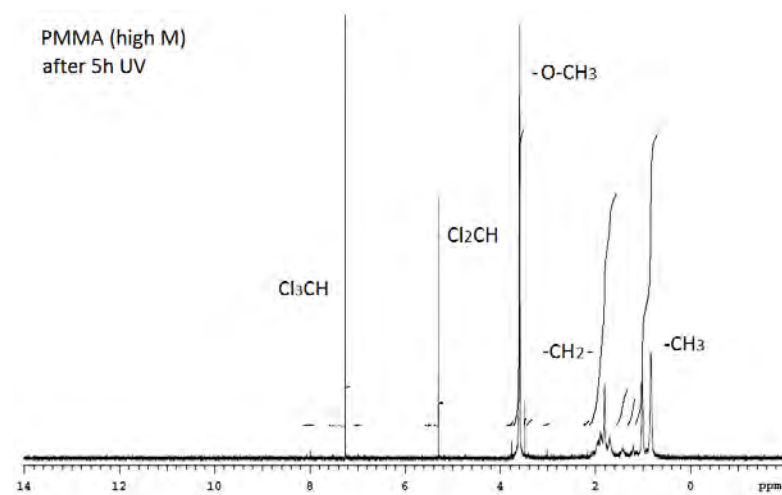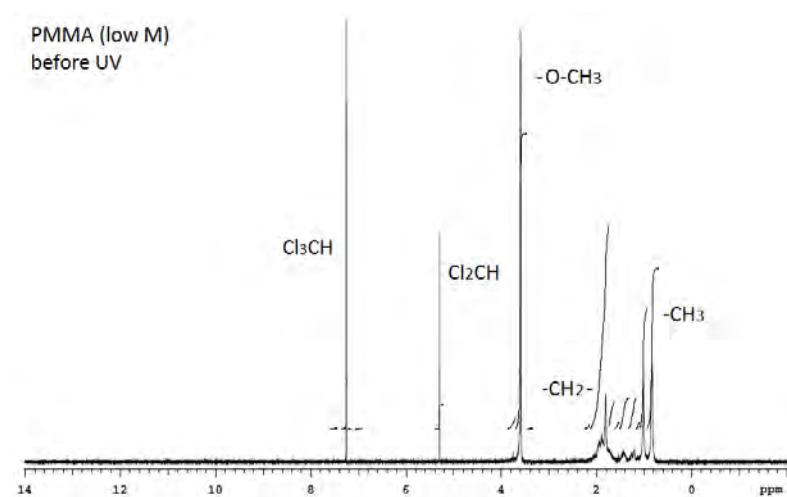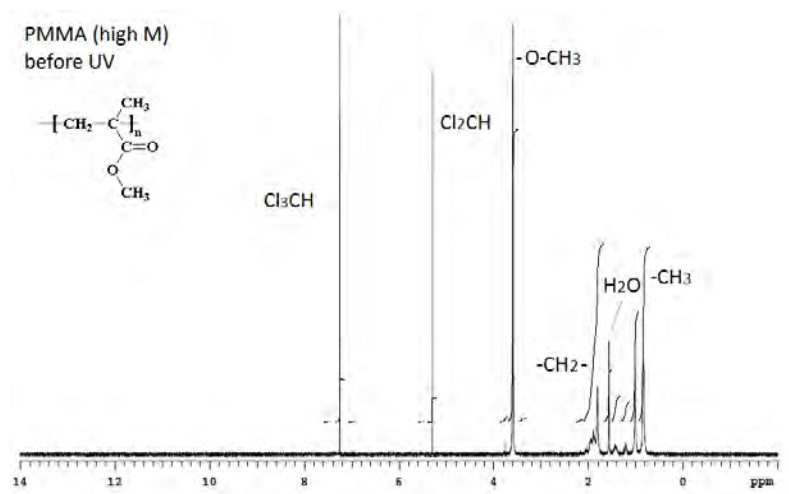
Figure 5. 7. NMR spectra of PMMA microfilms before and after 5h UV-light irradiation

DSC results of high and low molecular weight PMMA can be seen in Figure 5. 8. and 5. 9.. The glass transition temperature of high molecular weight PMMA microfilm does not change drastically after UV-light irradiation, even slight increase can be noted from 103.4 °C to 105.3 °C. The Tg of these microfilms were significantly lower than the 115.2 °C glass temperature of pristine, powder high molecular weight PMMA. In comparison, the glass transition temperature of low molecular weight PMMA decreased drastically after UV-light irradiation, from 114.3 °C to 94.4 °C. Also, the glass transition of the non-irradiated microfilm proceeds at similar temperature than the pristine, powder low molecular weight PMMA with 111.6 °C glass temperature.

Similarities in thermal degradations of PMMA samples with high and low molecular weights after photodegradation are revealed by their Tg and DTG plots, Figure 5. 10.. Also, the absence of peak for evaporation of DCM ($T_{boiling}$= 39.6 °C) shows that not high enough amount of DCM remained in the system after solvent casting that could be detected by TGA.

The first thermal degradation step of PMMA is initiated by radical transfer to the unsaturated chain ends followed by unzipping, typical to PMMA with vinyl termination [55] [56] [57]. Independent of molecular weight, this degradation step started at lower temperature after UV-light irradiation. Also the second degradation step linked to radical scissions of head-to-head linkages started at lower temperature and proceeded in wider temperature range in case of high molecular weight PMMA after irradiation than in the non-irradiated sample and the neat polymer powder [58]. In the DTG curve of low molecular weight PMMA after irradiation, this step could not be clearly detected. Furthermore, for both low and high molecular weight PMMA, the thermal degradation of the PMMA chains by random radical scission at the third step started at lower temperature and the process resulted wider DTG peak of UV-light irradiated samples than non-irradiated ones [57].
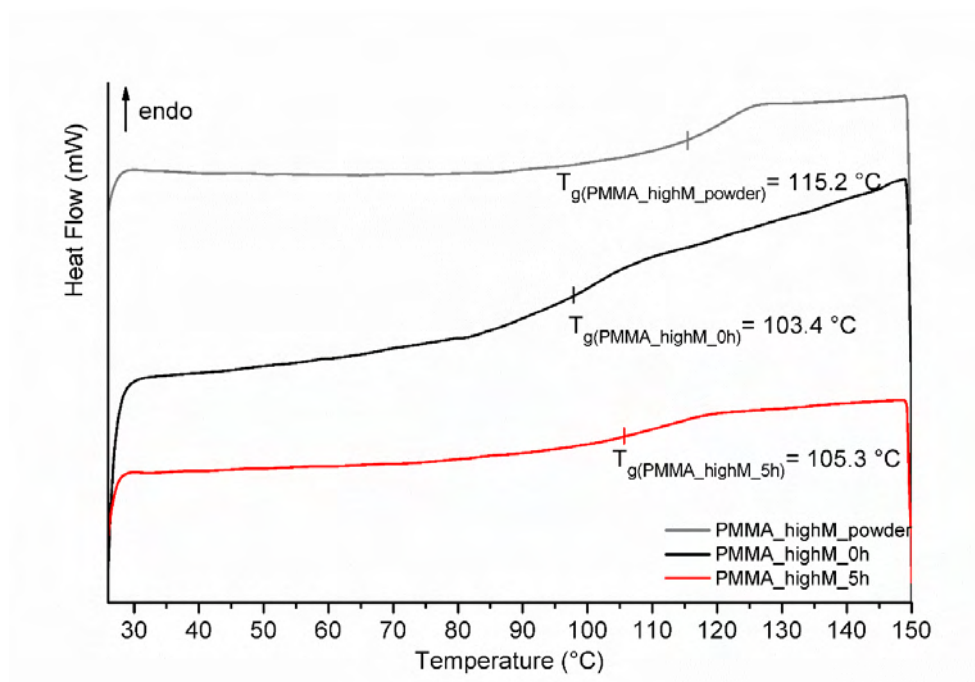
Figure 5. 8. DSC plot of PMMA (high M) microfilm before and after 5h UV-light irradiation
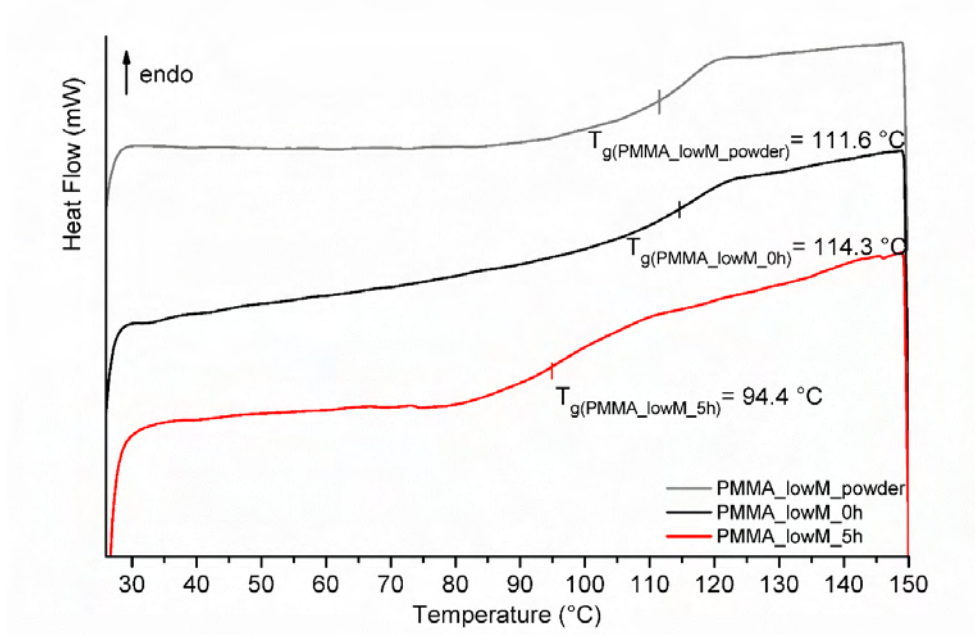
Figure 5. 9. DSC plot of PMMA (low M) microfilm before and after 5h UV-light irradiation

	PMMA (high M)					
	powder		0 h		5h	
	Weight fraction after offset	Peak	Weight fraction after offset	Peak	Weight fraction after offset	Peak
	(-)	(°C)	(-)	(°C)	(-)	(°C)
1st peak	0,97	187	0,87	152	0,89	105
2nd peak	0,9	292	0,79	296	0,83	203
3rd peak	0,00	365	0,00	365	0,01	346

	PMMA (low M)					
	powder		0 h		5h	
	Weight fraction after offset	Peak	Weight fraction after offset	Peak	Weight fraction after offset	Peak
	(-)	(°C)	(-)	(°C)	(-)	(°C)
1st peak	-	-	0,90	123	0,91	106
2nd peak	0,95	292	0,85	292	-	-
3rd peak	0,00	383	0,01	383	0,00	358

Figure 5. 10. TG and DTG plots of PMMA (high M) and PMMA (low M) microfilms before and after 5h l UV-light irradiation

5. 1. 2. Poly(styrene)

The weight of the PS nanofilms relative to their initial weight can be seen on Figure 5. 11.. However, significant weight loss in the first hour of UV-light irradiation could not be observed, later the mass decreases rapidly, even at a higher rate than the PMMA.
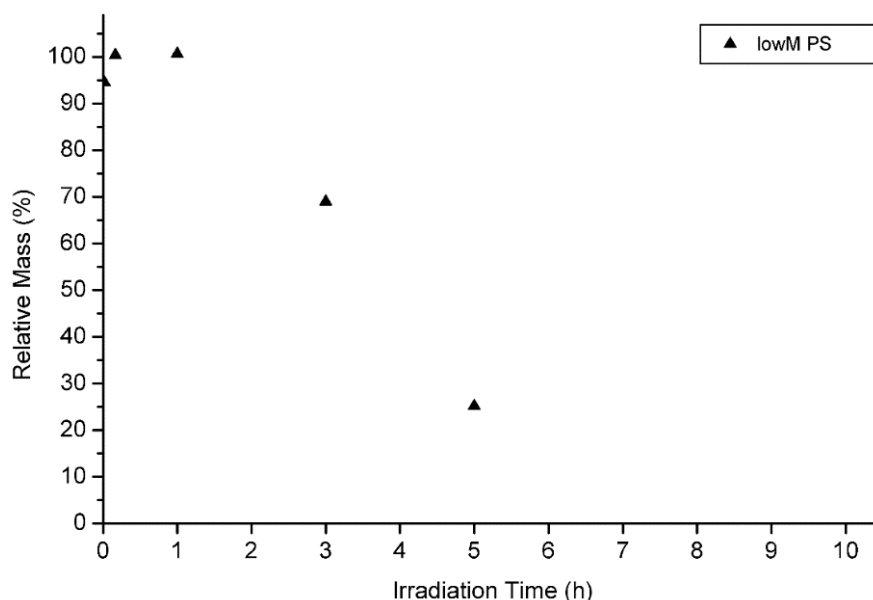
Figure 5. 11. Relative mass of PS nanofilm in function of UV-light irradiation time

IR spectra of non-irradiated and irradiated PS nanofilms are shown on Figure 5. 12.. Polystyrene gives several characteristic IR absorption peaks that could be detected even after 1-hour long UV-light irradiation. Its olefin main chain can be identified by the so-called long chain band at 720 cm^{-1} which is related to the bending (rocking) motion associated with four or more CH_2 groups in an open chain. Also, sp^3 C-H stretch occurs at 2950 cm^{-1}. Beside the main chain, also the aromatic ring of the PS can be identified by several peaks of the spectra. Ring stretch absorptions occur in pair at 1490 and 1440 cm^{-1}. Furthermore, out-of-plane (oop) bending of aromatic =C-H generally can be used to assign substitution on the ring, but in this case only one peak appears at 750 cm^{-1} and the other peak that is supposed to be at around 690 cm^{-1} for monosubstitution is not noticeable due to the high noise/signal ratio. Also, the sp^2 C-H stretch in the ring has IR absorption at 3020 cm^{-1} [49]. After 1-hour long UV-light irradiation the only change in the spectrum is the appearance of a relatively small carbonyl peak at 1750 cm^{-1}, but the characteristic peaks of PS are still present. Then after a longer, 5-hour UV-light irradiation, IR spectra shows drastic chemical change in the nanofilm. The characteristic peaks of PS disappear regarding the vibrational modes of both the main chain and the aromatic ring. Instead, there are broad carbonyl bands at 1750 cm^{-1} and broad bands between 1500 and 1300 cm^{-1} that might be given by many kinds of photodegradation products.
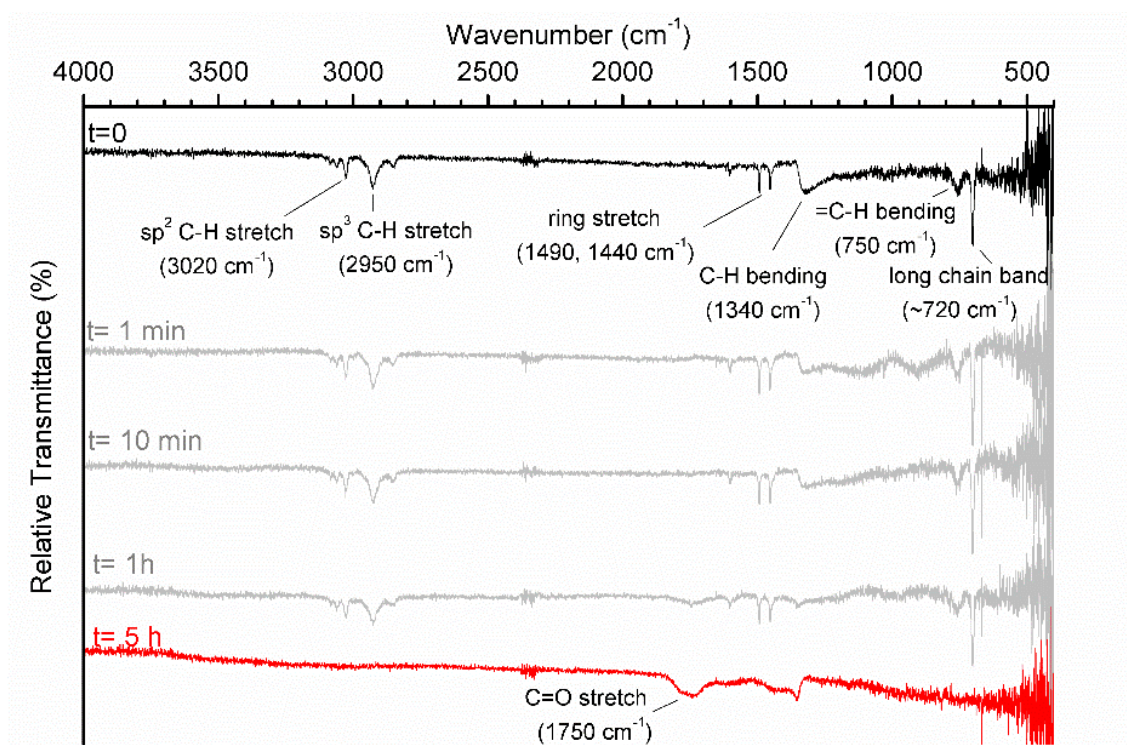
Figure 5. 12. IR-RAS spectra of PS nanofilms after different UV-light irradiation times

5. 2. Depolymerizable Polymers

5. 2. 1. Photo acid and base generators

Significant relative weight losses of the pure photo acid generators nanofilms could be indicated after UV-light irradiation, Table 5. 3... While AG1 nanofilm kept 74.1% of its initial weight after 1h irradiation, AG2 had higher weight loss and its mass decreased to 50.4%.

Table 5. 3. Relative mass of photo acid generator nanofilms after 1 h UV-light irradiation

	Irradiation Time	Relative Mass
	min	%
AG1 (PAGM)	60	74.1
AG2 (PAGI)	60	50.4

IR-RAS spectra of AG1 before and after UV-light irradiation are shown on Figure 5. 13.. The non-irradiated nanofilm shows multiple sharp IR absorption peaks. Among them there are many distinguishable characteristic peaks that confirm the presence of the functional groups of AG1. Trichloromethyl can be identified by C-Cl stretch that appears at 770 cm^{-1} and triazine ring by its characteristic peak at 1540 cm^{-1}. Also, aromatic group can be indicated by its ring stretch that results a peak pair at 1612 and 1475 cm^{-1} and out-of-plane (oop) bending of =C-H at 830 cm^{-1}, however the latest also present in the non-aromatic double bond. Aryl alkyl ethers give rise to two peaks that related to asymmetric C-O-C stretch, one at 1250 cm^{-1} that appears also on the spectrum of AG1 and one at 1040cm^{-1} which is not distinguishable in this case [49]. After UV-light irradiation, the spectrum of AG1 changes drastically. The peaks become so wide that cannot be resolved, however the presence of hydroxyl group can be assumed by the peak at 3200 cm^{-1} and carbonyl group by the peak at 1760 cm^{-1}. Also, the peak of C-Cl stretch disappear.

IR-RAS spectra of AG2 before and after UV-light irradiation are shown on Figure 5. 14.. In general, it is difficult to collect infrared spectral data for halogen-containing compounds because the C-X absorption occurs at very low frequencies [49]. This can be noticed also on the spectra of non-irradiated AG2; C-I stretch supposed to result peak at 600-485 cm^{-1}, but it cannot be indicated due to the high noise/signal ratio [49]. However, C-F stretch – as AG2 is a polyfluoroalkane- can be identified by the multiple strong band appearing in range of 1350-1100 cm^{-1} [59]. Besides, the sulfonate group of AG2 have two characteristic peaks at 1140 and 1060 cm^{-1} and also the tertbutyl group can be indicated by its C-H stretch at 2950 cm^{-1} and CH$_3$ bending at 1395 cm^{-1} [49]. In addition, the absorption peak at 1475 cm^{-1} can supposedly correspond to aromatic ring stretch. On the IR spectra of the UV-light irradiated AG2 the characteristic peaks of its cation (bis(4-tert-butylphenyl)iodonium) disappear; C-H stretch, aromatic ring stretch, and CH3 bending can not be indicated anymore. In contrast, the functional groups of its anion (perfluoro-1-butanesulfonate) still give distinguishable peaks, both polyfluoroalkane and sulfonate groups present even after irradiation.
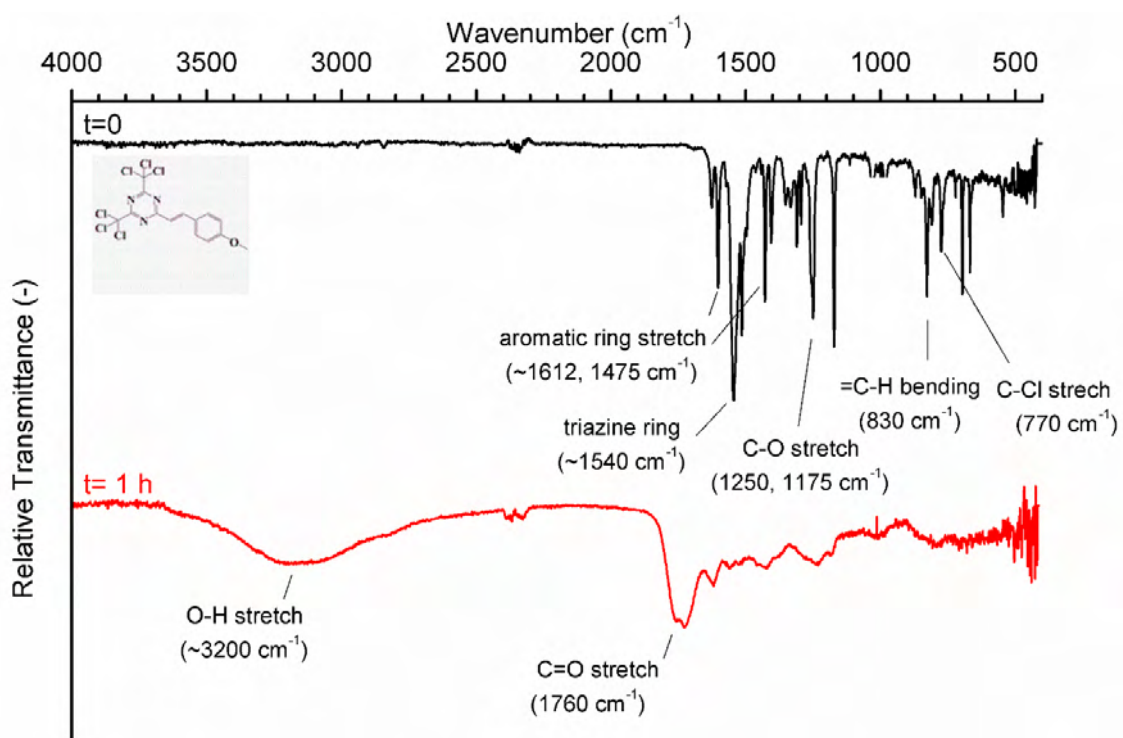
Figure 5. 13. IR-RAS spectra of AG1 nanofilm after 1-hour long UV-light irradiation
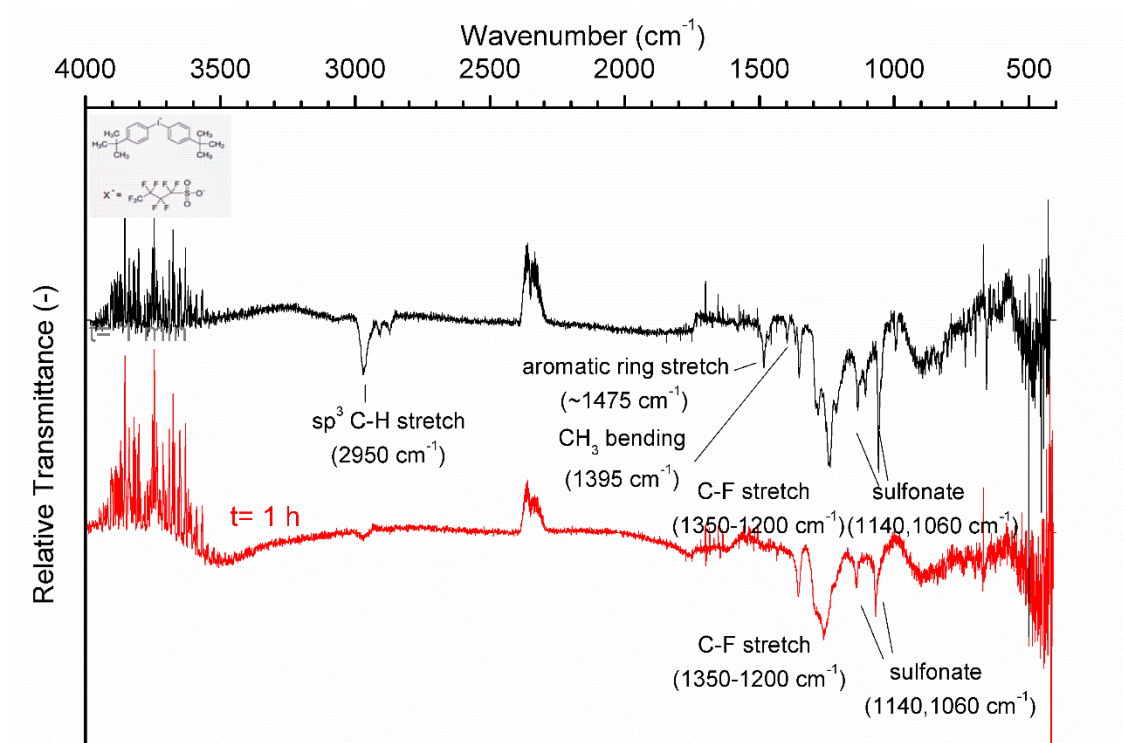
Figure 5. 14. IR-RAS spectra of AG2 nanofilm after 1-hour long UV-light irradiation

Also on nanofilm of photo base generator significant relative weight loss could be measured after 1-hour long UV-light irradiation, mass of BG decreased to 58.6%, Table 5. 4..

Table 5. 4. Relative mass of photo base generator nanofilm after 1 h UV-light irradiation

	Irradiation Time	Relative Mass
	min	%
BG	60	58.6

IR-RAS spectra of BG before and after UV-light irradiation are shown on Figure 5. 15.. The non-irradiated nanofilm shows many sharp IR absorption peaks. Among them there are some well-definable characteristic peaks, however in the fingerprint region peaks cannot be identified precisely due to complexity of the chemical structure and lack of IR spectral data on BG. On the spectrum, absorption peaks at 2970 and 2940 cm^{-1} belong to C-H stretch in methylene and methyl groups while the C-H stretch of anthryl group, which is expected to show up above 3000 cm^{-1}, is missing [49] [60]. Besides, the carbonyl group also gives strong, sharp peak at 1700 cm^{-1}. The peaks at 1430 and 1480 cm^{-1} cannot be related to a certain group of BG as they can belong to both aromatic ring stretch of the anthryl group and bending motions of methylene groups [49]. Similarly, two sharp peaks at 1274 and 1170 cm^{-1} and a broader, smaller one at 1068 cm^{-1} can belong to stretching vibrational motions of both C-O and C-N bonds. In general C-O bond is expected to give two band in range of 1330–1050 cm^{-1}; one strong at higher wavenumbers and one at lower wavenumbers [61]. In addition, Solanki et. al. observed one sharp peak belonging to C-O asymmetric stretch at 1074 cm^{-1} on the IR spectrum of benzyl carbamate [62]. Also, the amine group of BG can show IR absorption by C-N stretching in the fingerprint region generally from 1400 to 1000 cm^{-1} and in case of BG supposedly at two wavenumbers regarding the difference in inductive and resonance effect of alkyl and ester groups [49] [61]. After 1-hour long UV-light irradiation, the spectrum of BG changes drastically. The characteristic peaks disappear, there is only one broad peak on the IR spectrum at 1770 cm^{-1} that indicates the presence of carbonyl group in wide variety of different compounds. Thus, characteristic peaks of diethylamine (C-N stretch peak at 1350-1000 cm^{-1}, N-H stretch peak at 3300-3500 cm^{-1}) are missing as well.
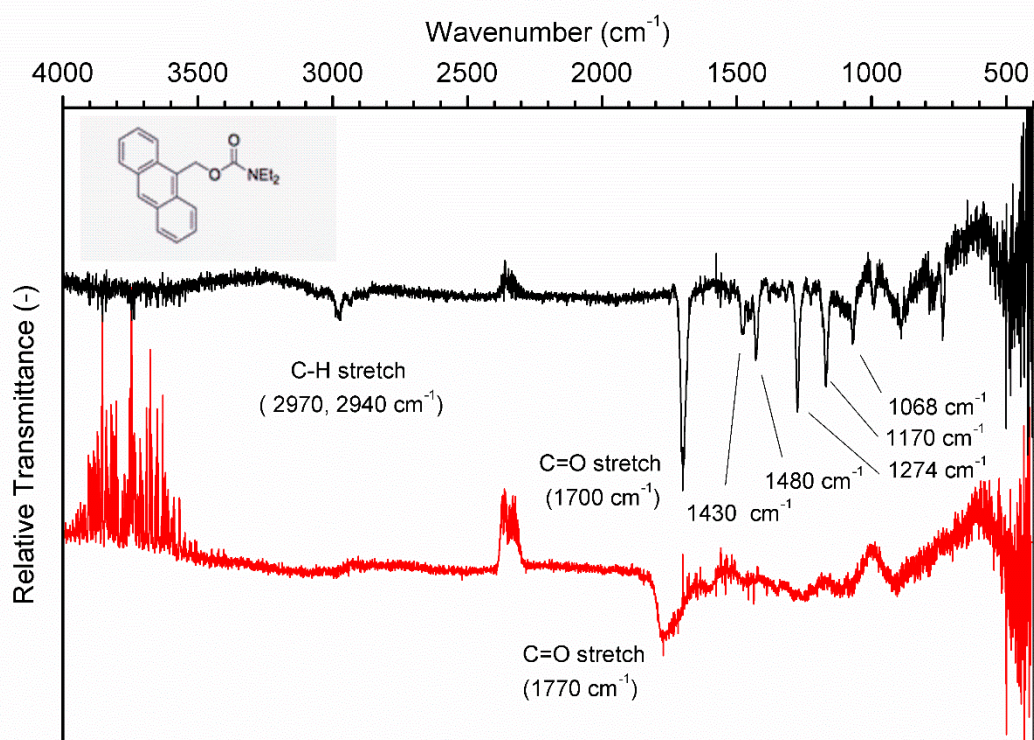
Figure 5. 15. IR-RAS spectra of PBG nanofilm after 1h UV-light irradiation

5. 2. 2. Poly(phthalaldehyde)

5. 2. 2. 1. PPhA-based nanofilms

The weight of PPhA, PPhA_AG1, and PPhA_AG2 nanofilms relative to their initial weight after different time period of UV-light irradiation can be seen in Figure 5. 16.. Upon irradiation, the weight of PPhA decreases rapidly and the weight loss occurs exponentially. The addition of photoacid generator further enhances this weight loss. PPhA_AG1 sample lost weight moderately faster than the pure polymer and the pure acid generator. In comparison, the PPhA_AG2 sample showed even faster weight loss than pure polymer and the PPhA_AG1 sample and similar to the pure polymer, its weight loss has an exponentially decreasing dependence on irradiation time. After 1-hour long UV-light irradiation, the PPhA kept 49% of its initial weight, while PPhA_AG2 nanofilms relative mass decreased to 20%.
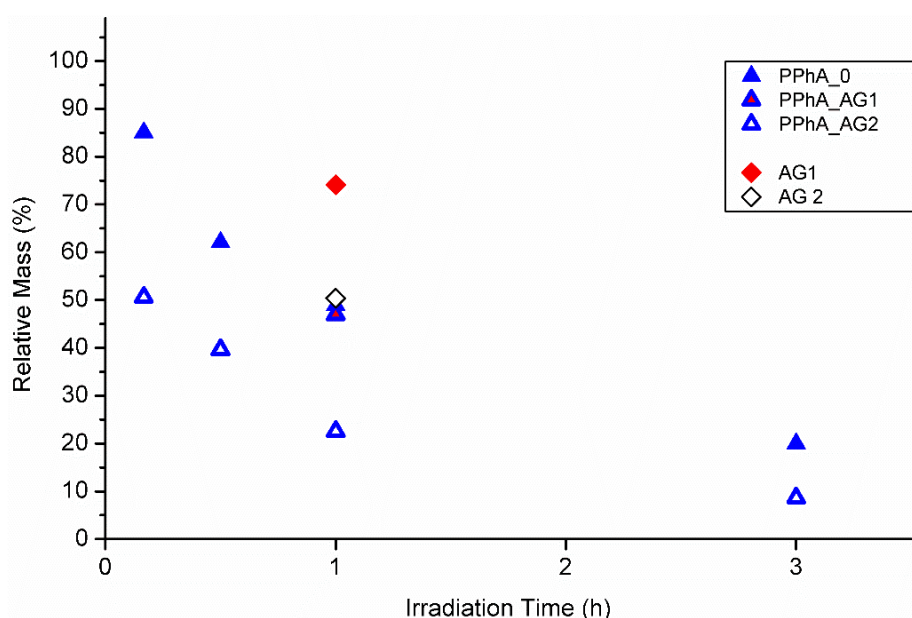
Figure 5. 16. Relative mass of PPhA nanofilms after different UV-light irradiation times

IR spectra of non-irradiated and irradiated PPhA nanofilms are shown on Figure 5. 17.. The non-irradiated sample give several sharp bands of which some can be assigned to certain functional groups of the repeating unit of the polymer. The aromatic ring can be identified by the =C-H out-of-plane (oop) bending that gives one sharp band at 760 cm^{-1} that indicates ortho and meta disubstitution of the ring while absorption via aromatic ring stretch can be assumed for the peak at 1470 cm^{-1}. In general, polymers with acetal linkages give four or five strong bands due to COCOC antisymmetric and symmetric stretchings in the region from 1200 to 1020 cm^{-1} that bands are often unresolved [49] [63]. Similar, it can be noticed in the case of PPhA, absorption peaks at 1100 cm^{-1} can be linked to the acetal link stretching motions. Besides, there is a peak at 1690 cm^{-1} on the spectrum that carbonyl peak`s position indicates the presence of aryl substituted aldehyde, supposedly belonging to the monomer of PPhA; o-phtalaldehyde (OPA). After 10-minute long UV-light irradiation, another much stronger sharp carbonyl band at 1770 cm^{-1} emerges while the characteristic bands that can be observed in

the spectrum of the non-irradiated polymer decrease or disappear. However, the presence of aromatic groups can be still indicated by the =C-H bending as well as acetal link might be present regarding broad absorption peak around 1100 cm^{-1}. After longer UV-light irradiation, samples give broad unresolved spectra with carbonyl peak at 1770 cm^{-1} and no indication of aromatic and acetal link.
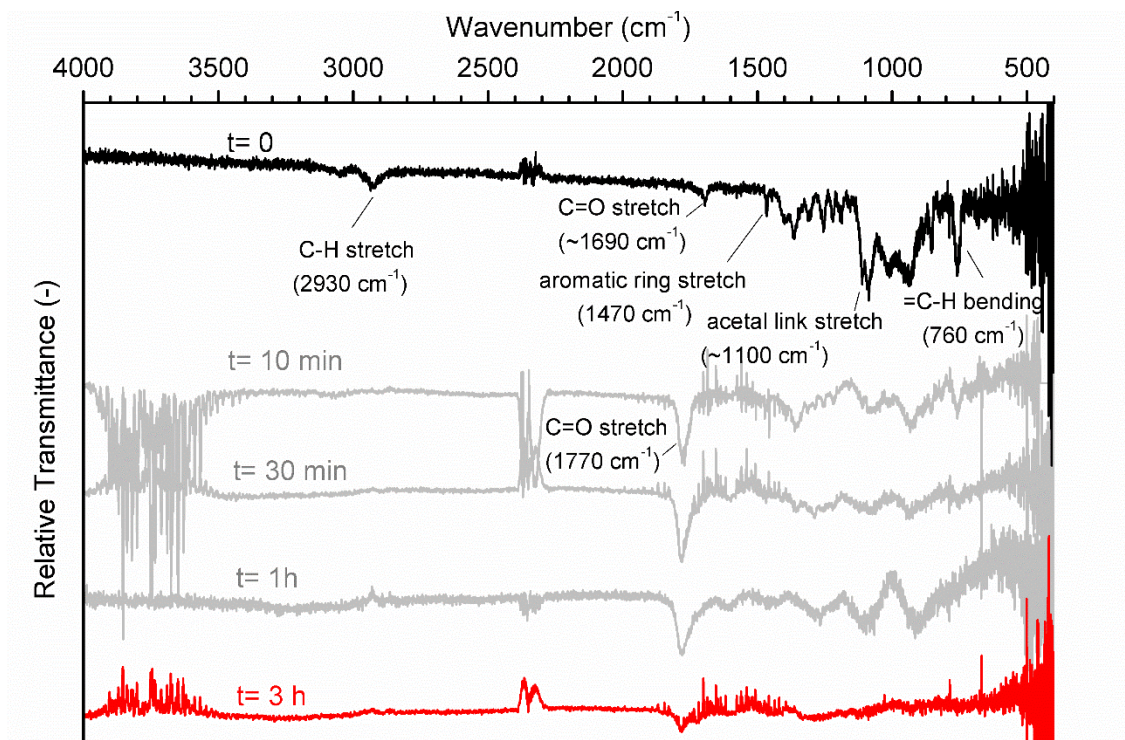
Figure 5. 17. IR-RAS spectra of PPhA nanofilms after different UV-light irradiation times

IR spectra of non-irradiated and 1-hour long UV-light irradiated PPhA_AG1 nanofilms are shown on Figure 5. 18.. The non-irradiated sample gives several bands that belong to functional groups of the polymer and AG1 (Figure 5. 13.). For example, PPhA with acetal linkage gives strong bands due to COCOC antisymmetric and symmetric stretchings in the region from 1200 to 1020 cm^{-1}, similar to that of pure PPhA. Moreover, AG1 can be distinguished by its peak at 1540 cm^{-1} that belongs to its triazine ring. Besides, aromatic ring that is present in both compounds can be indicated by aromatic ring stretch peak at 1460 cm^{-1}. In addition, the IR absorption at 760 cm^{-1} can be related to both C-Cl stretch of trichloromethyl group and =C-H bending of aromatic ring. After UV-light irradiation several characteristic bands disappear, for example acetal link of PPhA, and trichloromethyl and triazine of AG1, and aromatic ring of both. Instead, there are a couple of wide peaks on the spectra that hard to identify and a wide, strong carbonyl double bands at 1760 and 1730 cm^{-1}.

IR spectra of non-irradiated and UV-light irradiated PPhA_AG2 nanofilms are shown in Figure 5. 19.. In the spectrum of non-irradiated sample there are several peaks that belong to the PPhA and can be noticed also on the spectrum of the pure polymer but the characteristic peaks of AG2 are not distinguishable (Figure 5. 14.). The aromatic ring of the polymer can be identified by the =C-H out-of-plane (oop) bending that results one sharp peak at 760 cm^{-1} indicating ortho and meta disubstitution of the ring. Besides, the aromatic ring stretch occurs

based on the peak at 1470 cm^{-1}. Also, absorption by acetal link of the polymer can assumed by the unresolved peak group with similar to the peaks of pure PPhA at the region from 1200 to 1020 cm^{-1}. After 10-minute long UV-light irradiation the spectra of the irradiated samples dramatically different from the non-irradiated sample's. All of them show broad, poorly resolved bands next to a sharp carbonyl peak at 1770 cm^{-1}.

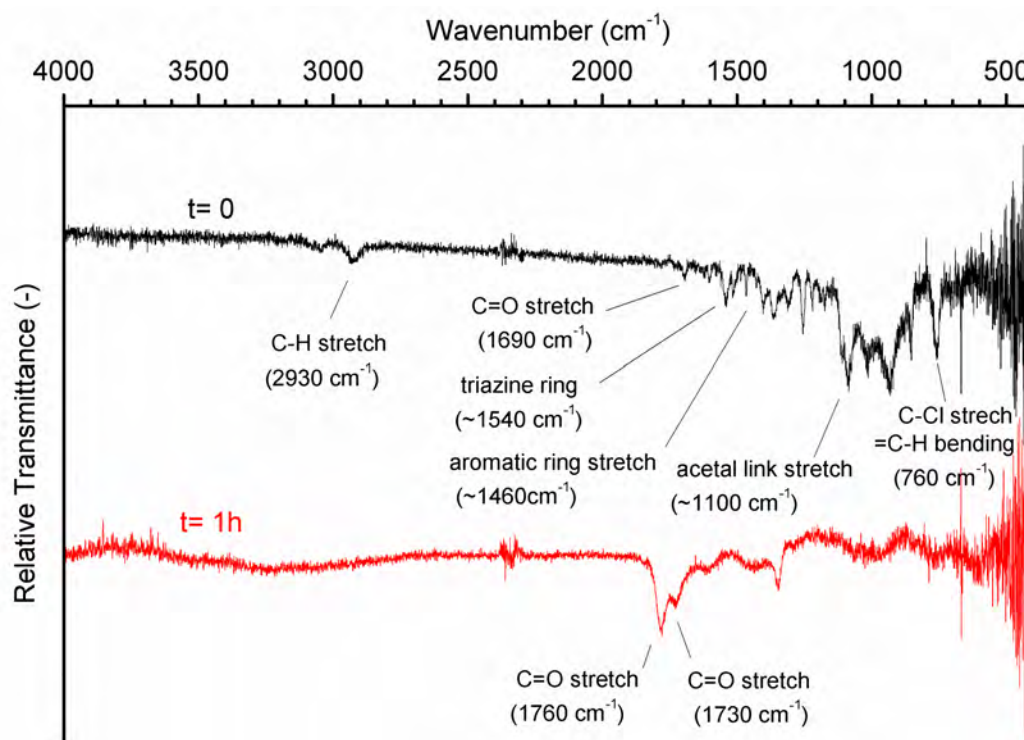**Figure 5. 18.** IR-RAS spectra of PPhA_AG1 nanofilm after 1-hour long UV-light irradiation
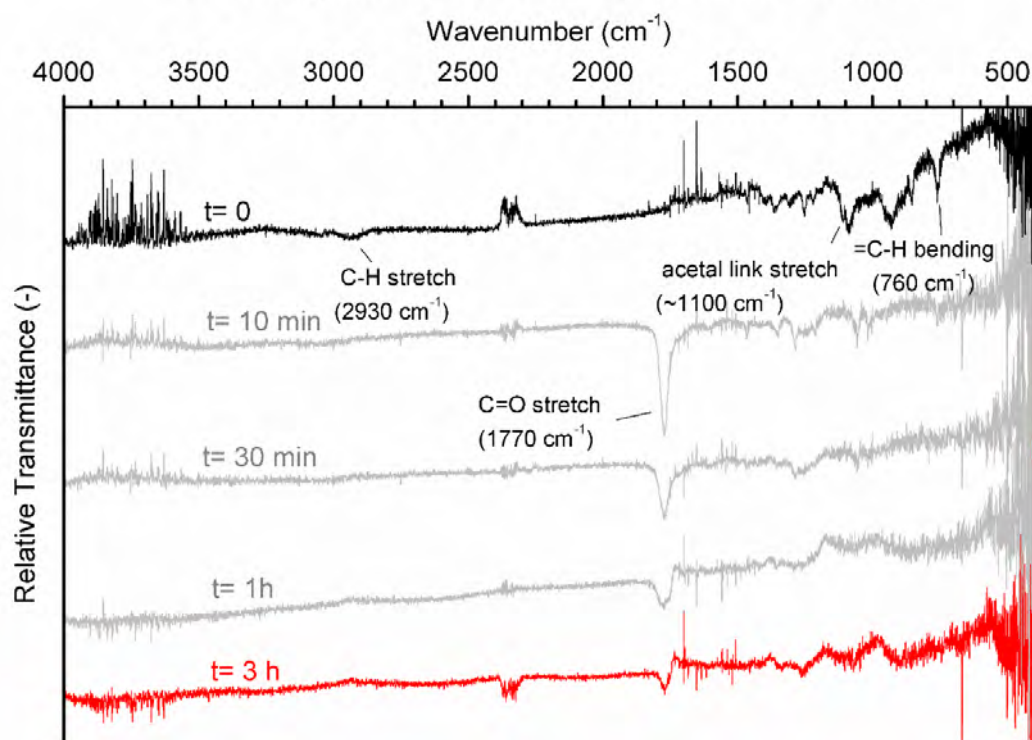
Figure 5. 19. IR-RAS spectra of PPhA_AG2 nanofilm after different UV-light irradiation times

5. 2. 2. 2. PPhA-based microfilms

There are significant visual differences between before and after 10-minute long UV-light irradiation of PPhA and PPhA_AG2 samples, Figure 5. 20.. The PPhA film without acid generator is a white, opaque, solid polymer film that becomes a yellow, viscous fluid under UV-light irradiation. Similar change in the appearance can be observed after UV light irradiation of PPhA_AG2 sample; its white, solid film turns deep brown, and even more fluid than PPhA after the same irradiation time.

PPhA_0		PPhA_AG2	
before UV	after 5 h	before UV	after 5 h
Remaining Relative Mass: 89,2 %		Remaining Relative Mass: 88,7 %	
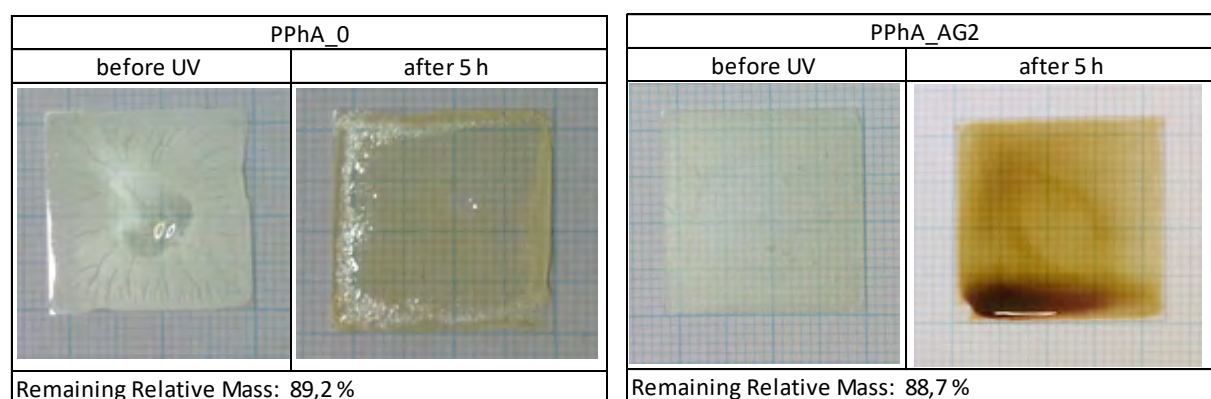
Figure 5. 20. Microfilm of PPhA and PPhA_AG2 (right) before and after 10 min UV-light irradiation and their remaining relative mass

The relative mass of pure PPhA microfilm decreases significantly during 10-minute long UV-light irradiation to 89.2 %, similar to its nanofilm that decreases to 85.0 % of its original weight. In comparison, PPhA_AG2 microfilm keeps more weight than its nanofilm; while the microfilm decreases to 88.7 %, the nanofilm decreases much more drastically to 62.0 %. Comparing PPhA and PMMA, weight losses of PPhA and PPhA_AG2 microfilms are significantly higher after 10 min UV-light irradiation than the PMMA microfilms after 5-hour long irradiation.

ATR-IR spectra of PPhA microfilm before and after UV-light irradiation are shown on Figure 5. 21. along with its pristine powder form and DCM. The non-irradiated PPhA microfilm gives the same characteristic bands as the PPhA nanofilm (see page 57) and PPhA powder. Also, the presence of DCM can be excluded based on the absence of C-Cl stretch peak. However, in comparison to the nanofilm, the bands are more distinguishable in the IR spectra of the microfilm after 10-minute long UV-light irradiation; rise of new bands and changes of relative peak intensities of the original peaks can be observed. After irradiation broad O-H stretch peak appears at ~3450 cm^{-1} and strong carbonyl peaks at 1760, 1720, 1690 cm^{-1}. Also new peaks bands next to the =C-H bending that might be caused by change in substitution of the aromatic ring. The change of the relative intensities can be observed; the carbonyl peak at 1690 cm^{-1} increased after UV-light irradiation relative to the peaks of the acetal link and =C-H bendings.

ATR-IR spectra of PPhA_AG2 microfilm before and after UV-light irradiation are shown on Figure 5. 22. along with spectra of its pristine powder form, AG2 powder and DCM. The non-irradiated PPhA_AG2 microfilm gives the same characteristic bands as the PPhA nanofilm

(see page 57) and PPhA powder. Furthermore, the presence of DCM can be excluded based on the absence of its absorption peaks. As in the case of PPhA, after 10-minute long UV-light irradiation the absorption peaks of PPhA_AG2 are more distinguishable than on the corresponding nanofilm`s spectrum; rise of new peaks and changes of relative peak intensities of the original peaks can be observed. On the spectrum of irradiated PPhA_AG2 broad O-H stretch band appears at ~3450 cm^{-1} and strong carbonyl peaks at 1760, 1690 cm^{-1}, however, in this case the peak at 1690 cm^{-1} is relatively lower than the one at 1760 cm^{-1}. Besides, several new bands rise next to the =C-H bending that might be caused by different substitutions of the aromatic rings. Similar to pure PPhA, also on the spectrum of irradiated PPhA_AG2 there is change in peak intensities compared to each other. The peak intensity of both carbonyl peaks at 1760 cm^{-1} and 1690 cm^{-1} increased relative to the peaks of the C-O stretch of the acetal link and =C-H bendings. Also, contrary to pure PPhA the carbonyl band at 1760 cm^{-1} -which is related to higher oxidation state- has relatively higher band intensity than the aldehyde carbonyl band at 1690 cm^{-1}.
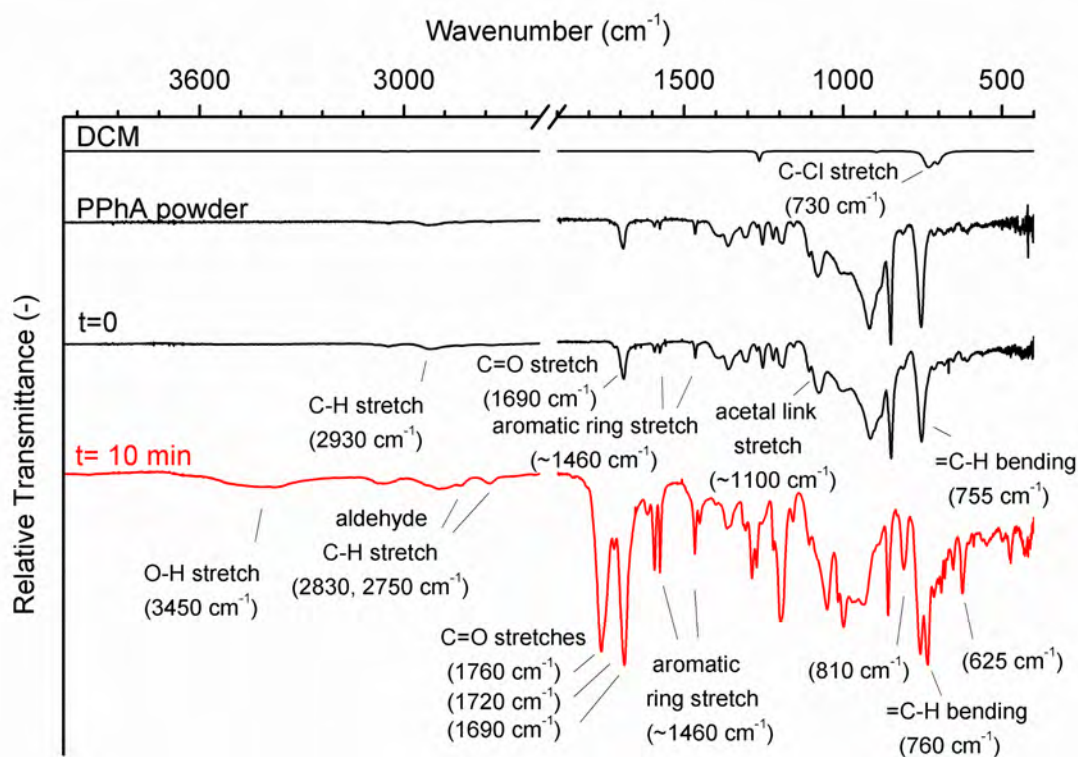
Figure 5. 21. ATR-IR spectra of DCM, PPhA powder and PPhA microfilms before and after 10-minute long UV-light irradiation

62
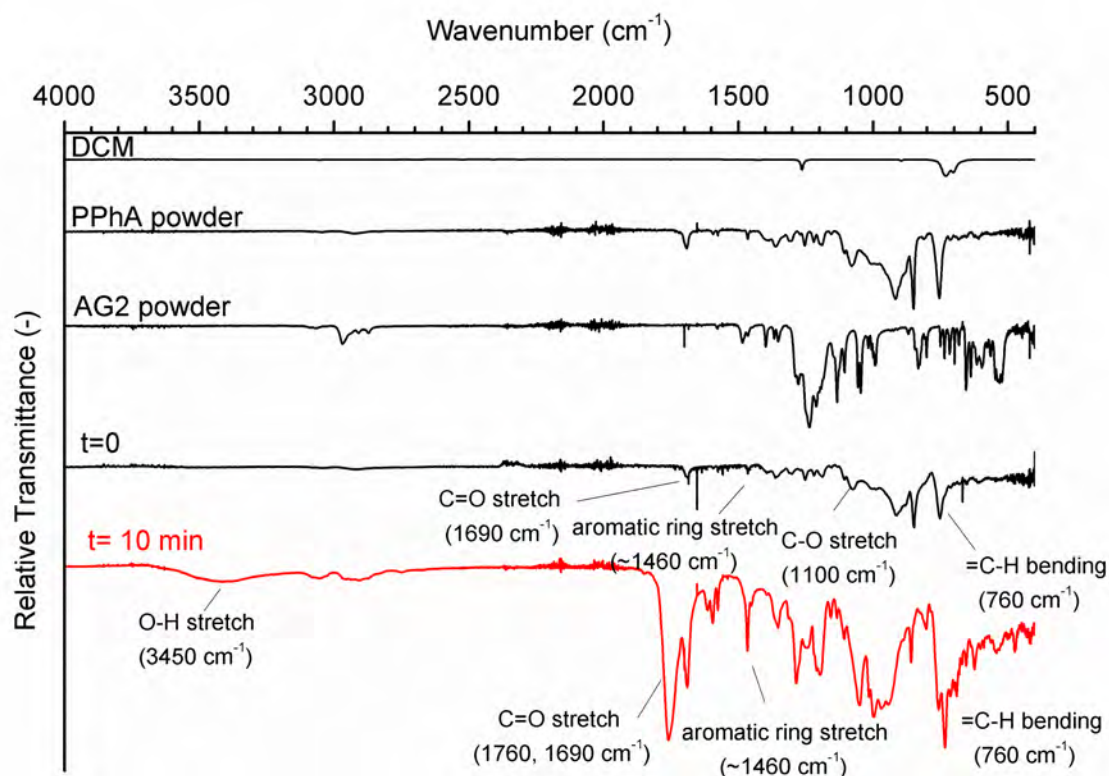
Figure 5. 22. ATR-IR spectra of DCM, PPhA powder and PPhA_AG2 microfilms before and after 10 minute UV-light irradiation

NMR spectra of PPhA and PPhA_AG2 microfilms before and after UV-light irradiation are very similar; apart from the acidic hydrogen of PPhA_AG2 the same type of protons can be identified by their peaks appearing at the same chemical shifts, Table 5. 5., 5. 6., Figure 5. 23.. In all spectra, not the PPhA but its monomer (OPA) could be detected beside DCM, water and non-identifiable "other" compounds related to peaks that cannot belong to OPA, DCM, water or acidic hydrogen. In addition, PPhA depolymerized when the microfilm samples were dissolved in chloroform as even non-irradiated samples contained only the monomer but not the PPhA after dissolution in chloroform, while the IR results prove that depolymerization did not occur after preparation of microfilms.

In detail, the most highly deshielded type of proton is at 10.5 ppm on every spectrum and belongs to the hydrogen in the aldehyde group of OPA. Then, peaks at 8.0 and 7.8 ppm belong to the hydrogens of the aromatic ring in ortho and para positions, respectively. Beside the characteristic peaks of the OPA, peak related to DCM at 5.3 ppm and water at 1.2 ppm appear as well [54]. Acidic hydrogen could be detected only in PPhA_AG2 samples at 1.3 ppm. NMR results also show that due to 10-minute long UV-light irradiation the fractions of hydrogen atoms in different compounds changed drastically. After irradiation the amount of the other compounds increased and no well-identifiable photoproduct could be detected based on appearance of more small, broad peaks at wide range of chemical shifts. Thus, the fraction of hydrogens in "new" photoproducts were estimated by the difference of the other compounds' hydrogen fractions before and after irradiation.

After 10-minute long UV-light irradiation of PPhA microfilm the fractions of hydrogen atoms belonging to OPA decreased with 60 % (with fraction 0.451) while the fraction of

hydrogens in new unidentifiable photoproducts was almost as much as this decrease (0.387). The deviance can be explained by that we do not have information on what kind of components evaporated during the measured weight loss that makes estimation less punctual. Besides, it can be noted that the ratio of hydrogens in aldehyde group and hydrogens in ortho and meta position in the aromatic ring do not decrease more than 3.7% after 10-minute long irradiation. This indicates that the remaining material after photodegradation is OPA and/or PPhA and depolymerization can be proposed as a possible photodegradation step. Similar phenomena, but in higher magnitude can be observed in PPhA_AG2 due to UV-light irradiation.

Moreover, in PPhA_AG2 microfilm the fractions of hydrogen atoms belonging to OPA decreased with 73 % (with fraction 0.505) while the fraction of hydrogens in new photoproducts was almost as much as this decrease (0.489). In this case the ratio of hydrogens in aldehyde group and hydrogens in ortho and meta position in the aromatic ring decreased maximum 10.7% upon UV-light irradiation which is higher than in case of pure PPhA. This can be related to the presence of other photodegradative reactions beside depolymerization.

Table 5. 5. Fractions of different types of H atoms in PPhA microfilms before and after 10 minute UV-light irradiation based on their NMR spectra

PPhA microlayer before UV				PPhA microlayer after 10 min UV			
Type of proton	Range of Integral		Fractions of hyrogen atoms	Type of proton	Range of Integral		Fractions of hyrogen atoms
	ppm				ppm		
CHO	10,5	10,6	0,243	CHO	10,5	10,6	0,096
CH (ortho)	8,0	8,0	0,254	CH (ortho)	8,0	8,0	0,104
CH (meta)	7,8	7,8	0,260	CH (meta)	7,8	7,8	0,107
CH_2Cl_2	5,3	5,3	0,004	CH_2Cl_2	5,3	5,3	0,061
H_2O	1,2	2,2	0,116	H_2O	1,2	2,2	0,123
acid	1,3	1,3	0,000	acid	1,3	1,3	0,000
other	-0,7	11,5	0,123	other	-0,7	11,5	0,123
				new	-0,7	11,5	0,387

Table 5. 6. Fractions of different types of H atoms in PPhA_AG2 microfilms before and after 10 minute UV-light irradiation based on their NMR spectra

PPhA_AG2 microlayer before UV				PPhA_AG2 microlayer after 10 min UV			
Type of proton	Range of Integral		Fractions of hyrogen atoms	Type of proton	Range of Integral		Fractions of hyrogen atoms
	ppm				ppm		
CHO	10,5	10,6	0,221	CHO	10,5	10,6	0,055
CH (ortho)	8,0	8,0	0,232	CH (ortho)	8,0	8,0	0,063
CH (meta)	7,8	7,8	0,235	CH (meta)	7,8	7,8	0,066
CH_2Cl_2	5,3	5,3	0,017	CH_2Cl_2	5,3	5,3	0,031
H_2O	1,2	2,2	0,173	H_2O	1,2	2,2	0,212
acid	1,3	1,3	0,062	acid	1,3	1,3	0,024
other	-0,7	11,5	0,059	other	-0,7	11,5	0,059
				new	-0,7	11,5	0,489

Figure 5. 23. NMR spectra of PPhA and PPhA_AG2 microfilms before and after 10-minute long UV-light irradiation

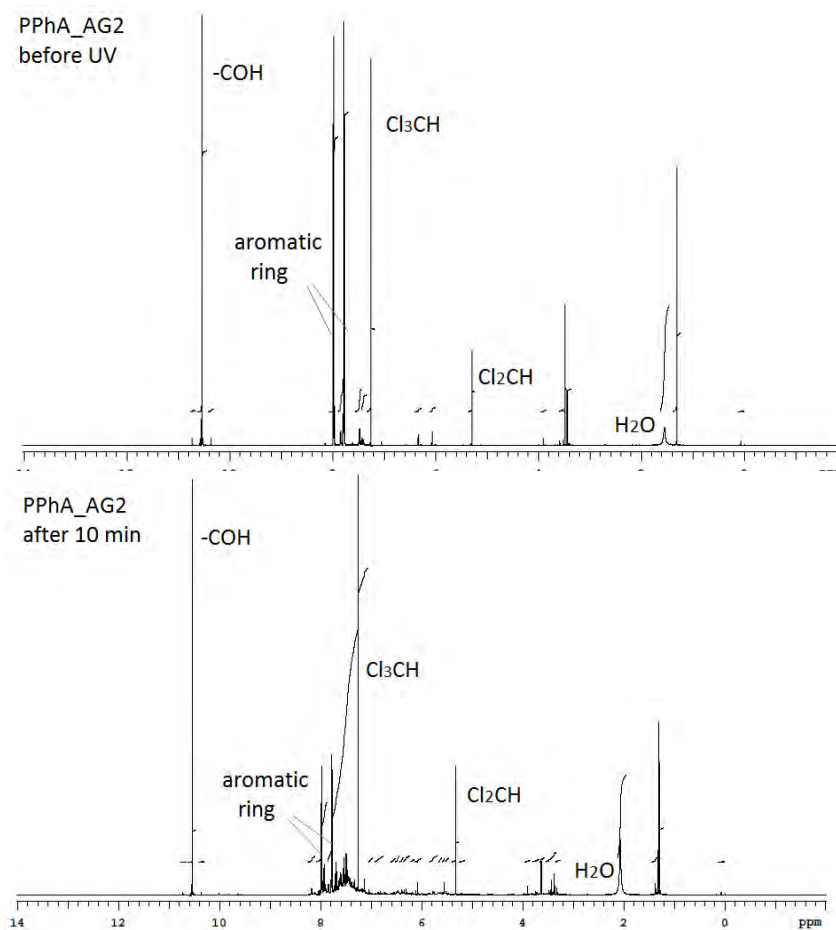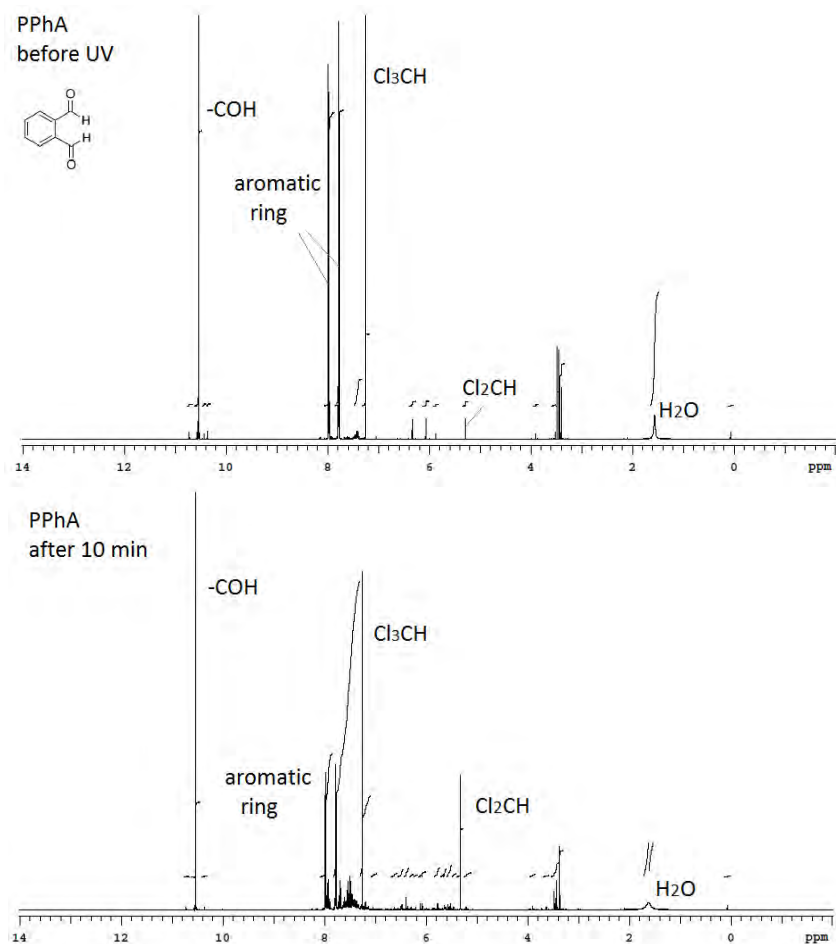Thermal degradation steps of PPhA microfilm samples before and after photodegradation are revealed by their TG and DTG plots, Figure 5. 24.. Both PPhA and PPhA_AG2 samples had absence of peak for evaporation of DCM ($T_{boiling}$= 39.6 °C) indicating that not high enough amount of it remained in the system after solvent casting that could be detected by TGA. The two degradation peaks of pristine polymer powder (163°C, 200 °C) appeared at slightly lower temperatures in PPhA and PPhA_AG2 films, 158°C, 197 °C and 161°C, 196 °C, respectively. This indicates that the same degradation mechanism might be assumed in these cases, but the solvent casting could result this slight shifting. Also, some deviation in the remaining weight fractions and the DTG peak heights of the degradation step occur that can caused by remaining solvent in the system. Nevertheless, the non-irradiated samples thermal degradation results in almost no remaining thermal degradation product and can be explained with the depolymerization of the PPhA to its volatile monomer, OPA [64]. In contrast, in both UV-light irradiated PPhA and PPhA_AG2 microfilms there were remaining material after their thermal degradation that shows the presence of other photoproducts than OPA and these products are probably not small, volatile organic molecules but very high molecular weight, non-volatile materials produced in multiple condensation steps during their photoreactions. However, it is important to note that in case of PPhA the fraction of this type of photoproduct was much less than in irradiated PPhA_AG2 samples. Also irradiated PPhA shows degradation step at 130 °C that can be linked to depolymerization of PPhA, furthermore its DTG peaks at 220°C and 350 °C can be related to thermal degradation and/or evaporation of less condensed photoproducts. These peaks are completely missing in the irradiated PPhA_AG2 sample and with the high remaining weight fraction they might indicate higher photodegradation rate of PPhA_AG2 than PPhA.

TGA plot of PPhA

TGA plot of PPhA_AG2

DTG plot of PPhA

DTG plot of PPhA_AG2

	PPhA					
	powder		0 h		10 min	
	Weight fraction after offset	Peak	Weight fraction after offset	Peak	Weight fraction after offset	Peak
	(-)	(°C)	(-)	(°C)	(-)	(°C)
1st peak	0.502	163	0.557	158	0.402	130
2nd peak	0.028	200	0.037	197	0.274	220
3rd peak	-	-	-	-	0.064	350

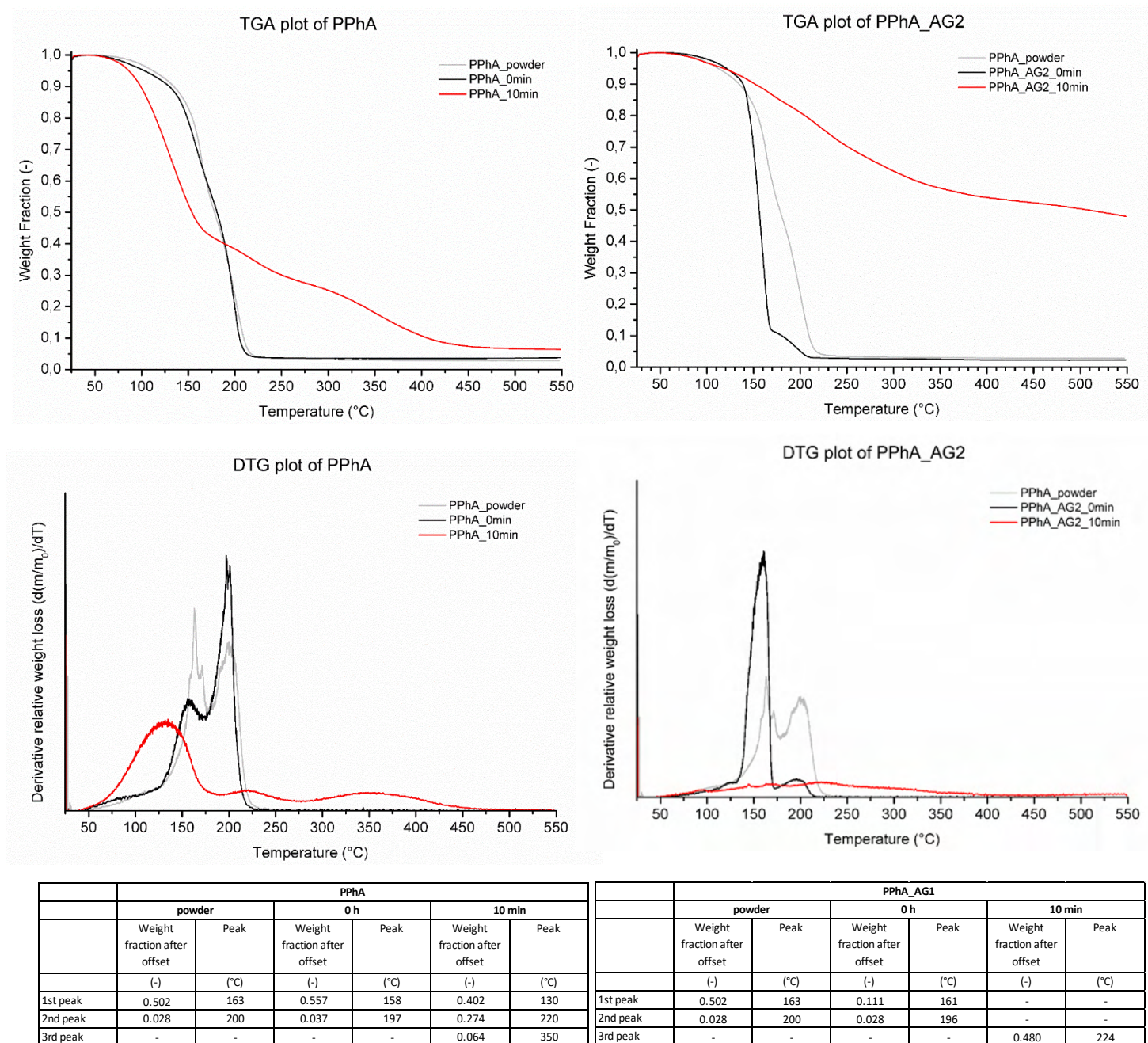|	PPhA_AG1					
	powder		0 h		10 min	
	Weight fraction after offset	Peak	Weight fraction after offset	Peak	Weight fraction after offset	Peak
	(-)	(°C)	(-)	(°C)	(-)	(°C)
1st peak	0.502	163	0.111	161	-	-
2nd peak	0.028	200	0.028	196	-	-
3rd peak	-	-	-	-	0.480	224

Figure 5. 24. TG and DTG plots of PPhA and PPhA_AG microfilms and pristine PPhA powder before and after 10 minute UV-light irradiation

5. 2. 3.Poly(propylenecarbonate)

Weight of PPC, PPC_AG1, and PPC_AG2 nanofilms relative to their initial weight after different time periods of UV-light irradiation can be seen on Figure 5. 25.. After 1-hour long irradiation the weight of PPC does not change, however after 3-hour long irradiation it was reduced to 92 %. The addition of photoacid generator slightly enhances the weight loss of PPC in the first hour of UV-light irradiation, but this effect becomes less significant after 3-hour long irradiation. After 1 hour, PPC_AG1 and PPC_AG2 samples lost weight higher than the weighted average of PPC and AG1, their relative mass was 85% and 88% instead of 97% and 95%, respectively. After 3-hour long relative mass of PPhA_AG1 and PPhA_AG2 decreased to 79% and 86%.

Figure 5. 25. Relative mass of PPC nanofilms after different UV-light irradiation times

IR spectra of non-irradiated and UV-light irradiated PPC nanofilms are shown on Figure 5. 26.. The same characteristic bands indicate the presence of carbonate and propylene groups of PPC in all spectra independent from irradiation time showing no significant chemical change upon UV-light. Carbonate group in the main chain of PPC can be identified by its strong band of carbonyl C=O stretch at 1760 cm^{-1} and C-O stretch can be indicated by the wide band at around 1300 cm^{-1} [65]. Also, C-H stretch of propylene group in the polymer chain shows characteristic IR absorption around 2950 cm^{-1} [49].
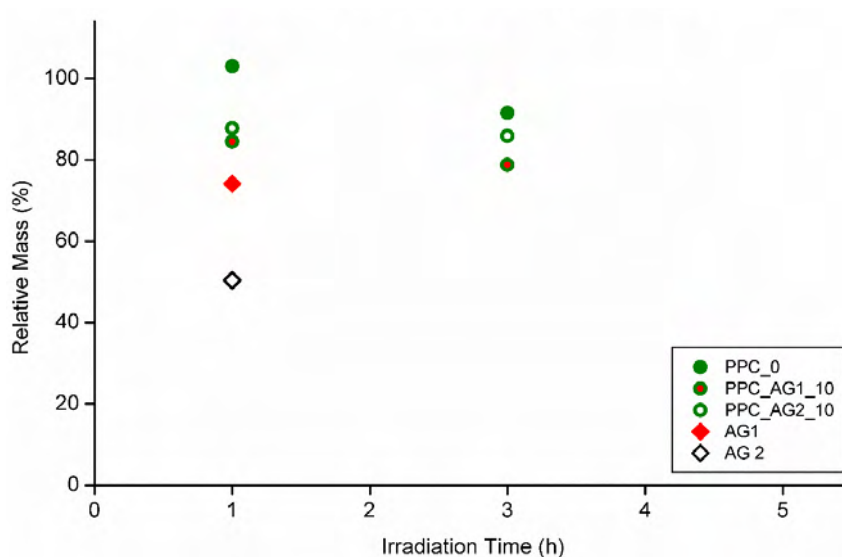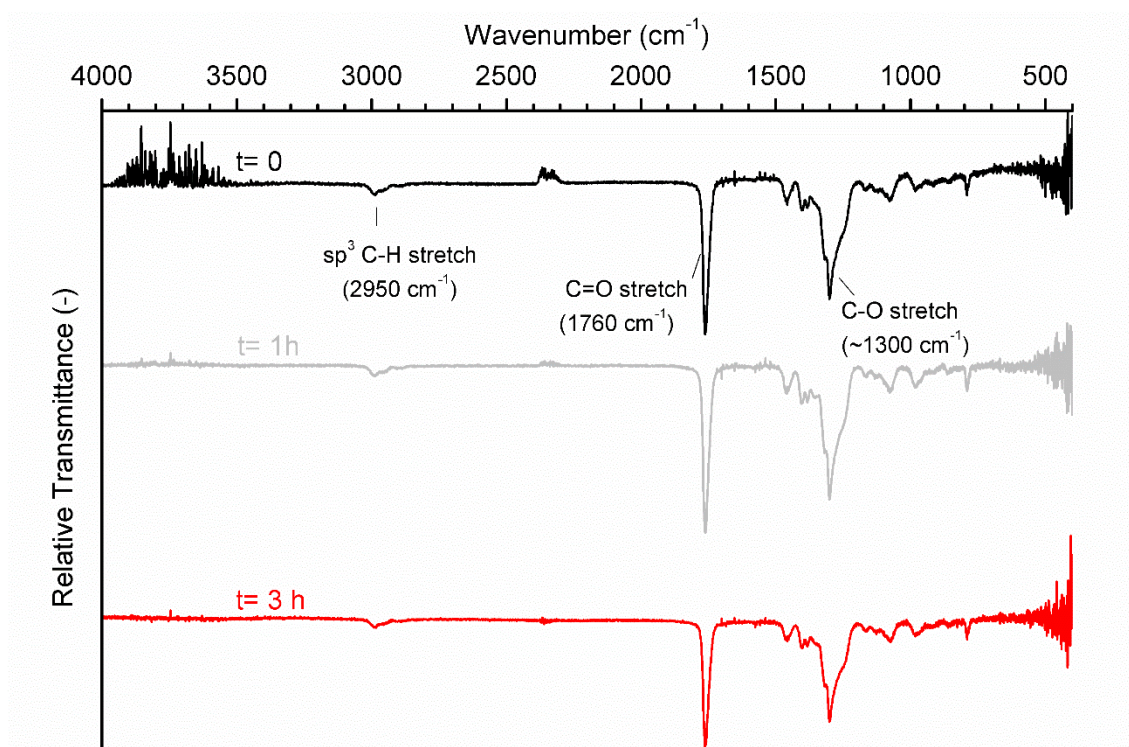
Figure 5. 26. IR-RAS spectra of PPC nanofilms after different UV-light irradiation times

IR spectra of non-irradiated and UV-light irradiated PPC_AG1 nanofilms are shown on Figure 5. 27.. The non-irradiated sample gives several peaks that can be connected to functional groups of the polymer and AG1. Carbonate and alkyl groups -similar to the pure PPC- can be identified by absorption peaks of C=O stretch at 1760 cm^{-1}, C-O stretch at 1300 cm^{-1}, and C-H stretch around 2950 cm^{-1}. Among the characteristic bands of AG1 only the absorption peak of triazine ring at 1540 cm^{-1} can be distinguished. After 1 and 3-hour long UV-light irradiations the spectra are similar, the characteristic peaks of PPC still appear while the triazine ring of AG1 cannot be detected.

IR spectra of PPC_AG2 nanofilms before and after UV-light irradiations are shown on Figure 5. 28.. On the IR spectrum of non-irradiated sample there are several bands that belong to functional groups of the polymer, but none to the AG2. Carbonate and alkyl groups of the PPC can be identified by absorption peaks of C=O stretch at 1760 cm^{-1}, C-O stretch at 1300 cm^{-1}, and C-H stretch around 2950 cm^{-1}. After 1 and 3-hour long UV-light irradiations the spectra remain unchanged, the characteristic peaks of PPC still appear at the same wavenumbers.
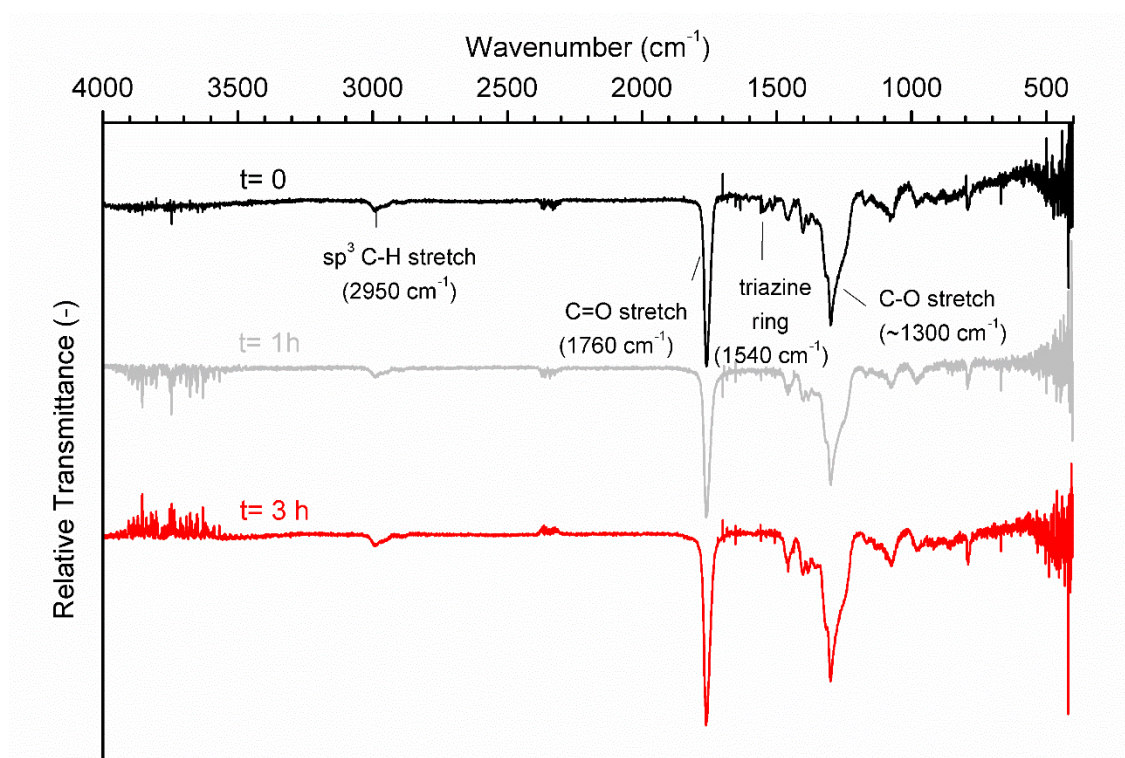
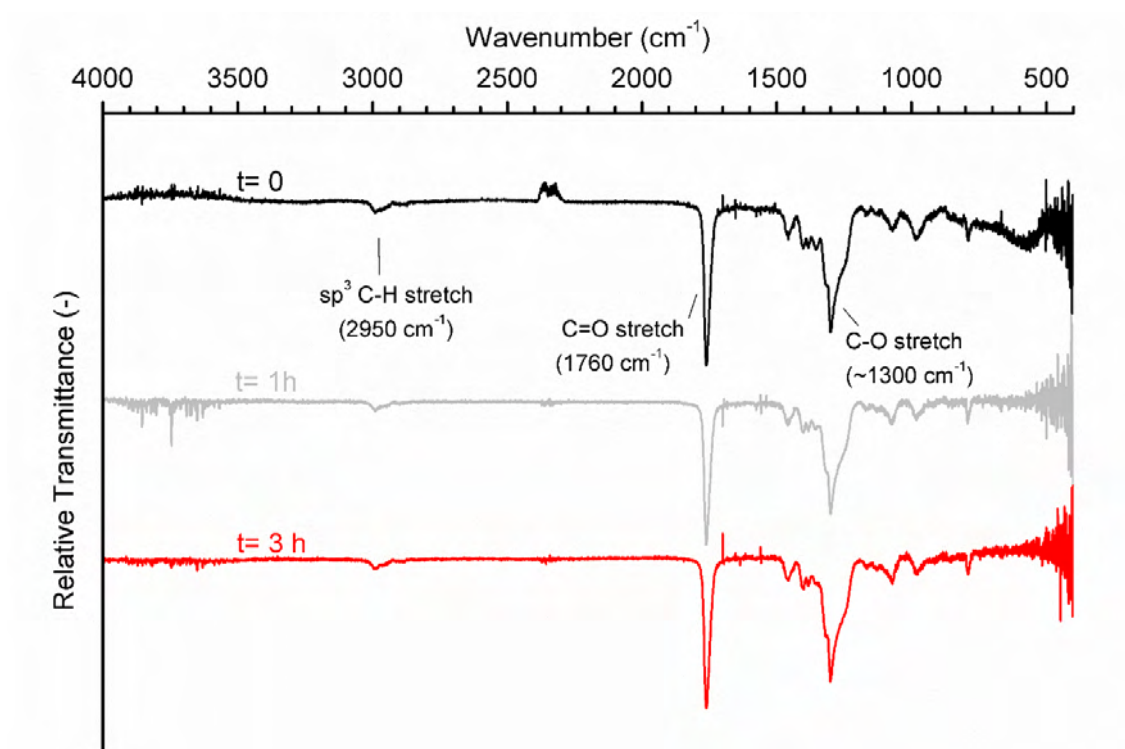**Figure 5. 27.** IR-RAS spectra of PPC_AG1 nanofilms after different UV-light irradiation times

Figure 5. 28. IR-RAS spectra of PPC_AG2 nanofilms after different UV-light irradiation times

5. 2. 1. Poly(1-hexadecene-sulfone)

The weight of PSu and PSu_BG nanofilms relative to their initial weight after different time periods of UV-light irradiation can be seen on Figure 5. 29.. Upon irradiation, there is no significant change in the weight of PSu as even after 3-hour long irradiation it kept 98% of its initial weight. Adding photo base generator to the PSu does not change its rate of weight loss; the relative mass of PSu_BG after 1-hour long irradiation was 97%, slightly higher than weighted average of PS and BG after the same irradiation time which was 94%. Also, after 3-hour long UV-light irradiation its relative mass remains high, 93%.

Figure 5.29. Relative mass of PSu nanofilms after different UV-light irradiation times

IR spectra of non-irradiated and UV-light irradiated PSu nanofilms are shown on Figure 5. 30.. All spectra are independently from irradiation time show no significant chemical change upon UV-light. There are three vibration modes of PSu that can be identified by their absorption peaks. At high wavenumber of the spectra, at 2920 cm^{-1}, absorption peaks of sp^3 C-H stretch appear. Next, the methylene group can be identified by its bending motion resulting peak at 1465 cm^{-1}. Besides, the presence of sulfone group is indicated by its stretching vibrational motions giving peaks at 1320 and 1120 cm^{-1} [49].

IR spectra of non-irradiated and UV-light irradiated PSu_BG nanofilms are shown in Figure 5. 31.. Before UV-light irradiation there are absorption peaks of both PSu and BG in the spectrum. PSu can be indicated by its C-H stretch (2920 cm^{-1}), CH$_2$ bending (1465 cm^{-1}), and S=O stretching (1320, 1120 cm^{-1}). The presence of BG can be detected only by its carbonyl band (1700 cm^{-1}). After UV-light irradiation the characteristic bands of PSu remain unchanged, but the carbonyl band of BG at 1700 cm^{-1} disappeared.

Figure 5. 30. IR-RAS spectra of PSu nanofilms after different UV-light irradiation times
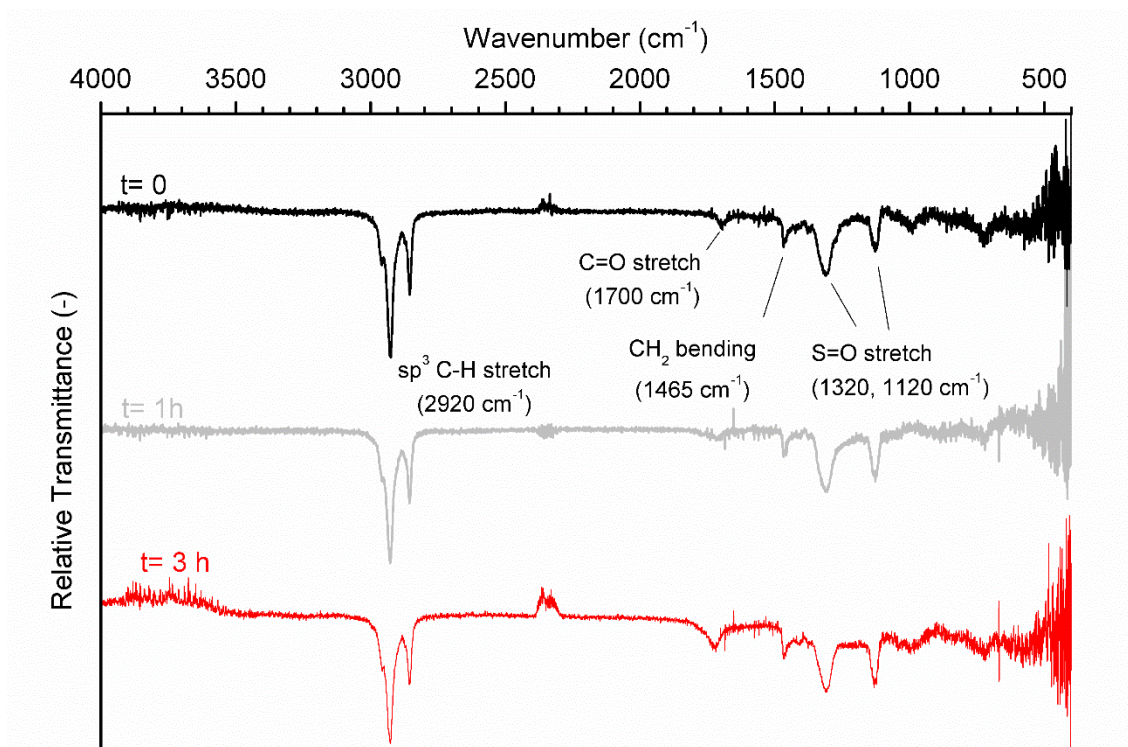
Figure 5. 31. IR-RAS spectra of PSu_BG nanofilms after different UV-light irradiation times

5. 3. Photocrosslinkable Polymer

5. 3. 1. Poly(vinylcinnamate)

The weight of PVCi nanofilms relative to their initial weight after different time periods of UV-light irradiation can be seen on Figure 5. 32.. Upon UV-light irradiation, the weight of PVCi does not change after 1-hour long irradiation time, but significant decrease can be observed upon further UV-light explosion; after 3-hour long irradiation; the relative mass of PVCi was reduced to 78%.
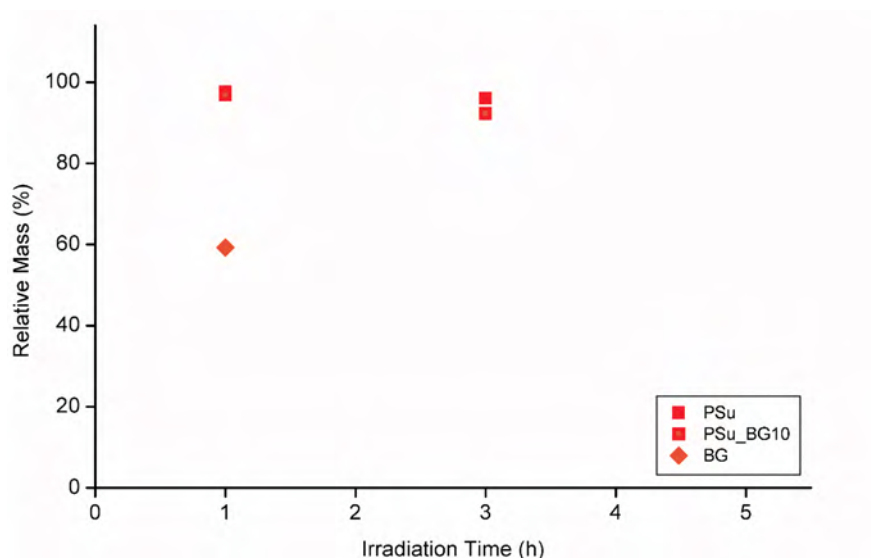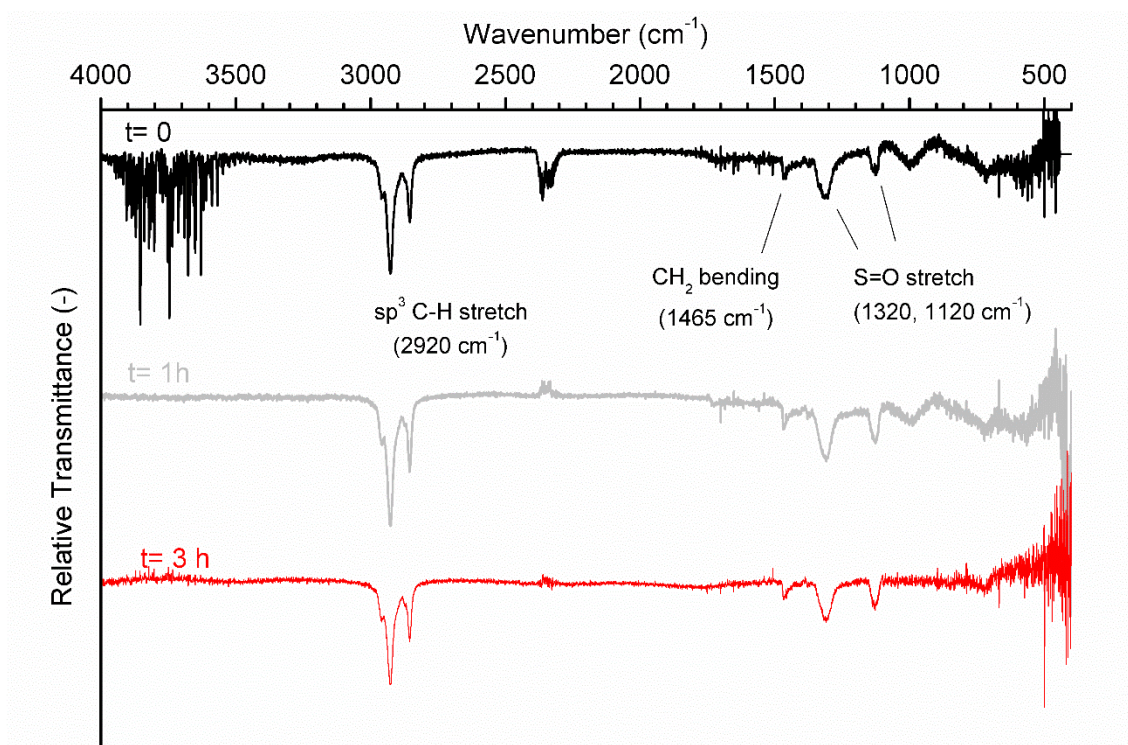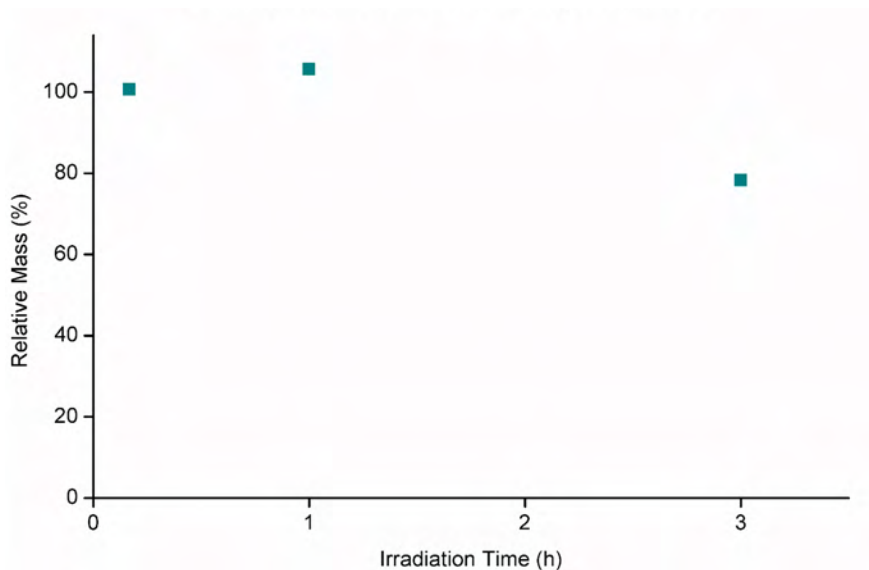

Figure 5. 32. Relative mass of PVCi nanofilms after different UV-light irradiation times

IR spectra of non-irradiated and UV-light irradiated PVCi nanofilms are shown in Figure 5. 33.. The non-irradiated sample give several sharp bands among them some can be assigned to certain functional groups of PVCi. Methylene group in the main chain of PVCi can be identified by its long chain bending motion that results sharp peak around 770 cm^{-1} on the spectrum and the C-H stretch that gives peak around 2950 cm^{-1}. Also, ester link between the main and side chain shows IR absorption giving strong carbonyl band at 1716 cm^{-1} and C-O stretching bands around 1300 cm^{-1}. Besides, the presence of the double bond of PVCi can be noted by its absorption band at 1163 cm^{-1}. The aromatic ring can be identified by aromatic ring stretch related to absorption peaks at 1570 and 1490 cm^{-1} [49]. After UV-light irradiation the characteristic bands of PVCi disappear. Instead, in the spectra there is only one wide carbonyl band around 1750 cm^{-1} indicating the presence of carbonyl groups in wide variety of different compounds.
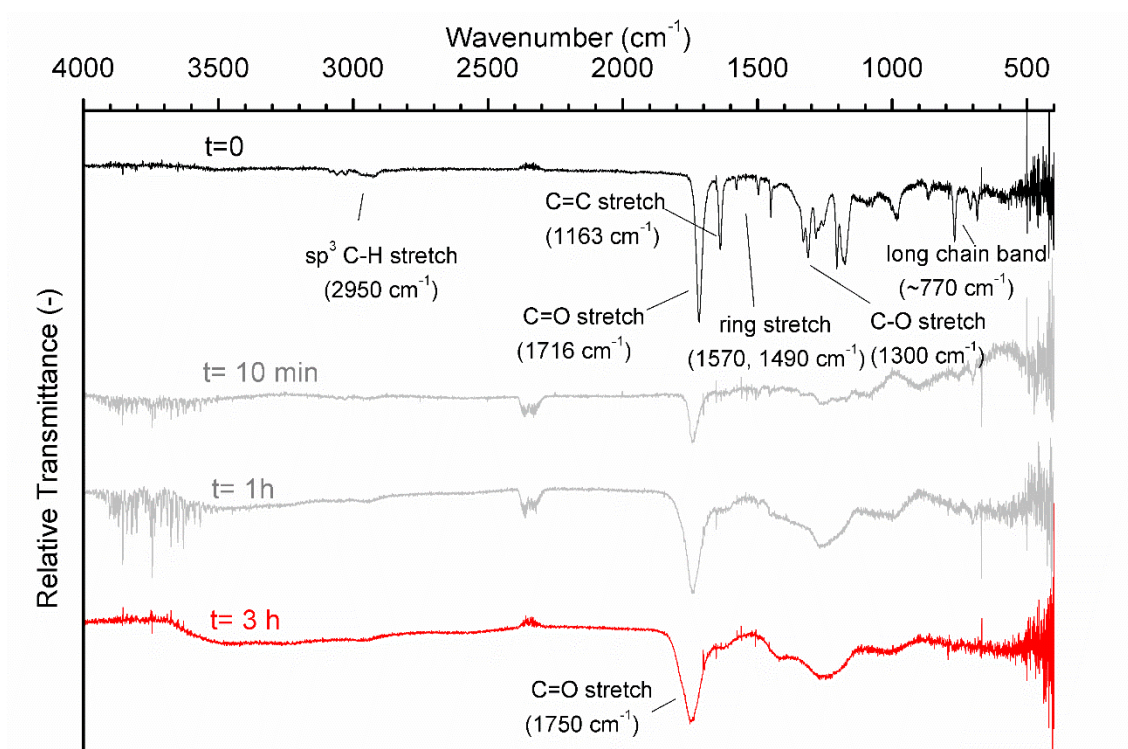
Figure 5. 33. IR-RAS spectra of PVCi_BG nanofilms after different UV-light irradiation times

6. Discussion

6. 1. Photodegradable Polymers

6. 1. 1. Commodity Polymers

6. 1. 1 .1. Poly(methyl methacrylate)

The weight loss phenomena of high and low molecular weight PMMA polymers upon UV-light irradiation observed on both nano- and microfilms is in correspondence with the literature. However, Carbaugh et. al reported higher weight loss rate for lower molecular weight PMMA films with micrometer-range thickness while in our case there was no significant difference in the rate of the relative weight decrease by molecular weight of PMMA measured on both nano- and microfilms [66]. Based on our results, it can be assumed that the formation and leaving of volatile photoreaction products happened in the same rate for the low and high molecular weight polymers. Regarding the thickness of the irradiated polymer samples, relative weight of nanofilms decrease at much higher rate than microfilms . This is expected considering that same dose of irradiation was used on smaller amount of material [3]. Also, in nanofilms elimination of degradation products are less diffusion limited.

The presence of the same chemical groups -characteristic to PMMA- could be detected with IR and NMR spectroscopy before and after UV-light irradiation independent of molecular weight and film thickness. As there are not any new bands in both IR and NMR spectra after irradiation, it is shown that reactions such as photolysis of methyl or ester side chain and crosslinking did not occur in a detectable amount. This can be explained by that the polychromatic UV-light was irradiated with relatively high dosage for these reaction pathways [3]. However, in the IR spectra band broadening appear after increased irradiation time indicating changed chemical environment of the detected groups. Accordingly, direct photodissociation of main chain and following unzipping can be proposed as photodegradation mechanism that caused the above mentioned weight losses in PMMA samples.

Major change in the physical properties of low and high molecular weight PMMA upon UV-light irradiation was shown by DSC and TGA measurements and indicated also by the visible contraction of the surface of their microfilms. Based on DSC measurements, the glass transition temperature of low molecular weight PMMA decreased drastically due to UV-light irradiation, while on high molecular weight PMMA film this could not be observed. As glass temperature of polymers drops rapidly at a critical, relatively low molecular weight (described by Flory Fox equation), the low molecular weight PMMA might suffered so many chain-scission reactions that its molecular weight decreased below this point [67]. The lack of glass temperature decrease for high molecular weight can be explained by that its high initial molecular weight did not decrease below this critical molecular weight. The DTG curves of the low and high molecular weight PMMA showed that UV-light irradiation resulted their thermal degradation steps shift to lower temperatures that can be linked to chemical changes in the polymer chains upon irradiation that made them more prone to engage in radical reactions of the thermal degradation. This was especially noticeable for the reactions of the chain ends at low temperature and for the random radical scission reactions at high temperature. Also, the absence of new peak on the DTG curves indicates that the similar thermal degradation processes might occur but at lower temperatures.

In summary, both high and low molecular weight PMMA suffered photodegradation that proceeded through the same mechanism and at the same rate, based on their weight losses and other physical and chemical changes. The mechanism of the photodegradation can be assumed to have happened via main-chain scission and incomplete unzipping of the polymer chain to its monomers. Also, it is shown that direct irradiation with mercury short-arc UV lamp results much higher degree of photodegradation in PMMA with nanometer-range thickness than in micrometer-range.

6. 1. 1. 2. Polystyrene

Polystyrene nanofilm shows no weight loss upon UV-light irradiation during the first hour, however presence of small carbonyl peak on its IR spectrum after 1-hour of irradiation may indicate that the photooxidation of the PS starts before it loses weight. The photooxidative degradation mechanism in PS nanofilm is confirmed also by its IR spectrum after 5-hour long irradiation having broad carbonyl peak possibly belonging to many kinds of degradation products with higher oxidation states than polystyrenes. This agrees with the literature that describes photooxidation typical for PS in air [29]. Therefore, it can be assumed that the observed weight loss at longer UV-light irradiation is the result of photooxidative degradation of the chain *via* peroxy radical that can be evolved in multiple photoreactions to produce volatile products beside non-volatile ones. In addition, delay in the photodegradation of solid polystyrene might occur due to two possible reasons (i) the energy acquired by excitation can be lost by vibrational relaxation (ii) solid state photooxidation is dependent on the oxygen diffusion into the polymer [27]. Even though the weight loss did not occur immediately, it is still remarkably high and can be explained by that in nanofilms effect of diffusion control is decreased for both oxygen and volatile photoproducts.

6. 1. 2. Depolymerizable polymers

6. 1. 2. 1. Photo acid and base generators

To enhance depolymerization, photocatalysts were used and the substances were also studied separately. In AG1 all C-Cl bonds were cleaved upon 1-hour long UV-light irradiation, thus the generation of Cl radical and formation of HCl can be assumed, however the product does not contain the expected triazine and aryl alkyl ether groups, but higher oxidation state carbonyl compounds. Therefore, in our case multiple photooxidative reactions of AG1 under UV-light is proposed next to acid generation. Similar to AG1, aromatic and even alkyl groups of AG2 got photodegraded upon UV-light based on its IR spectrum. However, as the characteristic bands of the anion (perfluoro-1-butanesulfonate) of the expectedly forming acid appear on the spectrum, the acid generation can be assumed in AG2 as well. In case of BG based on its spectrum after UV-light irradiation, formation of basic diethylamine did not occur. Instead, photooxidation of the photobase generator happened, therefore presence of basic species should not be considered during photodegradation of PSu_BG.

6. 1. 2. 2. Polyphthalaldehyde

The rapid weight loss of PPhA upon UV-light irradiation measured on the PPhA-based nano-and microfilms agrees with publications; weight loss caused by photo-induced depolymerization of PPhA is highly studied due to its use as positive photoresist in lithographic

applications [32]. Thus, the observed weight loss of PPhA-based samples might be linked to depolymerization. This assumption is supported also by that addition of photo acid generator to PPhA caused highly more rapid weight loss in a similarly exponential decrease by irradiation time. This shows that similar depolymerization reaction might have happened but with lowered activation energy and higher reaction rate due to catalytic role of photo generated acid.

Based on IR, NMR, QCM-D and TGA results, photodegradation process of pure PPhA-based samples primarily happened via depolymerization and further photodegradation of the monomer, OPA. In PPhA microfilm NMR and IR results showed that after UV-light irradiation the remaining material contained decreased amount, but mainly chemically unchanged PPhA (minimum 96.3% of the PPhA remained unchanged). Acetal link was still detected by ATR-IR characteristic to the main chain and NMR indicated ratios of hydrogens in aldehyde group and aromatic ring typical to monomer after spontaneous, not UV-light induced depolymerization of the remaining polymer in UV-light irradiated PPhA microfilm. This shows that the main chain and aromatic ring in PPhA typically did not take part in photoreactions that would change ratios of hydrogens in the repeating unit and later in the monomer (like addition, elimination, and substitution), rather depolymerization of PPhA proceeded upon UV-light irradiation. Depolymerization of PPhA had proposedly higher reaction rate and is a more dominant process than main chain scission or removal of end cap groups due to UV-light irradiation because of the measured rapid decrease in weight of PPhA nano- and microfilm that enhanced after addition of photo acid generator. However, it can be assumed that the extensive depolymerization happened after a UV-light induced main chain scission or end cap group removal as the bare chain is thermodynamically labile [30]. Unfortunately, the amount of OPA formed during irradiation could not be directly quantified as the pristine PPhA powder already contained OPA and it can be observed on both microfilm and nanofilm that OPA got consumed in further photoreactions upon UV-light. Oxidization of OPA can be assumed as carbonyl group was detected by IR on both nano-and microfilms after irradiation. In nanofilms only higher oxidation states than aldehyde were present after 10-minutes of irradiation with absorption around 1770 cm^{-1} while in microfilms OPA still could be indicated next to these bands. It can be explained by that in nanofilms lower amount of polymer got irradiated with the same dose than in microfilms. Also, in nanofilms the corresponding carbonyl band became broader by increased irradiation time that shows wide variety of oxidation states of photoproducts that probably formed via multiple photoreactions from OPA. However, the presence of multiple photoproducts that are hard to distinguish was typical also to irradiated microfilm based on broad peaks on TGA curve and its NMR spectrum. In addition, oxidization of the monomer to 2-carboxybenzaldehyde was observed on cyclic PPhA sample after monochromatic irradiation (365 nm, 1.70 mW cm^{-2}, 3 min) by Hernandez et. al. showing that aldehyde group of OPA is prone to oxidise upon UV-light [40]. In this case the absence of other photoproduct than 2-carboxybenzaldehyde might be explained by the use of monochromatic light, while in our study polychromatic irradiation resulted more types of photoreactions of OPA.

Similar to pure PPhA, based on IR, NMR, QCM-D and TGA results depolymerization of PPhA and photoreaction of OPA upon UV-light irradiation can be proposed in case of PPhA_AG2 samples as well. However, NMR result of irradiated PPhA_AG2 microfilm showed that there is decreased ratio of hydrogens in the aldehyde group and hydrogens in aromatic ring compared to pure PPhA microfilm. This can be caused by that i) aldehyde group of generated OPA rapidly reacted in further photoreactions before photoreactions of its

aromatic ring ii) not aldehyde group formed after main chain scission. It is hard to distinguish between the two possibilities and their parallel proceeding cannot be excluded as well. Nevertheless, this phenomena was moderate; even in extreme case maximum 10.7% of the repeating unit could not depolymerize to OPA, but another aromatic compound. Also, oxidation of the nano- and microfilms upon UV-light irradiation was higher than in case of pure PPhA samples, based on corresponding IR and NMR results. Moreover, formation of higher molecular weight products can be assumed based on DTG curve of irradiated PPhA_AG2 microfilm than in pure PPhA microfilm. The higher oxidation and condensation reaction rate can be explained by formation of OPA in higher rate that reacts further, but also the presence of acidic hydrogen could catalyse photoreactions that might not happen in PPhA films otherwise.

6. 1. 2. 3. Poly(propylenecarbonate)

Poly(propylenecarbonate) nanofilm shows moderate weight loss upon UV-light irradiation, much lower than PMMA, PS, and PPhA after 3-hour long irradiation. Even with addition of photo acid generator only small increase of weight loss could be achieved. Interestingly, unlike in PPhA, AG1 had higher effect on weight loss of PPC than AG2. Based on IR spectra of PPC-based nanofilms photodegradation occurred upon UV-light irradiation as there was no change in IR spectra after UV-light irradiation. However, it can be assumed that the activation energy of depolymerization reaction could not be lowered enough with the presence of acidic substance.

6. 1. 2. 4. Poly(1-hexadecane-sulfone)

Poly(1-hexadecane-sulfone) nanofilm does not show relevant weight loss upon UV-light irradiation. Even with addition of photo base generator the slight weight decrease is related only to the photodegradation of BG while the PSu remained unchanged. The absence of chemical change in the polymer was showed also by the IR spectrum before and after UV-light irradiation. The high photostability of the pure PSu can be explained by that its long olefin chain makes the polymer more stable that their short-chain counterparts [37]. Also, as generation of basic compounds from BG upon UV-light irradiation could not be proven, possible catalytic effect of BG on depolymerization cannot be further discussed.

6. 2. Photocrosslinkable Polymer

6. 2. 1. Poly(vinylcinnamate)

The expected crosslinking reaction of poly(vinylcinnamate) could not be detected after 10-minute long irradiation on its nanofilm based on the absence of C=C IR absorption band. Moreover, QCM-D measurements showed weight decrease of the polymer after 3-hour long irradiation that shows photodegradation of the polymer. Based on IR-RAS spectrum of the corresponding nanofilm this degradation occurred via photooxidation. Proposedly, to achieve controlled photocrosslinking of PVCi monochromatic light with shorter irradiation time should be used.

6. 3. Comparison of polymers

The weightloss in nanofilms and mechanism of the photodegradation of the studied polymers are summarized in Figure 6. 1.. PPhA showed the fastest weight loss that can be explained with its depolymerization upon UV-light and further reaction of the generated monomer. Compared to PPhA, in PSu and PPC the expected depolymerization reaction is much more restricted, probably due to their higher ceiling temperature [36] [37] [34] [35]. Depolymerization upon UV-light is observed also in PMMA, however in this case the unzipping is incomplete and it can explain the slower photodegradation than in PPhA. Interestingly, PS - that degraded with a different mechanism, photooxidation- lost weight more rapidly than PMMA but still not as fast as PPhA. In case of PVCi photocrosslinking could not be achieved but instead undesired photooxidative degradation happen upon UV light that was still moderate compared to PS. In general, it was shown that not only reaction mechanism but also the reaction rate (and related activation energy) has essential role to achieve rapid photodegradation; in case of PPhA photodegradation could be increased with catalysis.
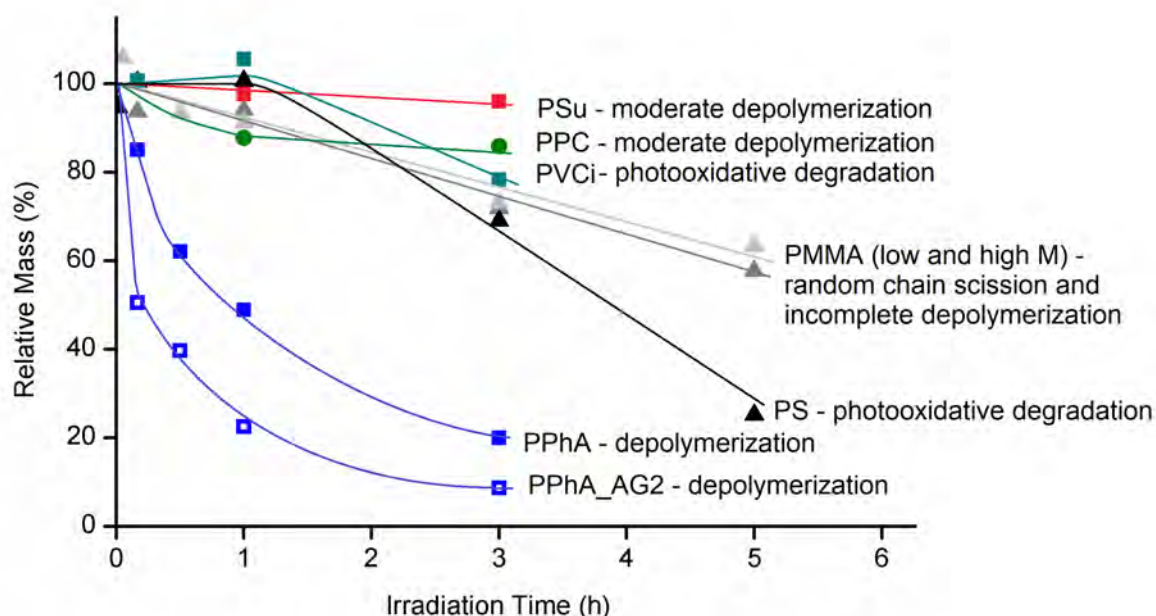

Figure 6. 1. Relative mass and photodegradation mechanism of studied nanofilms in function of UV-light irradiation time (with eyeliners)

7. Conclusion

Chemical changes and mass loss of different polymer nanofilms upon UV-light could be measured relatively fast and easy with coupling QCM-D and IRRAS methods. Due to the robustness of the measurement procedure, several types of polymers could be compared and evaluated on their suitability as possible microcapsule walls under the same UV-light irradiation conditions. An important advantage is that polymers photodegradation could be studied on their nanofilms that have the same thickness range as microcapsule wall thickness. Besides, in case of PMMA and PPhA additional chemical (ATR-IR, NMR) and physical (TGA, DSC) characterization supported the results gained with QCM-D and IRRAS. Also, it is important to note that more rapid photodegradation could be observed on nanofilms than on microfilms making studying possible degradation mechanisms less time consuming.

Six different kinds of polymers (PMMA, PS, PPhA, PPC, PSu, PVCi) were studied, in case of PMMA with two different molecular weights and in case of depolymerizable polymers (PPhA, PPC, PSu) with added photo catalyst in addition to the neat polymer. The weight loss rate of PMMA is independent of molecular weight. However, Tg decreased significantly upon UV-light irradiation in lower molecular weight PMMA in contrast to high molecular weight PMMA. Among the depolymerizable polymers, high catalytic effect of the added photo catalysator could be observed only in PPhA. In PSu and PPC, the depolymerization remained restricted proposedly due to their higher ceiling temperature.

Among the studied polymers the most suitable candidate as microcapsule wall is PPhA, preferably with added photo acid generator as it showed rapid photodegradation and its microfilm shifted to liquid phase upon UV-light irradiation. Its chemical characterization also showed that lower dose and use of monochromatic light with the suitable wavelength for inducing depolymerization but not to cause further reaction of the monomer might be beneficial in case of use as microcapsule wall.

Bibliography

[1] Bédard M. F., Polymeric Microcapsules with Light Responsive Properties for Encapsulation and Release, Advances in Colloid and Interface Science, 158, 2–14, 2010.

[2] Guillet , Polymer Photophysics Photochemistry, ISBN 0521347831, Cambridge University Press, 1985.

[3] Wochnowski C., Polymer Degradation and Stability 89, 252-264, 2005.

[4] Miller K. J., Macromolecules,26, 4945-4952, 1993.

[5] Fedynyshyn T. H., J. Vac. Sci. Technol. B, 18(6), 3332-3339, 2000.

[6] McKeen L. W., The Effect of UV Light and Weather on Plastics and Elas- tomers, ISBN: 978-1-4557-2851-0, Elsevier Inc., 2013.

[7] "Arslan-Tontul S., Single and double layered microencapsulation of probiotics by spray drying and spray chilling, Food Science and Technology 81, 160-169, 2017".

[8] Anal A. K., Recent advances in microencapsulation of probiotics for industrial applications and targeted delivery, Trends in Food Science Technology, 18 (5), 240-251, 2007.

[9] Li Y., Novel Charged Microcapsules as Templates for Layer-by-Layer Assembly of Polyelectrolytes and Adsorption of Lipid Bilayer, Master Thesis, Chalmers University of Technology, Gothenburg, 2011.

[10] Milián, Y. E., A review on encapsulation techniques for inorganic phase change materials and the in fluence on their thermophysical properties, Renewable and Sustainable Energy Reviews 73, 983–999, 2017.

[11] Esser-Kahn A. P., Triggered Release from Polymer Capsules, Macromolecules, 44, 5539–5553, 2011.

[12] De Geest B. G., Self-Rupturing Microcapsules, Advanced Materials, 17, 2357-2361, 2005.

[13] Paulo F., Design of Experiments for Microencapsulation Applications: A Review, Materials Science and Engineering C 77, 1327–1340, 2017.

[14] Marturano V., Light-Responsive Polymer Micro- and Nano-Capsules, Poly- mers, 9, 8, 2017.

[15] Alarcón C.H., Stimuli Responsive Polymers for Biomedical Applications, Chem. Soc. Rev., 34, 276–285, 2005.

[16] Lefebvre E., Poster, 7th International Materials Education Symposium, 2015.

[17] Fomina N., Photochemical mechanisms of light-triggered release from nanocar- riers, Advanced Drug Delivery Reviews, 64, 1005–1020, 2012.

[18] Wei J., Multi-Stimuli-Responsive Microcapsules for Adjustable Controlled- Release, Adv. Funct. Mater., 24, 3312–3323, 2014.

[19] Yi Q., Externally Triggered Dual Function of Complex Microcapsules, AC- SNano, 7, 10, 8693-8705, 2013.

[20] Kaitz, J. A., Depolymerizable polymers: preparation, applications, and future outlook, MRS Communications, 5, 191-204, 2015.

[21] Krevelen D. W., Properties of Polymers, ISBN 978-0-08-054819-7, Elsevier, 2009.

[22] Chen K., Fabrication of Ultraviolet-responsive Microcapsules via Pickering Emulsion Polymerization Using Modified Nano-silica/Nano-titania as Pickering Agents, RSC Adv., 5, 13850–13856, 2015.

[23] Rabek J. F., Photodegradation of Polymers, ISBN-13:978-3-642-80092-4, Springer, 1996.

[24] Stedwell C. N., Laser Photodissociation and Spectroscopy of Mass-separated Biomolecular Ions, ISBN 978-3-319-01252-0, Springer, 2013.

[25] Visakh, P. M., Photochemical Behavior of Multicomponent Polymeric-based Materials, ISBN 978-3-319-25196-7, Springer, 2016.

[26] Atkins P., Physical Chemistry, ISBN: 1-4292-1812-6, Oxford University Press, 2010.

[27] Rabek J. F., Polymer Photodegradation, ISBN: 978-94-011-1274-1, Springer, 1995.

[28] Yousif E., Photodegradation and photostabilization of polymers, especially polystyrene: review, SpringerPlus, 2:398, 2013.

[29] Rabek J. F., Journal of Polymer Science: Polymer Chemistry Edition, 12, 273-294, 1974.

[30] Tsuda M., Journal of Polymer Science: Part A: Polymer Chemistry, 35, 77-89, 1997.

[31] DiLauro A. M., Macromolecules, 46, 3309-3313, 2013.

[32] Ito H., Development of New Advanced Resist Materials for Microlithography, Journal of Photopolymer Science and Technology, 21, 4, 475-491, 2008

[33] Schwartz J. M., Journal of Polymer Science, part A: Polymer Chemistry, 55, 1166-1172, 2016.

[34] Li X. H., Thermal decomposition characteristics of poly(propylene carbonate) using TG/IR and Py-GC/MS techniques, Polymer Degradation and Stability, 81, 157-165, 2003.

[35] Spencer T. J., Decomposition of poly(propylene carbonate) with UV sensitive iodonium salts, Polymer Degradation and Stability, 96, 686-702, 2011.

[36] Lawrie K., Extreme ultraviolet (EUV) degradation of poly(olefin sulfone)s: Towards applications as EUV photoresisits, Radiation Physics and Chemistry, 80, 236-241, 2011.

[37] Thompson L. F., A New Family of Positive Electron Beam Resists - Poly(Olefin Sulfones), J. Electrochem. Soc.: Solid-state science and technology, 120, 12, 1722-1726, 1973.

[38] Sasaki T., Journal of Polymer Science: Part A: Polymer Chemistry, 47, 602-613, 2009.

[39] Shirai M., UV-curable positive photoresists for screen printing plate, Polym Int, 65:362-370, 2016.

[40] Hernandez H. L., Triggered Transience of Metastable Poly(ohthalaldehyde) for Transient Electronics, Adv. Mater, 26, 7637-7642, 2014.

[41] Kuramoto, Patent Application Publication, US 2011/0233048 A1, 2011.

[42] Fouassier J. P., Photoinitiators for Polymer Synthesis: Scope, Reactivity and Efficiency, ISBN:9783527332106, Wiley, 2012.

[43] Frings R. B., Photoreactions of polyvinylcinnamate: laser flash photolysis studies, Journal of Photochemistry, Volume 17, Issue 1, 50, 1981.

[44] Tsuda M., Some Aspects of the Photosensitivity of Poly(vinyl Cinnamate), Journal of Polymer Science: Part A, Vol. 2, pg. 2907-2916, 1964.

[45] Inoue m., Photocontrol of Solvent Responsiveness of Structural Colored Balloons, Langmuir, 29, 7047-7051, 2013.

[46] Reviakine I., Hearing What You Cannot See and Visualizing What You Hear: Interpreting Quartz Crystal Microbalance Data from Solvated Interfaces, Anal. Chem., 83, 8838–8848, 2011.

[47] Andersson Trojer M. A., Modification of microcapsules for controlled release, PhD Thesis, Chalmers University of Technology, 2012.

[48] Liu G., QCM-D Studies on Polymer Behavior at Interfaces, ISBN 978-3-642-39790-5, Springer, 2013.

[49] Pavia D. L., Introduction ro Spectroscopy, ISBN 0495114782, Brooks/Cole, 2009.

[50] Fussman C. R., High energy laser propagation in various atmospheric conditions utilizing a new, accelerated scaling code, MSc Thesis, Naval Postgraduate School, 2014.

[51] Takahashi M., Terahertz Vibrations and Hydrogen-bonded Networks in Crystals, Crystals, 4, 74-103, 2014.

[52] Höhne G. W. H., Differential Scanning Calorimetry, ISBN 978-3-642-05593-5, Springer, 2003.

[53] Gabott P., Principles and Applications of Thermal Analysis, ISBN-13: 978-1-4051-3171-1, Blackwell Publishing Ltd, 2008.

[54] Fulmer G. R., NMR Chemical Shifts of Trace Impurities: Common Laboratory Solvents, Organics, and Gases in Deuterated Solvents Relevant to the Organometallic Chemist, Organometallics, 29, 2176–2179, 2010.

[55] Ferriol M., Thermal degradation of poly(methyl methacrylate) (PMMA): modelling of DTG and TG curves,Polymer Degradation and Stability, 79, 271–281, 2003.

[56] Manring L. E., Thermal Degradation of Saturated Poly(methyl methacrylate), Macromolecules, 21, 530-532, 1988.

[57] Manring L. E., Thermal Degradation of Poly(methyl methacrylate) 2. Vinyl-Terminated Polymer, Macromolecules, 22, 2673-2677, 1989.

[58] Manring L.E., Thermal Degradation of Poly(methyl methacrylate). 3. Polymer with Head-to-Head Linkages, Macromolecules, 22, 4654-4656, 1989.

[59] Zhang K., Destruction of Perfluorooctane Sulfonate (PFOS) and Perfluorooctanoic Acid (PFOA) by Ball Milling, Environ. Sci. Technol., 47, 6471 – 6477, 2013.

[60] Bauschlicher C. W., Infrared spectra of polycyclic aromatic hydrocarbons: methyl substitution and loss of H, Chemical Physics 234, 79-86, 1998.

[61] Pretsch E., Structure Determination of Organic Compounds, ISBN 978-3-540-9, Springer, 2009.

[62] Solanki S. S. B., Growth and characterization of organic single crystal benzyl carbamate, Journal of Crystal Growth 427, 24–28, 2015.

[63] Lin-Vien D., The Handbook of Infrared and Raman Characteristic Frequencies of Organic Molecules, ISBN 0-12-451160-0, Academic Press, 1991.

[64] Köstler S., Amphiphilic Block Copolymers Containing Thermally Degradable Poly(phthalaldehyde) Blocks, Journal of Polymer Science: Part A: Polymer Chemistry, Vol. 47, 1499–1509, 2009.

[65] Hsu T.-J., Block copolymerization of carbon dioxide with cyclohexene oxide and 4-vinyl-1-cyclohexene-1,2-epoxide in based poly(propylene carbonate) by yttrium–metal coordination catalyst, Polymer, 43, 4535–4543, 2002.

[66] Carabaugh D. J., Dry photolithography through ultraviolet radiation-induced photo-etching of polymethyl methacrylate, Thin Solid Films, 615, 423-426, 2016.

[67] O`Driscoll K., Chain-Length Dependence of the Glass Transition Temperature, Macromolecules, 24, 4479-4480, 1991.